MaN 47

TID-4500, UC-32
Mathematics and Computers

LAWRENCE LIVERMORE LABORATORY
University of California/Livermore, California/94550

UCRL-51688

NUMERICAL EVALUATION OF SOMMERFELD INTEGRALS

R. J. Lytle
D. L. Lager

MS. date: October 23, 1974

Foreword

This work was sponsored by the Defense Advanced Research Projects Agency, under the direction of Mr. James Goodwyn and was monitored by Dr. Donald E. Barrick of NOAA.

Contents

NUMERICAL EVALUATION OF SOMMERFELD INTEGRALS

Abstract

The integrals expressing the interaction of electromagnetic sources with the ground are known as Sommerfeld integrals. Although these integrals have been known since 1909, and although approximate analytical expressions have been determined for a wide variety of conditions, there are still many applications for which sufficiently accurate results for Sommerfeld integrals need to be determined. This report describes a number of numerical integration methods which have been found to be particularly effective. All possible combinations of the electric dipole source and receiver location and orientation are considered. A computer program based upon these methods is available upon request. This computational algorithm has many applications in the areas of antenna design and evaluation, geophysical investigations, studies of environmental effects on communication systems, and the interaction and coupling effects of EMP into hardened systems.

Introduction

We concern ourselves with determining the interaction of electromagnetic fields with the ground. Specifically, we address the problems depicted in Figs. 1 through 4. These figures depict all the possible combinations of source and receiver locations relative to ground. We also consider all possible combinations of source and receiver orientations. Although these problems are classic, there are still a wide variety of situations where sufficiently accurate results need to be determined; thus, the effort described in

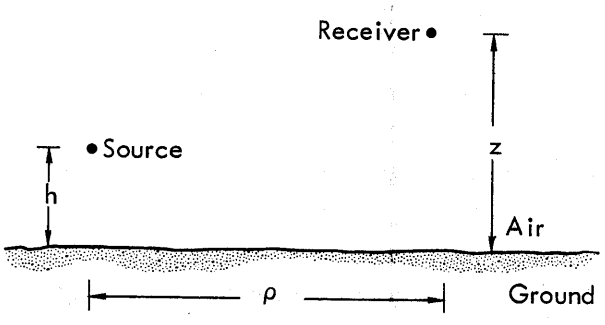

Fig. 1. Source and receiver locations are both above ground.

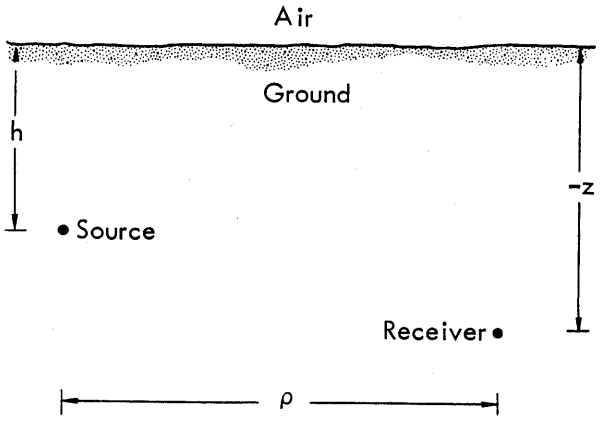

Fig. 2. Source and receiver locations are both below ground.

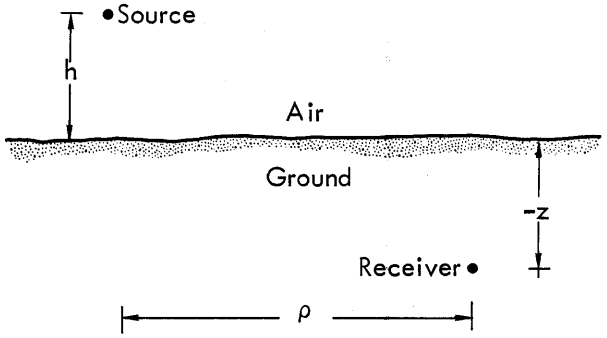

Fig. 3. Source is above ground and receiver is below ground.

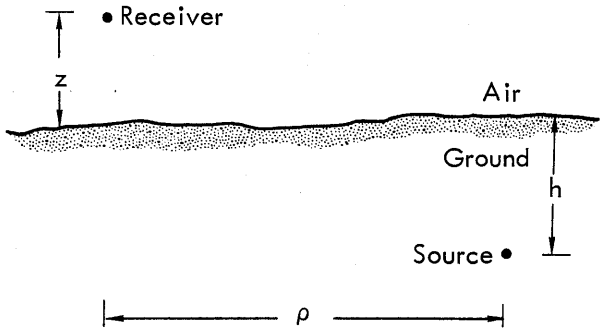

Fig. 4. Source is below ground and receiver is above ground.

this report was initiated. We have pursued a numerical integration approach, where the integrals to be evaluated are known as Sommerfeld integrals, in honor of Arnold Sommerfeld (who determined the exact integral expressions describing the physical phenomena).

In 1909, Arnold Sommerfeld derived the equations governing the electromagnetic fields generated by an electric dipole located above the ground.[1] For certain operating conditions, Sommerfeld approximately evaluated the integral expressions describing the fields by using approximate methods of integration in the complex domain. However, the methods used to evaluate the fields from these integral expressions are approximate, and are unfortunately not applicable for all ranges of operating conditions.

Since those initial investigations, numerous individuals have worked to expand the range of applicability of approximate formulas for Sommerfeld integrals (see the bibliography for an abbreviated list). Approximate formulas exist for conditions when the source (or receiver) is either buried or elevated. However, certain parameter bounds have to be satisfied before the various approximate formulas can be effectively used.

Many applications fall into situations where approximate evaluations of the Sommerfeld integrals are sufficiently accurate, particularly when the separation distance between source and receiver is large. The range of applicability of the approximate formulas depends upon the medium parameters (relative dielectric constant and conductivity) as well as the frequency, and the relative locations of source, receiver, and ground. The approximate formulas typically become more accurate for larger values of the dielectric constant, larger conductivity of the ground, and greater separation between source, receiver, and ground.

Although there are many situations when the Sommerfeld integrals can be approximated by sufficiently accurate analytic expressions, there are still numerous applications when sufficiently accurate analytic approximations for the Sommerfeld integrals do not exist. These situations particularly occur for small-to-moderate separation distances between source, receiver, and ground. We recognized that for these situations, some effective numerical integration procedure should be developed specifically for the general Sommerfeld integrals.

It is possible to numerically evaluate Sommerfeld integrals, regardless of the parameters, by using brute force integration. However, this can be so expensive that it may not be economically feasible to apply the results to the wide variety of problems of interest.

What is needed is a rapid, sufficiently accurate means of evaluating Sommerfeld integrals for the complete range of parameters of interest. This includes large, intermediate, and small values of dielectric constant and ground conductivity, and for any separation between source, receiver, and ground. The intent of the work described in this report was to generate a procedure that was sufficiently general that it would enable us to evaluate Sommerfeld integrals, both accurately and rapidly, for the full range of interesting parameters. We present the results of our efforts herein.

No claim is made that the general formulation presented herein is better for a specific problem than some other formulation which one might use. What is presented is a formulation that can be applied to a wide range of problems. The resultant code accuracy, timing, storage requirements, and computation algorithms are set up as "straw men" that may possibly be improved, not only for specific problems, but also for general problems. The computer program based upon the algorithms discussed herein is available upon request. An accompaning computer manual describes in detail the interaction of these numerous algorithms. An interchange and comparison of computer programs pertaining to this general problem is encouraged and welcomed. In this way, the difficulties presented by Sommerfeld integrals will most rapidly become a thing of the past.

There have been some approximate numerical integration procedures previously developed specifically for Sommerfeld integrals. Representative approaches include: (1) using asymptotic methods which assume the refractive index is large,[2] (2) using spline functions to represent part of the integrand and then analytically evaluating the resultant integral in terms of Lommel functions,[3] (3) a brute force numerical integration procedure utilized for a buried source in a dissipative medium (see water),[4] and (4) an alteration of the contour of integration used in conjunction with approximate analytic results (utilized for a buried vertical source and a buried vertical receiver).[5] These approaches have been demonstrated to be sufficiently accurate for a wide range of situations. The work described in this report was carried out so that the results could be applied to the general problem, as well as to problems which satisfy a number of "nice" criteria.

Applications

The problem of determining the current on an antenna located in close proximity to the ground-air interface (with the antenna either elevated or buried) is one which has undergone extensive investigation. Two reasons for the considerable longevity of this topic are that it is a problem of great practical interest and

that a solution for arbitrarily shaped antennas is difficult to obtain.

Numerical techniques applied to wire antenna structures in free space have been notably successful in predicting the complex interactions among the wire elements comprising the antenna structure.[6] These same numerical procedures can also be used for wire antenna configurations in close proximity to ground. The kernel of the governing integral equation is different for antennas near ground than it is for antennas in free space, but similar spatial sampling criteria, interpolation methods, junction treatments, basis functions, loading considerations, feed region models, and matrix solution techniques can be used. The form of the free-space-kernel, modified to account for the interaction of the wire elements with the ground, is commonly called the Sommerfeld integral for the ground interaction problem.

By coupling standard integral equation methods used for analysis of wire antenna structures with Somerfeld integral evaluations, it is possible to accurately model a number of structures and situations of practical significance. For example, one can accurately predict the polarization, beamwidth, bandwidth, near fields, gain, efficiency, input impedance, self-impedance, mutual impedance, phase center of antenna, ground screen effects, and environmental influence (rain, tide level, ground type, temperature) for antennas in close proximity to ground using the combined Sommerfeld integral/integral equation approach. This approach requires accurate and rapidly convergent methods both for evaluating the Sommerfeld integrals and for solving integral equations. These criteria have been satisfied for the integral equation methods for a number of antennas in free space. Due to the great practical importance of knowing the performance characteristics of antennas in close proximity to ground, the effort described in this report was extended towards developing an accurate, rapidly convergent, and sufficiently general procedure for evaluating Sommerfeld integrals.

In addition to the above information which one may desire about the antenna system and its interaction with the ground, further applications of the Sommerfeld/integral equation procedure include (among many others): design and data reduction considerations relating to telecommunication systems utilizing through-the-earth links; system design and data inversion studies pertaining to electromagnetic geophysical investigations; predicting ground losses; current attenuation loss; antenna wire loss; corona loss for high power systems; where and what size insulators are required; regions of significant interaction with the ground; where, what size, and what shape ground screens are desirable; accurately predicting low-angle and surface-wave radiation patterns; and modeling influence of guy wires.

Another area of application of the Sommerfeld/integral equation procedure is that the numerical results generated by the general approach can be used to extend the region of application of formulae approximating the Sommerfeld integrals. If approximate but sufficiently accurate formulae for Sommerfeld integrals can be used for all ranges of parameters of interest, then the antenna-in-proximity-to-ground problem becomes of the same order of difficulty(calculationally) as the

antenna-in-free-space problem. Our first attempt at extending the range of applicability of approximate formulas will be described in a forthcoming report.

Prelude to the Mathematical Details

We assume that the reader is familar with the contents of the book,[7] Dipole Radiation in the Presence of a Conducting Half-Space, written by Alfredo Baños, Jr. The notation used by Baños is also used in this report. The reader is of course referred to this book for background details. Baños also gives a very interesting historical account of efforts at evaluating Sommerfeld integrals.

The vertical and horizontal electromagnetic field expressions have been developed by Baños in terms of U and V integrals (his notation), which are defined in Appendix A. We are concerned with evaluating the U and V integrals and derivatives of these integrals. Our approach is to determine numerically effective ways of generating rapidly convergent results. We have somewhat arbitrarily settled upon using the Riemann sheet specification used by Baños, i.e., the vertical branch cut formulation. After briefly reviewing the effect of this choice of branch cut location, we investigate the behavior of the various components of the U and V integrands on the upper Riemann sheet. This detailed investigation enables us to visualize the tradeoffs involved in choosing one contour of integration versus another contour. This led us to specific contours of integration for both the Bessel and Hankel function representation of the U and V integrals. The results are expressed in terms of an approach based on numerical algorithms only and an approach based on a combination of approximate analytic results and a numerical algorithm.

The effect on the numerical procedures of the location of source and receiver, the relative dielectric constant (ϵ_r), and the ratio of ground conduction currents to displacement currents (p), is demonstrated.

Effect of Choice of Branch Cuts

The U and V integrands include the factors γ_1 and γ_2, where $\gamma_1 = (\lambda^2 - k_1^2)^{1/2}$ and $\gamma_2 = (\lambda^2 - k_2^2)^{1/2}$. The square root operation involved in determining γ_1 and γ_2 means that they are multiple-valued functions (two possible roots each). Branch points for γ_1 and γ_2 occur at $\lambda = k_1, \infty$ and $\lambda = k_2, \infty$, respectively. To determine uniquely the result of the square root operation, a branch cut connecting the two branch points of γ_1 (and γ_2) needs to be specified. There are an infinite number of ways of connecting the branch points. However, only the two special cuts which have previously received the most interest are discussed herein. These two branch cuts are the fundamental cuts of Sommerfeld and the vertical cuts used in the numerical study utilized in the body of this report.

The fundamental branch cuts of Sommerfeld are specified by the condition Re $(\gamma_1) = 0$ and Re $(\gamma_2) = 0$. With this choice, one of the two possible Riemann sheets for γ_1 is specified by Re $(\gamma_1) \geq 0$ and the second Riemann sheet is specified by Re $(\gamma_1) \leq 0$. A similar choice is made for the Riemann sheets for γ_2.

Since k_1 is complex, the fundamental branch cut specification Re $(\gamma_1) = 0$ dictates that the fundamental cuts for γ_1 follow hyperbolas, depicted by the wiggly lines in Fig. 5. Since k_2 is a real number, the fundamental branch cut specification Re $(\gamma_2) = 0$ dictates that the fundamental cuts for γ_2 are "degenerate hyperbolas" following the imaginary axis and the real axis between $-k_2$ and k_2 (see the wiggly lines in Fig. 5).

With two Riemann sheets for γ_1 and also two for γ_2, the combination of the functions γ_1 and γ_2 requires a four-sheeted Riemann surface. This of course holds

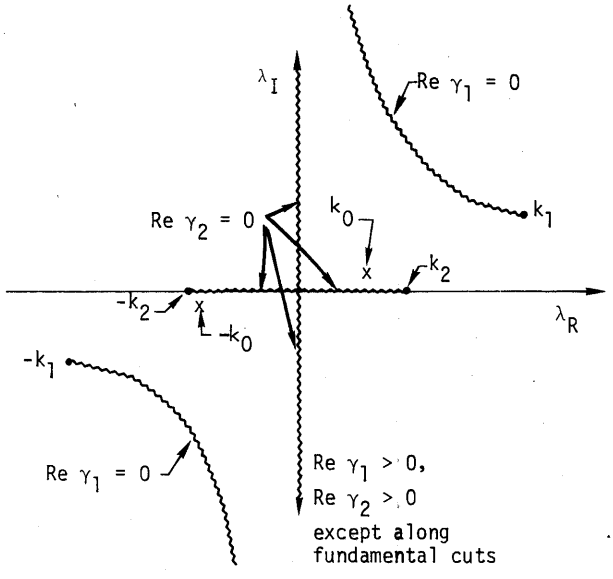

Fig. 5. The fundamental branch cuts are Re $(\gamma_1) = 0$ and Re $(\gamma_2) = 0$, where $\gamma_1 = (\lambda^2 - k_1^2)^{1/2}$ and $\gamma_2 = (\lambda^2 - k_2^2)^{1/2}$.

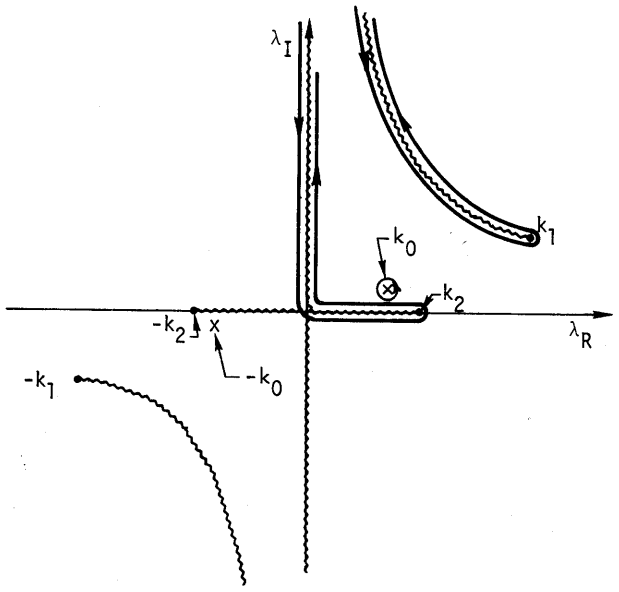

Fig. 6. The solid lines denote Sommerfeld's contour of integration and the fundamental cuts are represented by wiggly lines. Note the integration around the pole at $\lambda = k_0$.

regardless of the choice of branch cut location. Following Sommerfeld, one specification of the choice of roots on each Riemann sheet is given in Table 1. The contour of integration used by Sommerfeld in his initial investigations is shown in Fig. 6. Note that this path of integration always remains on Sheet I [with Re $(\gamma_1) \geq 0$ and Re $(\gamma_2) \geq 0$]. This path of integration lies on both sides of the fundamental branch cuts. The presence of a real (not virtual) pole on Sheet I can cause some numerical integration difficulties for the fundamental branch cut integrations.

The vertical branch cuts used in this numerical study, Fig. 7 (and also used by Baños, among others) are a second possible choice of branch cut. These cuts have the advantage that there is no real pole on Sheet I (for the vertical cuts). There is a virtual pole on Sheet I (for the

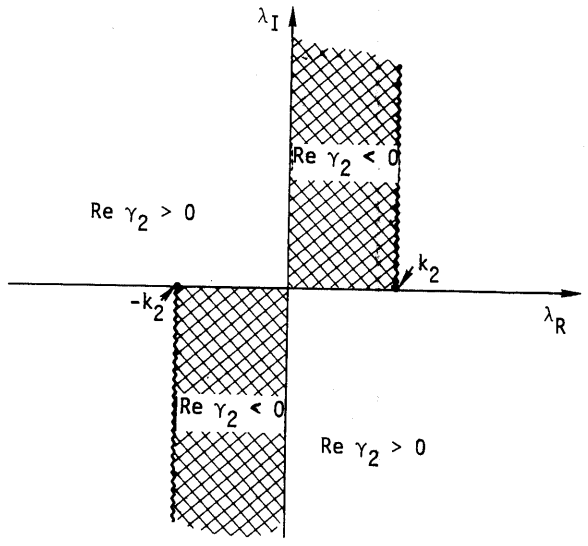

Fig. 7. For vertical branch cuts, the variation of the Re (γ_2) on the first Riemann sheet can have Re $(\gamma_2) > 0$ and Re $(\gamma_2) < 0$, where $\gamma_2 = (\lambda^2 - k_2^2)^{1/2}$.

vertical cuts), but its effective influence is not as great as that of the real pole on Sheet I (for the fundamental cuts). Hence, the demands on the numerical integration for the vertical cuts is expected to be less severe than for the fundamental cuts. It is possible that other branch cuts might be a better choice, but time limitations prevented us from pursuing alternative choices.

The use of vertical branch cuts for γ_1 and γ_2 dictates that Re (γ_1) and Re (γ_2) are no longer greater than zero over the complete Sheet I (or any other sheet). The region where Re (γ_2) and Re (γ_1) are less than zero is well delineated however, and the shaded regions in Figs. 7 and 8 define these regions. The mathematical operation involved in determining the choice of square root on Sheets I to IV (for the vertical cuts) was given in Table 1).

Due to the different branch cuts (fundamental and vertical), and consequent different dependency of γ_1 and γ_2 upon the Riemann sheet number, the quantities γ_1, γ_2, and the denominator of the V integrand $N(\lambda)$ $[N(\lambda) = k_1^2 \gamma_2 + k_2^2 \gamma_1]$, evaluated at $\lambda = k_0$ have different results. To illustrate this difference, the dependency of these quantities upon sheet number and choice of cuts is given in Table 2. Note the presence of real and virtual poles in both formulations, but that the real and virtual poles occur on different sheets in the two formulations. This comparison of the effect of the choice of branch cuts has been included to attempt to clear up possible questions in the reader's mind regarding the relative effect of the cut choice. As stated before, we have arbitrarily used the vertical cut choice in all our numerical studies.

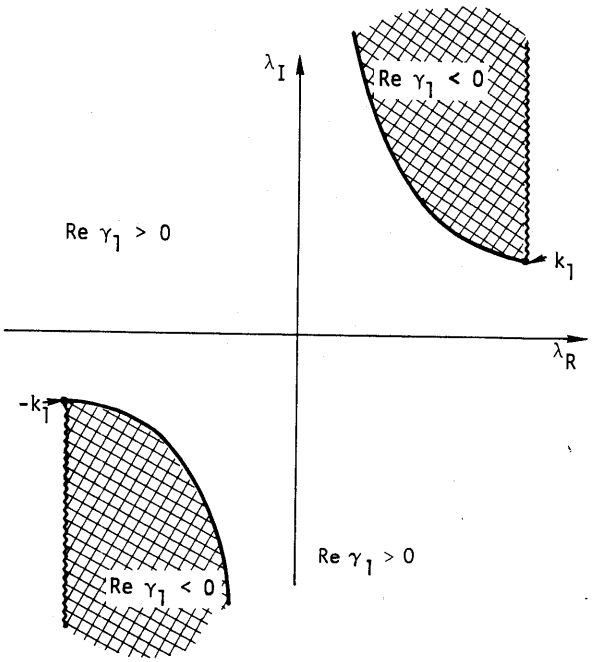

Fig. 8. For vertical branch cuts, the variation of the Re (γ_1) on the first Riemann sheet can have Re $(\gamma_1) > 0$ and Re $(\gamma_1) < 0$, where $\gamma_1 = (\lambda^2 - k_1^2)^{1/2}$.

Table 1. Comparison of branch cut choices. Item: Specification of γ_1 and γ_2 for each sheet.

Fundamental cuts

$$\gamma = \sqrt{\lambda^2 - k^2}$$

Sheet	Re γ_1	Re γ_2
I	≥ 0	≥ 0
II	≤ 0	≥ 0
III	≥ 0	≤ 0
IV	≤ 0	≤ 0

Vertical cuts

$$\gamma = \sqrt{\lambda - k}\ \sqrt{\lambda + k}$$

$$\sqrt{\lambda - k} = |r| \exp(i\xi)$$
$$\sqrt{\lambda + k} = |s| \exp(i\psi)$$

Sheet	ξ	ψ
I	$\frac{-3\pi}{4} \leq \xi \leq \frac{\pi}{4}$	$\frac{-3\pi}{4} \leq \psi \leq \frac{\pi}{4}$
II	$\frac{-\pi}{4} \leq \xi \leq \frac{3\pi}{4}$	$\frac{-3\pi}{4} \leq \psi \leq \frac{\pi}{4}$
III	$\frac{-3\pi}{4} \leq \xi \leq \frac{\pi}{4}$	$\frac{-\pi}{4} \leq \psi \leq \frac{3\pi}{4}$
IV	$\frac{-\pi}{4} \leq \xi \leq \frac{3\pi}{4}$	$\frac{-\pi}{4} \leq \psi \leq \frac{3\pi}{4}$

Table 2. Comparison of branch cut choices. Item: Behavior of γ_1, γ_2, and N at $\lambda = k_0$.

Fundamental cuts

$$\gamma_1(k_0) = \begin{cases} -i\dfrac{k_0 k_2}{k_1}, & \text{sheets I and III} \\ +i\dfrac{k_0 k_2}{k_1}, & \text{sheets II and IV} \end{cases}$$

$$\gamma_2(k_0) = \begin{cases} -i\dfrac{k_0 k_1}{k_2}, & \text{sheets III and IV} \\ +i\dfrac{k_0 k_1}{k_2}, & \text{sheets I and II} \end{cases}$$

$$N(k_0) = \begin{cases} -2i\, k_0 k_1 k_2, & \text{sheet III} \\ 0, & \text{sheets I and IV} \\ +2i\, k_0 k_1 k_2, & \text{sheet II} \end{cases}$$

Vertical cuts

$$\gamma_1(k_0) = \begin{cases} -i\dfrac{k_0 k_2}{k_1}, & \text{sheets I and III} \\ +i\dfrac{k_0 k_2}{k_1}, & \text{sheets II and IV} \end{cases}$$

$$\gamma_2(k_0) = \begin{cases} -i\dfrac{k_0 k_1}{k_2}, & \text{sheets I and II} \\ +i\dfrac{k_0 k_1}{k_2}, & \text{sheets III and IV} \end{cases}$$

$$N(k_0) = \begin{cases} -2i\, k_0 k_1 k_2, & \text{sheet I} \\ 0, & \text{sheets II and III} \\ +2i\, k_0 k_1 k_2, & \text{sheet IV} \end{cases}$$

Integrand Component Behavior

The U and V integrands (Baños' notation, see also Appendix A – Mathematical Formulas) are composed of the product of either a Bessel or a Hankel function, an exponential factor $\exp(-\gamma_1 a - \gamma_2 b)$, a factor of either $1/(\gamma_1 + \gamma_2)$ (for the U integral) or $1/N(\lambda)$ (for the V integral), and a factor of λ. The variation of these factors with λ dictates which integration contours are numerically most effective. The influence of these factors throughout the λ plane, particularly near the origin and $\lambda = k_2$, is particularly important. These terms depend upon the medium parameters [ϵ_r and $p = \sigma/(\omega\epsilon_0\epsilon_r)$], as well as λ; thus, results are described below for a range of medium parameters to see their influence.

Figures 9 and 10 illustrate the behavior of the Bessel function (real and imaginary) as functions of the argument z. Note the exponential growth in $J_0(z)$ as Im (z) is increased. Also note the oscillatory behavior of $J_0(z)$ as Re (z) is varied.

Figures 11 and 12 depict the behavior of the Hankel function (real and imaginary) as functions of the argument z. A smooth variation of $H_0^{(1)}(z)$ with z is indicated, except for z near zero or near the negative Im (z) axis [wherein lies the branch cut for the ln z behavior of $H_0^{(1)}(z)$]. Note that the magnitude of $H_0^{(1)}(z)$ decreases as Im (z) is increased.

The factor $\exp(-\gamma_1 a - \gamma_2 b)$ depends only on the terms $\gamma_1 a$ and $\gamma_2 b$. The term $\gamma_2 b$ can be represented by $\gamma_2 b = k_2 b$

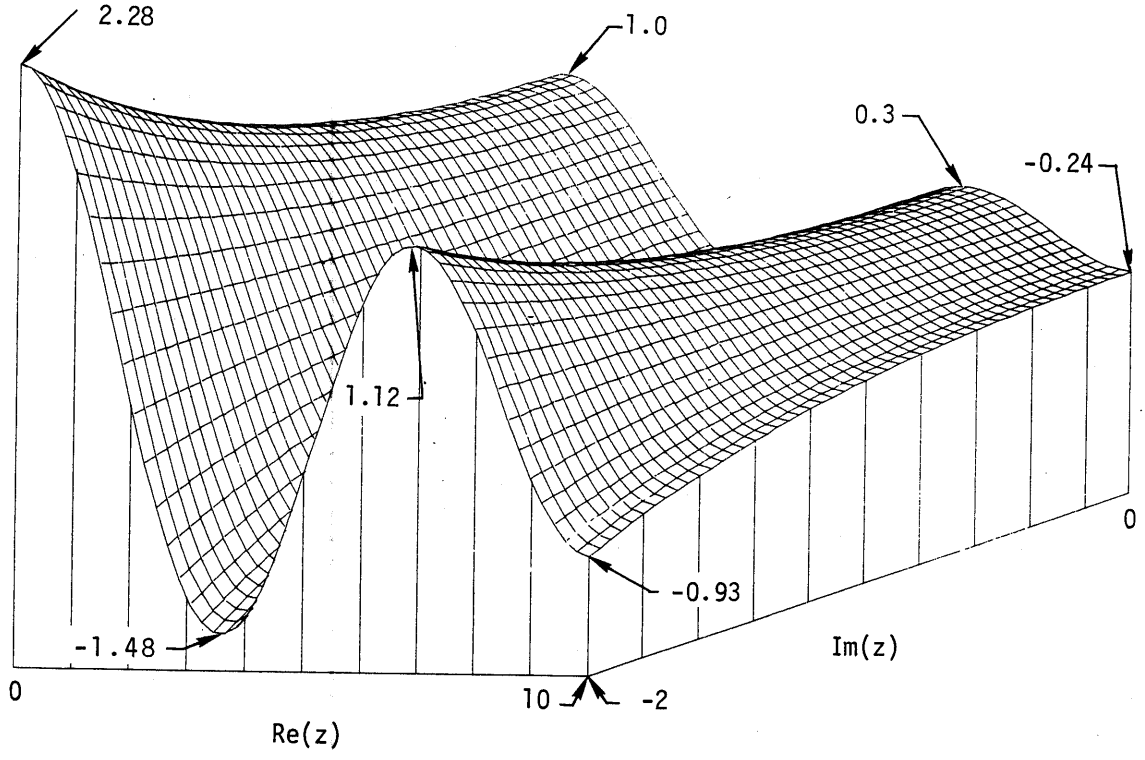

Fig. 9. The Re $(J_0(z))$ oscillates along the Re (z) axis and increases parallel to the Im (z) axis.

$[\text{Re}\,(\gamma_2/k_2) + i\,\text{Im}\,(\gamma_2/k_2)]$. This factorization gives two separate terms, one ($k_2 b$) dependent on source/receive location and one $[\text{Re}\,(\gamma_2/k_2) + i\,\text{Im}\,(\gamma_2/k_2)]$ dependent on λ and the ground parameters. Since the source-receiver location term is a constant (independent of λ), then the dependence of $\gamma_2 b$ as a function of λ and the ground parameters alone can be demonstrated by normalized curves.

Figures 13 and 14 illustrate the variation of Re (γ_2/k_2) and Im (γ_2/k_2), respectively, with λ. The presence of the vertical branch cut at Re $(\lambda/k_2) = 1$ and Im $(\lambda/k_2) \geq 0$ is evident in these figures. Also evident in Fig. 13 is the fact that Re $(\gamma_2) > 0$ everywhere on the first (upper) Riemann sheet, except when $\lambda_I > 0$ and $0 < \text{Re}\,(\lambda/k_2) < 1$, or $\lambda_I < 0$ and $-1 < \text{Re}\,(\lambda/k_2) < 0$ (also see Fig. 7).

Figures 15 through 19 and 20 through 24 show the behavior of Re (γ_1/k_2) and Im (γ_1/k_2), respectively, upon location in the λ plane and with medium parameters (ϵ_r and p). These factors dictate the variation of $\gamma_1 a = k_2 a\,[\text{Re}\,(\gamma_1/k_2) + i\,\text{Im}\,(\gamma_1/k_2)]$ with λ and medium parameter. Notice that from Figs. 15 through 19 there is not much variation of Re (γ_1/k_2) with λ for small λ, except when ϵ_r is small and p is also small (Fig. 15). Similar remarks are true for Im (γ_1/k_2). There is a slight dependence of Re (γ_1/k_2) and Im (γ_1/k_2) upon λ, but it is not dramatic. The variation of these terms with the medium parameters, ϵ_r and p is more apparent, with the effect primarily influencing the absolute amplitude of the factor.

The factor $1/(\gamma_1 + \gamma_2)$ is plotted in Figs. 25 through 29 and 30 through 34,

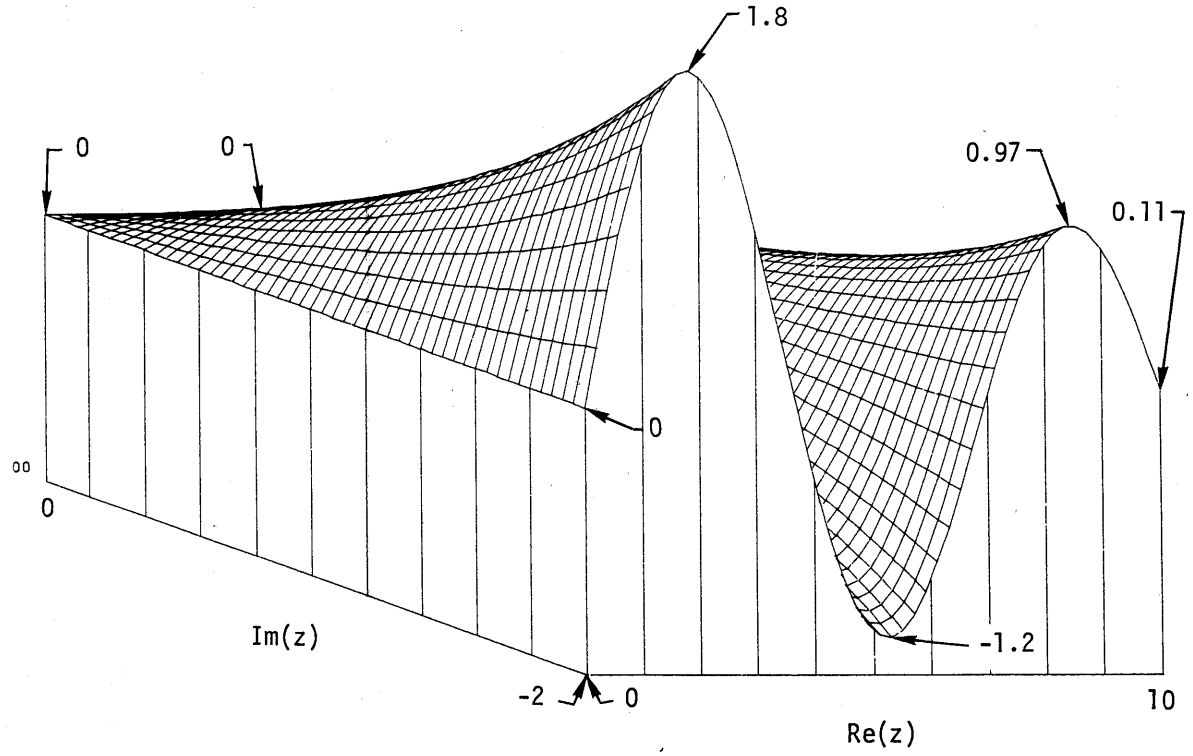

Fig. 10. The Im $(J_0(z))$ oscillates along the Re (z) axis and increases parallel to the Im (z) axis.

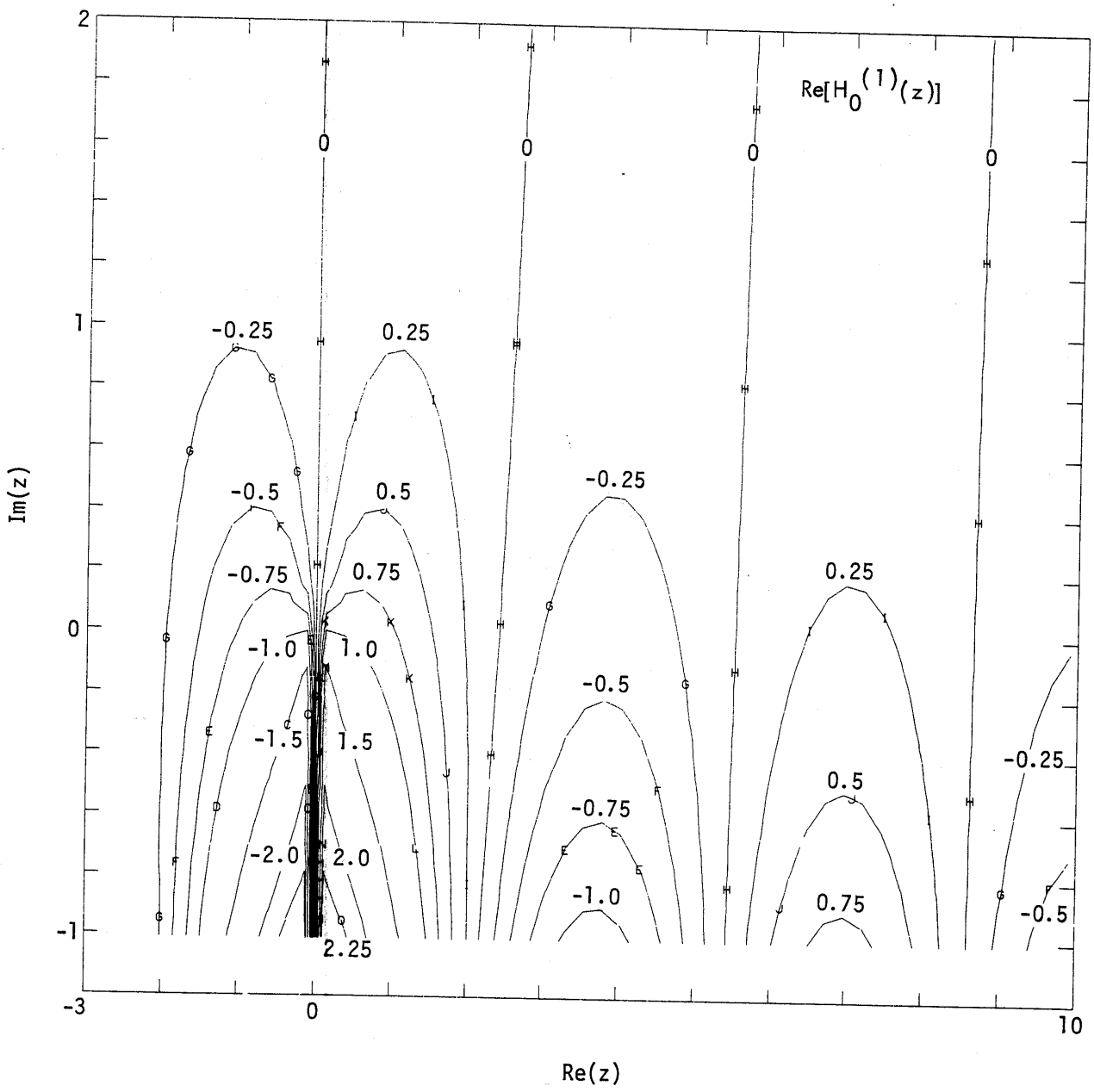

Fig. 11. The Re $(H_0^{(1)}(z))$ varies rapidly near the branch cut along the negative Im (z) axis.

respectively, as $|1/(\gamma_1 + \gamma_2)|$ and $\underline{/1/(\gamma_1 + \gamma_2)}$. The effect of the vertical branch cut at Im $(\lambda) \geq 0$ and Re $(\lambda/k_2) = 1$ is evident in these figures. Also indicated is the fact that the term $1/(\gamma_1 + \gamma_2)$ is reasonably well-behaved both in magnitude and phase except near the branch cut. There is some dependence of these results upon the medium parameters, but the variation is not spectacular.

The factor $1/N(\lambda)$, which occurs in the V integrand, has a most spectacular variation with λ and with medium parameters. Figures 35 through 39 and 40 through 44, respectively, illustrate the variation of $|1/N(\lambda)|$ and $\underline{/1/N(\lambda)}$. The presence of the vertical branch cut is

evident in both the magnitude and phase results. The magnitude results in Figs. 35 through 39 indicate a peaking behavior near the vertical branch cut, with the peak located on the side specified by Re $(\lambda/k_2) > 1$. The width of the peak is decidedly influenced by the medium parameters, with the width of the peak being smaller for larger ϵ_r or p. The magnitude function is well behaved for $0 \leq$ Re $(\lambda/k_2) < 0.8$. The magnitude variation away from the real axis [especially below Re $(\lambda/k_2) = 1$] is smooth. The phase function $\angle 1/N(\lambda)$ is also reasonably well behaved except very near the vertical branch cut (see Figs. 40 through 44).

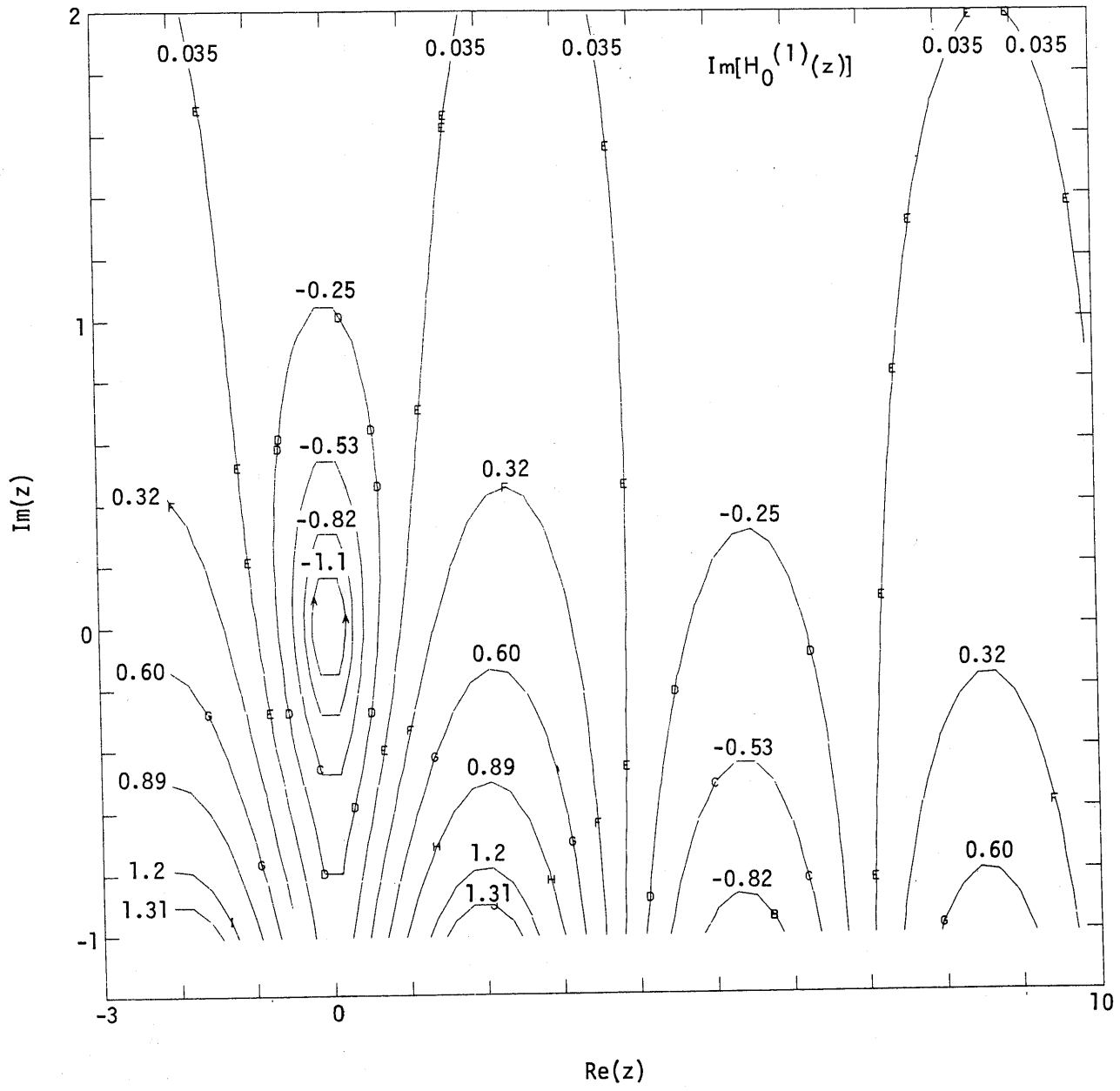

Fig. 12. The Im $(H_0^{(1)}(z))$ is reasonably well behaved except in the near vicinity of z = 0.

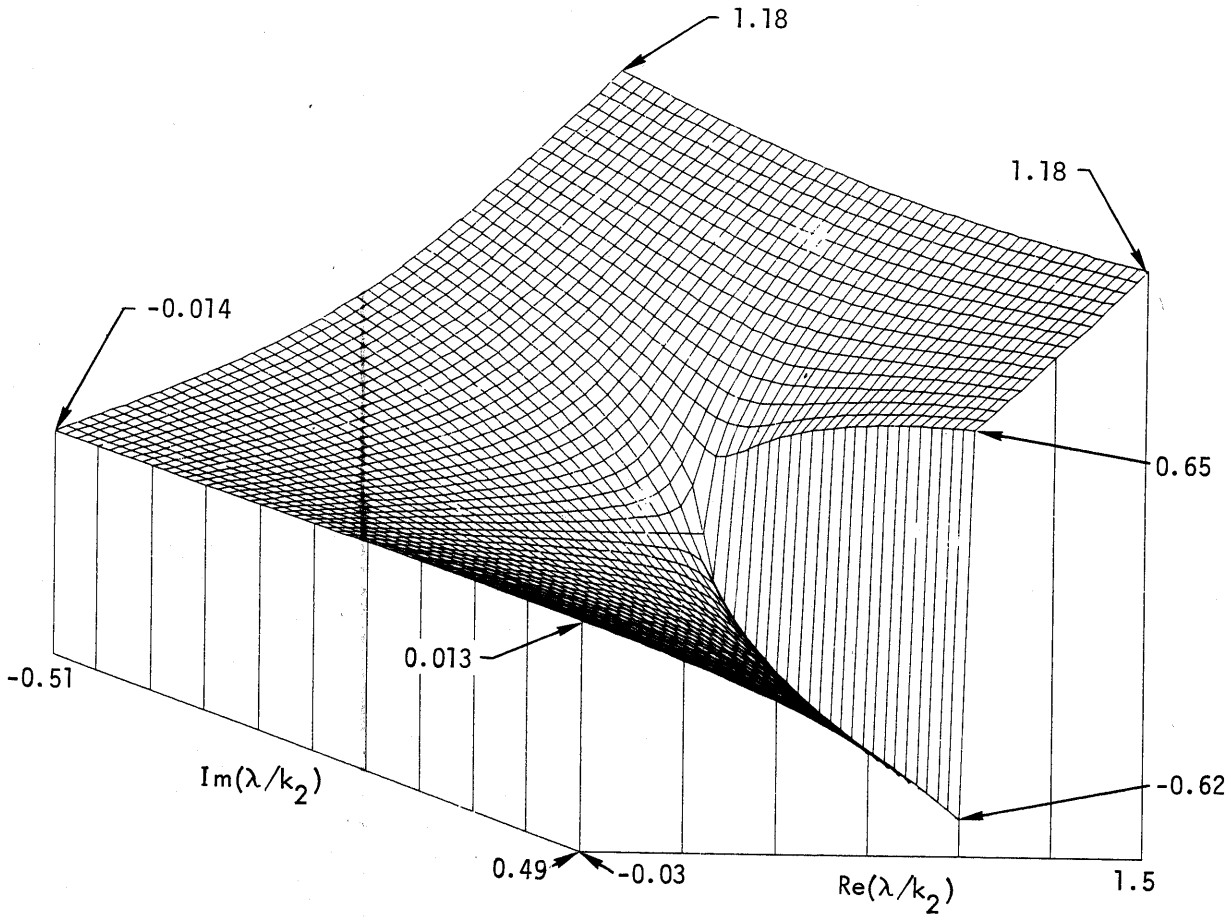

Fig. 13. The Re (γ_2/k_2) is smoothly varying except along the vertical branch cut emanating from $\lambda = k_2$.

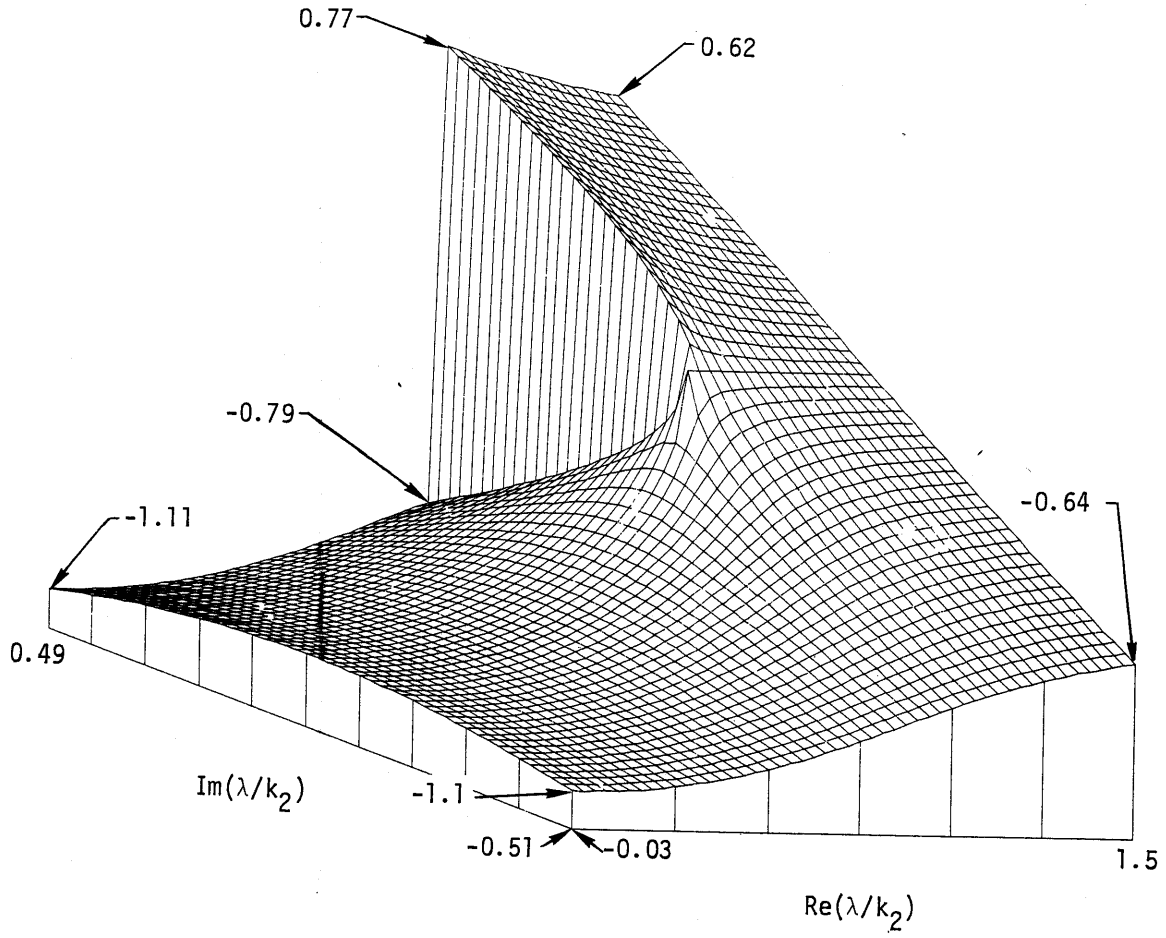

Fig. 14. The Im (γ_2/k_2) is well behaved except along the vertical branch cut emanating from $\lambda = k_2$.

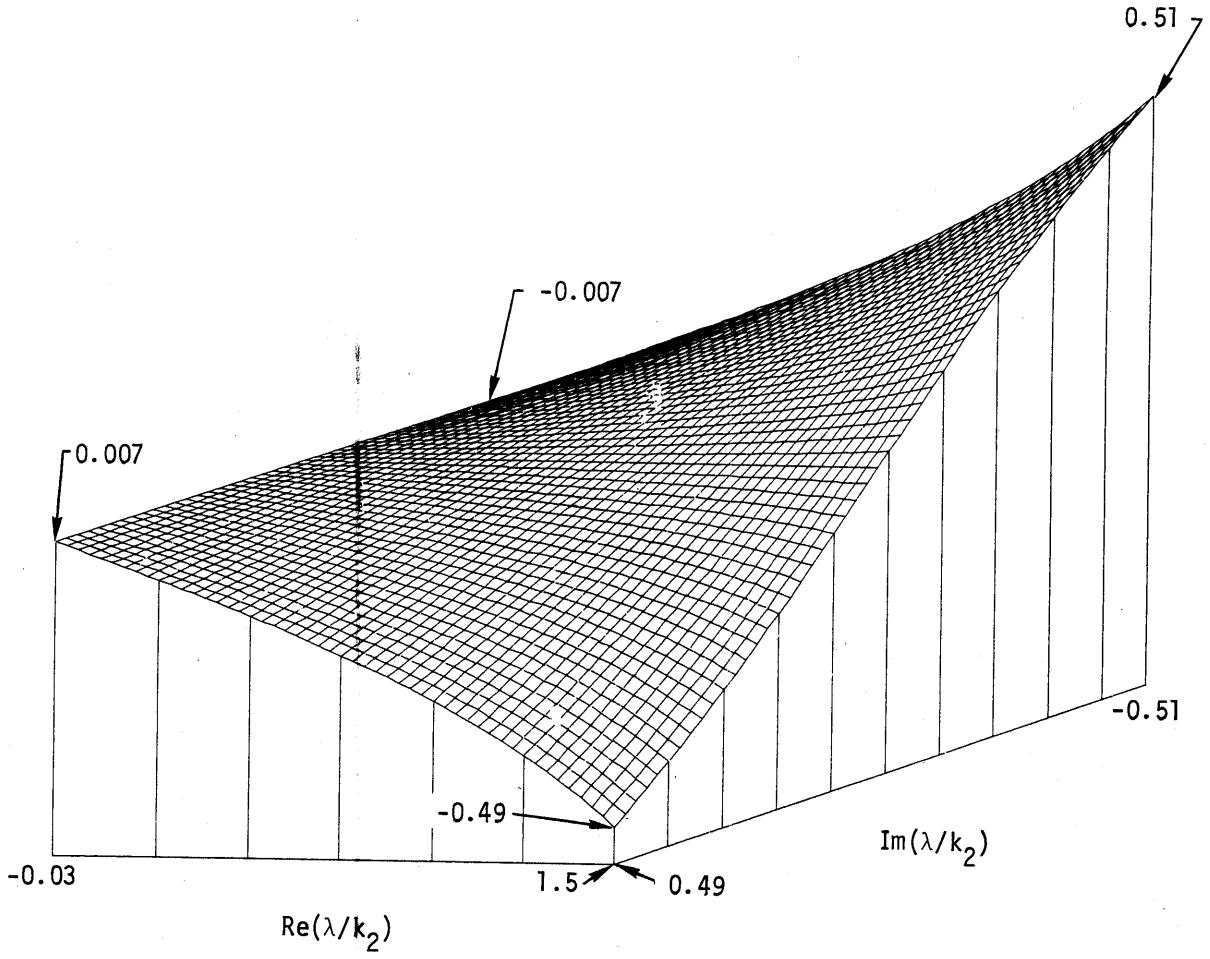

Fig. 15. The Re (γ_1/k_2) is a smooth function for $\epsilon_r = 4$ and $p = 0$.

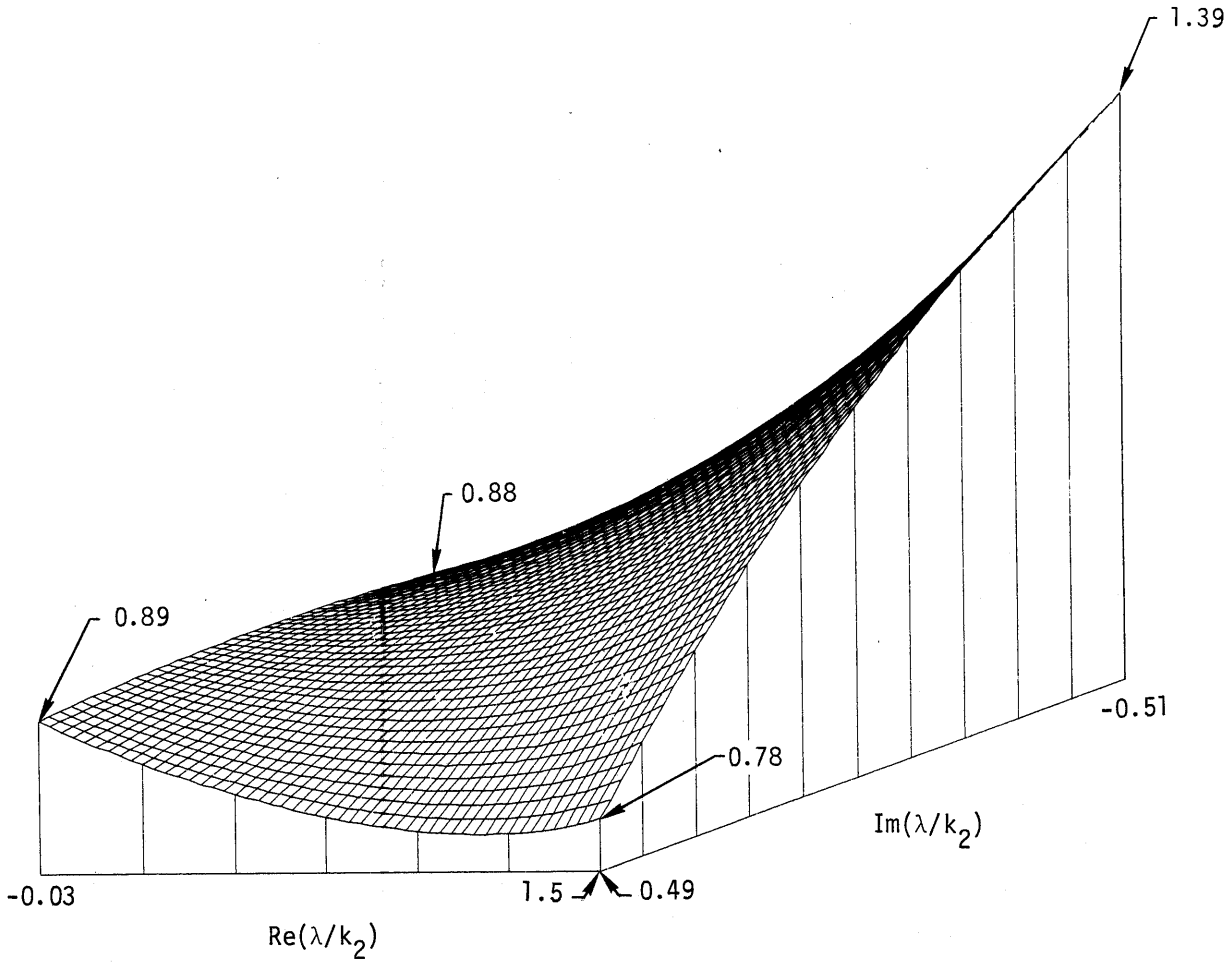

Fig. 16. The Re (γ_1/k_2) is a smooth function for $\epsilon_r = 4$ and $p = 1$.

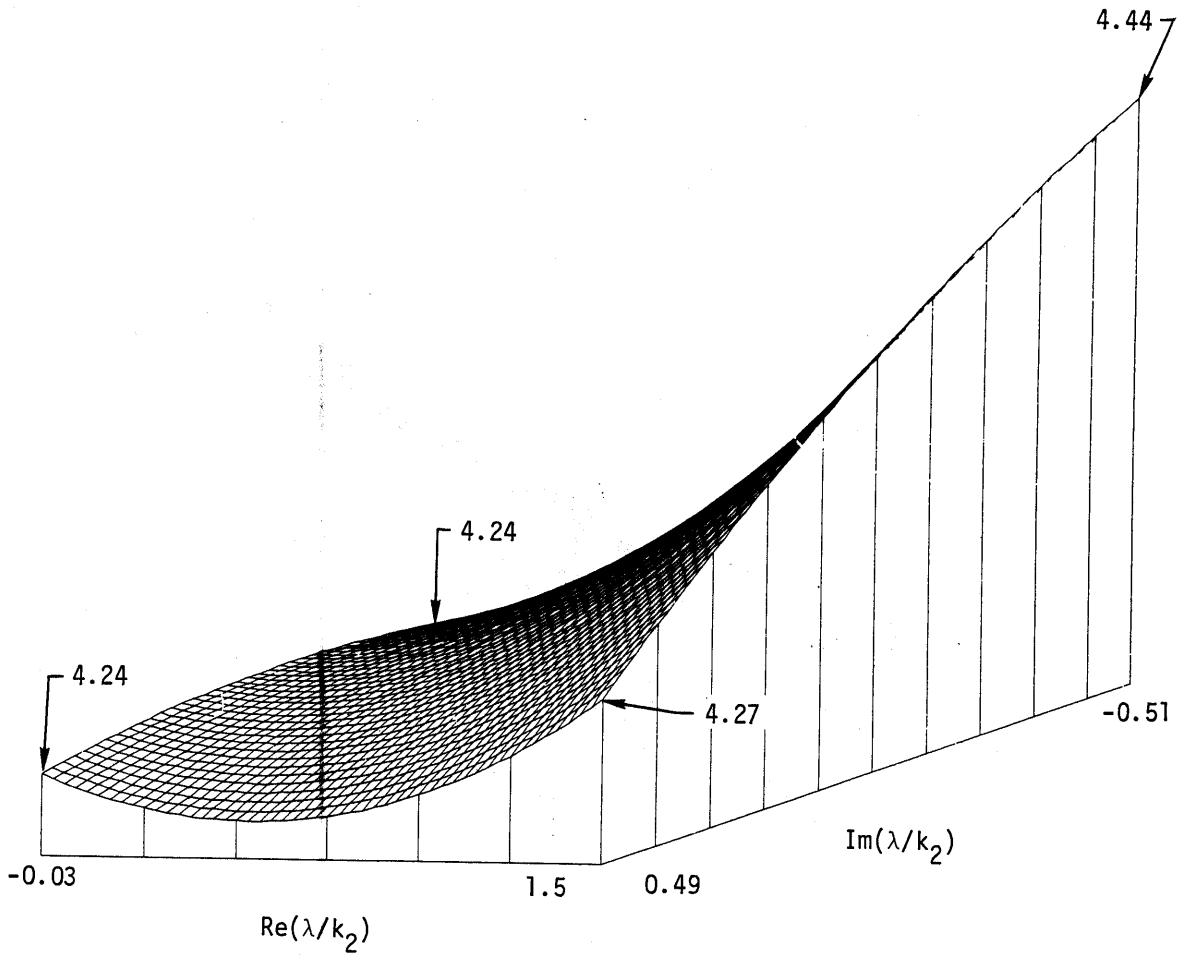

Fig. 17. The Re (γ_1/k_2) is a smooth function for $\epsilon_r = 4$ and $p = 10$.

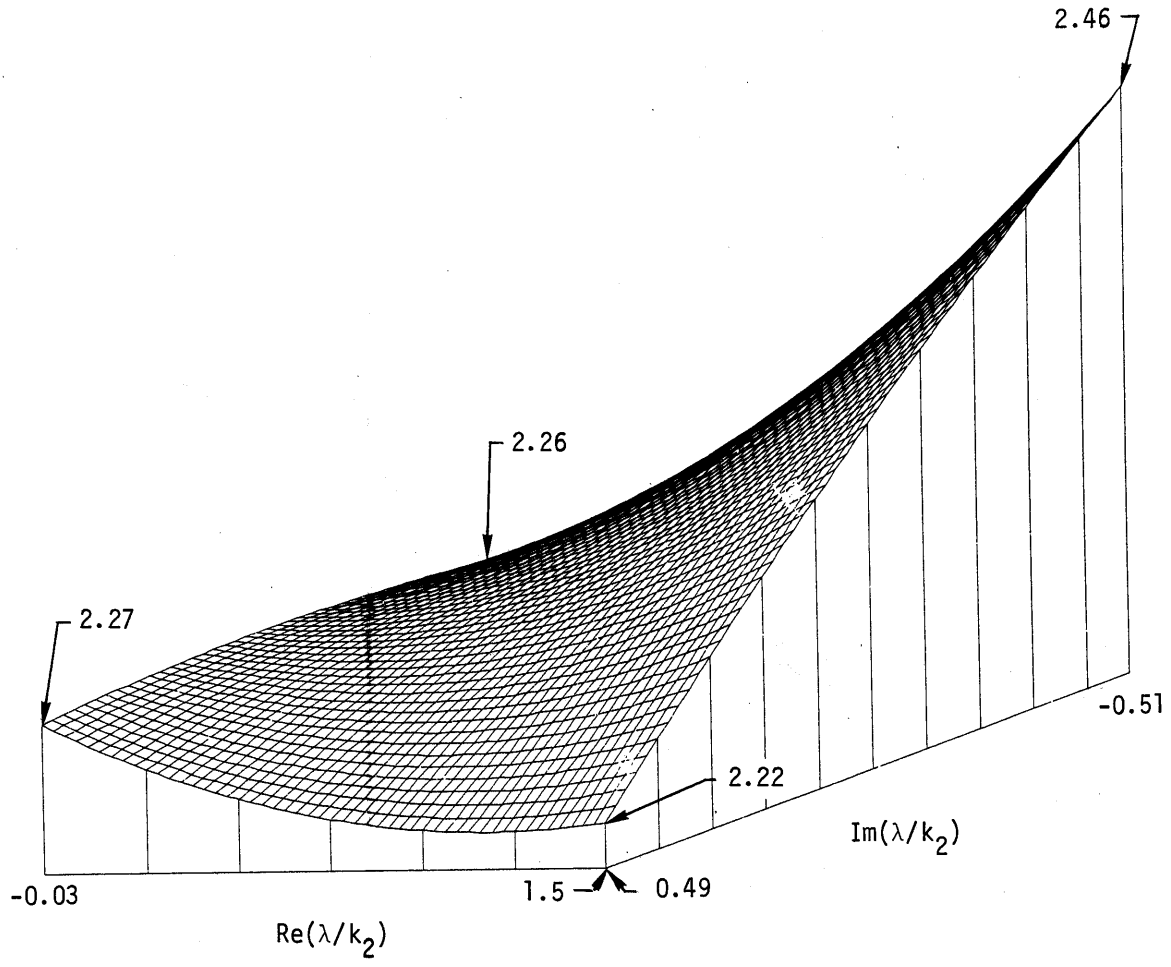

Fig. 18. The Re (γ_1/k_2) is a smooth function for $\epsilon_r = 25$ and $p = 1$.

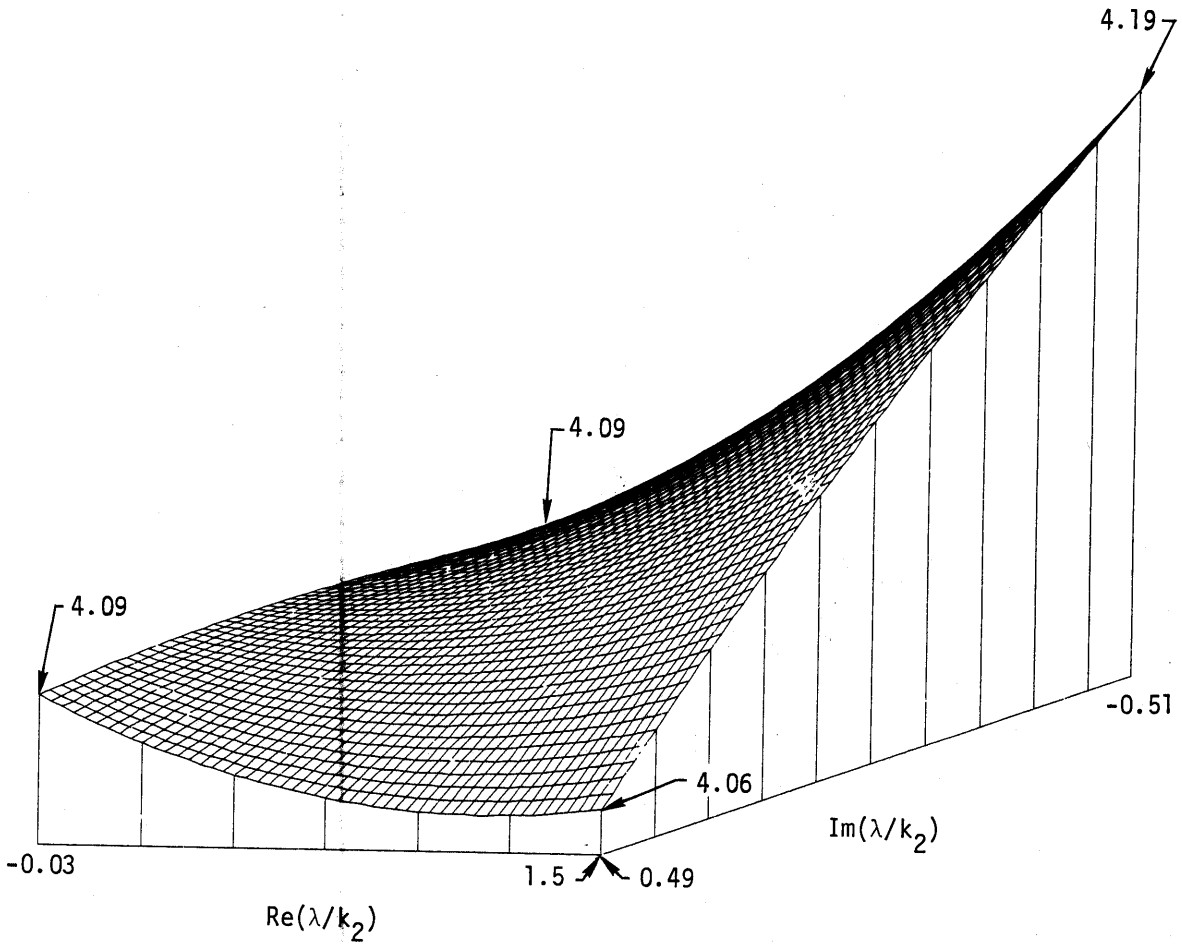

Fig. 19. The Re (γ_1/k_2) is a smooth function for $\epsilon_r = 81$ and $p = 1$.

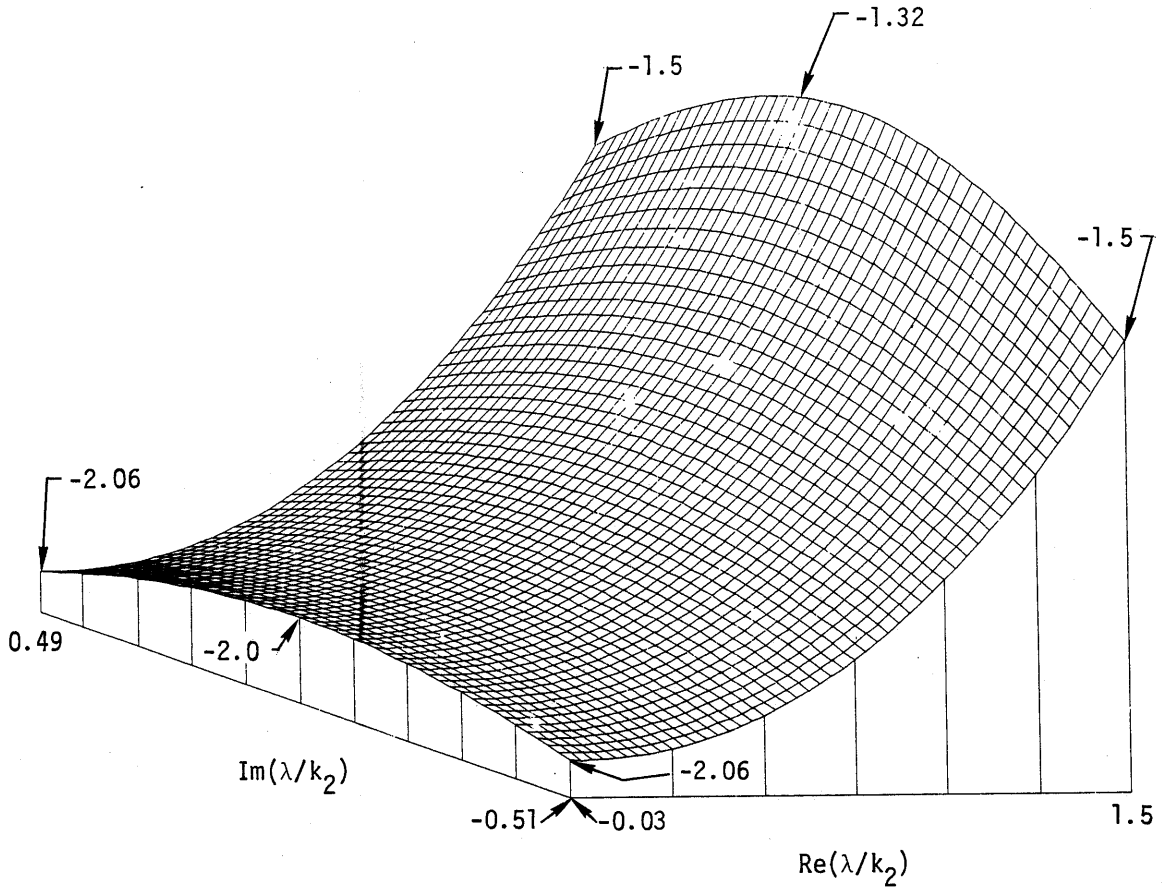

Fig. 20. The Im (γ_1/k_2) is a smooth function for $\epsilon_r = 4$ and $p = 0$.

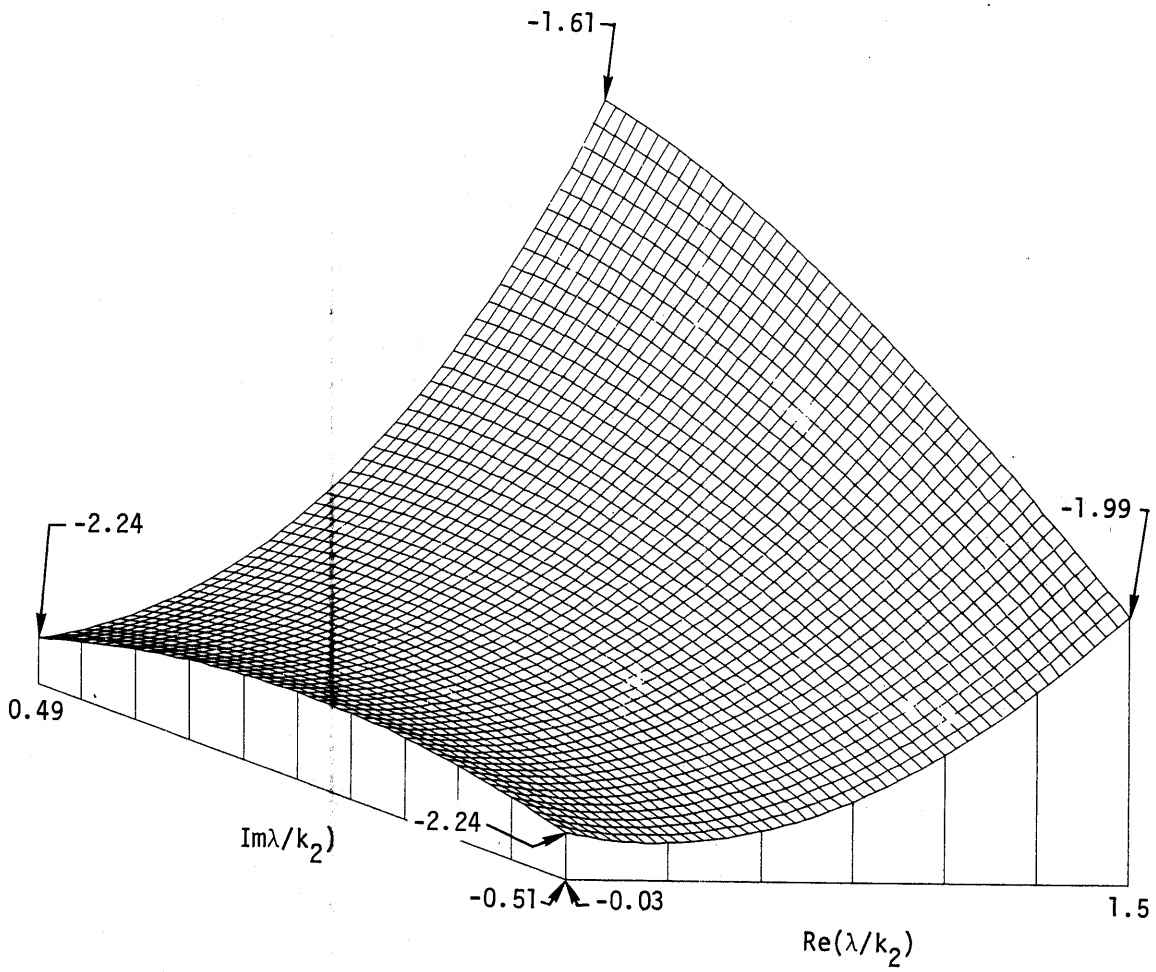

Fig. 21. The Im (γ_1/k_2) is a smooth function for $\epsilon_r = 4$ and $p = 1$.

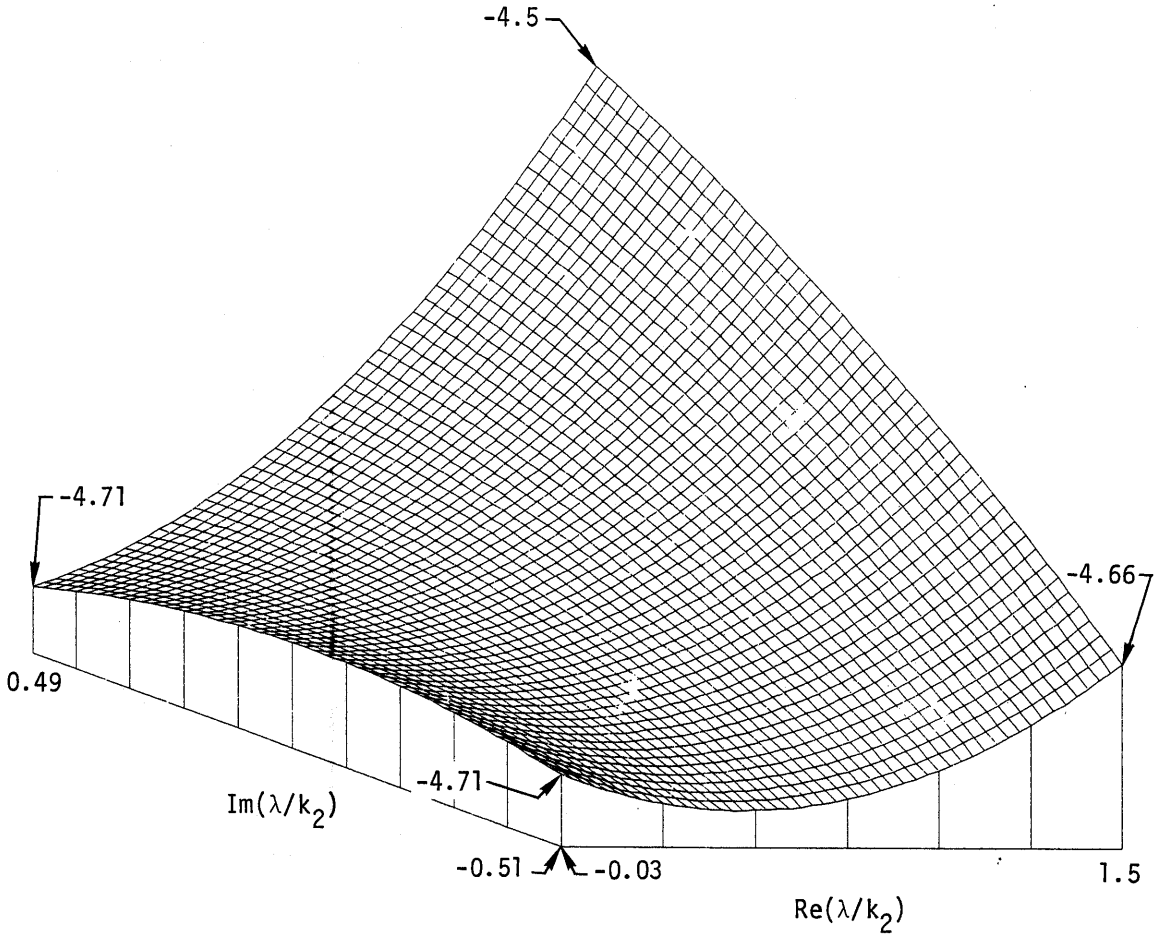

Fig. 22. The Im (γ_1/k_2) is a smooth function for $\epsilon_r = 4$ and $p = 10$.

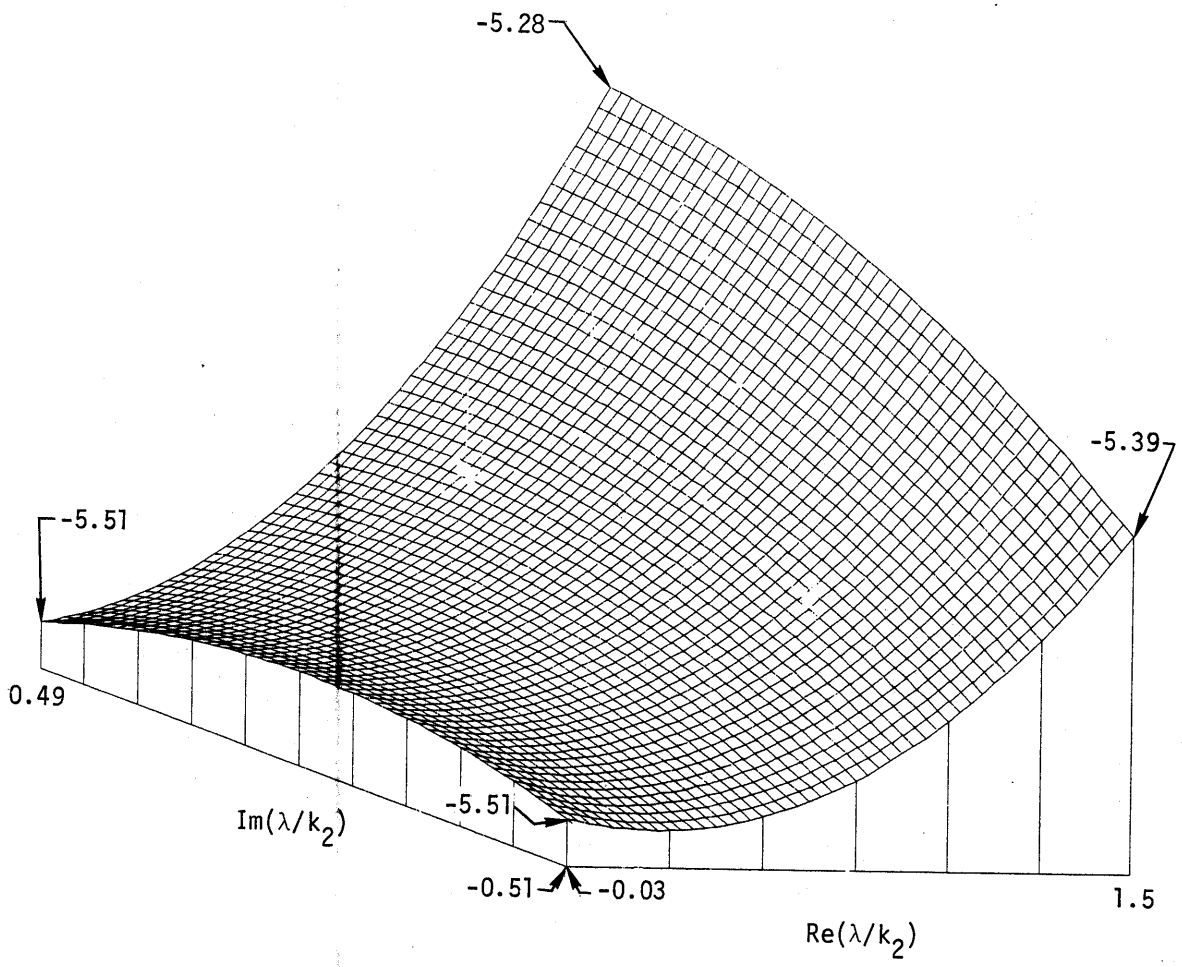

Fig. 23. The Im (γ_1/k_2) is a smooth function for $\epsilon_r = 25$ and $p = 1$.

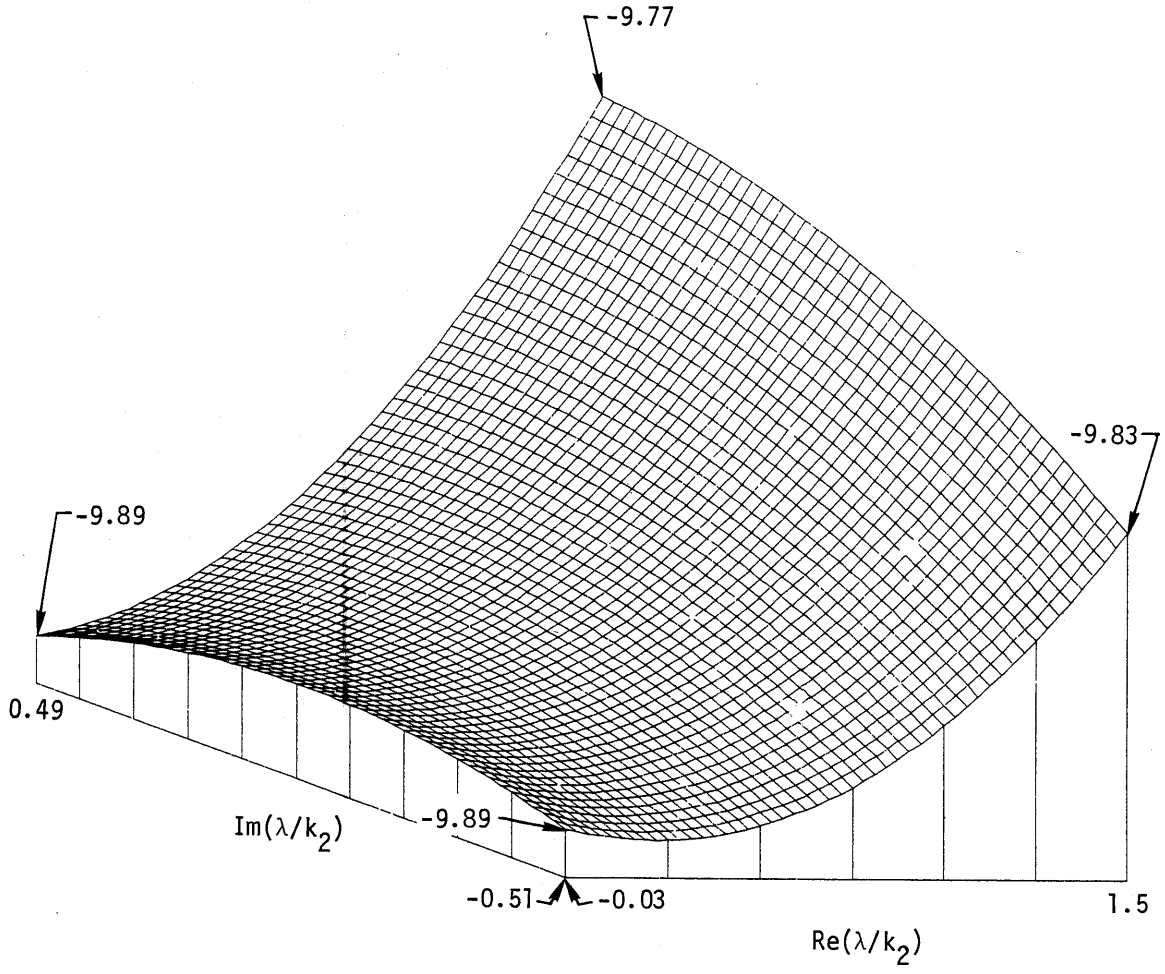

Fig. 24. The Im (γ_1/k_2) is a smooth function for $\epsilon_r = 81$ and $p = 1$.

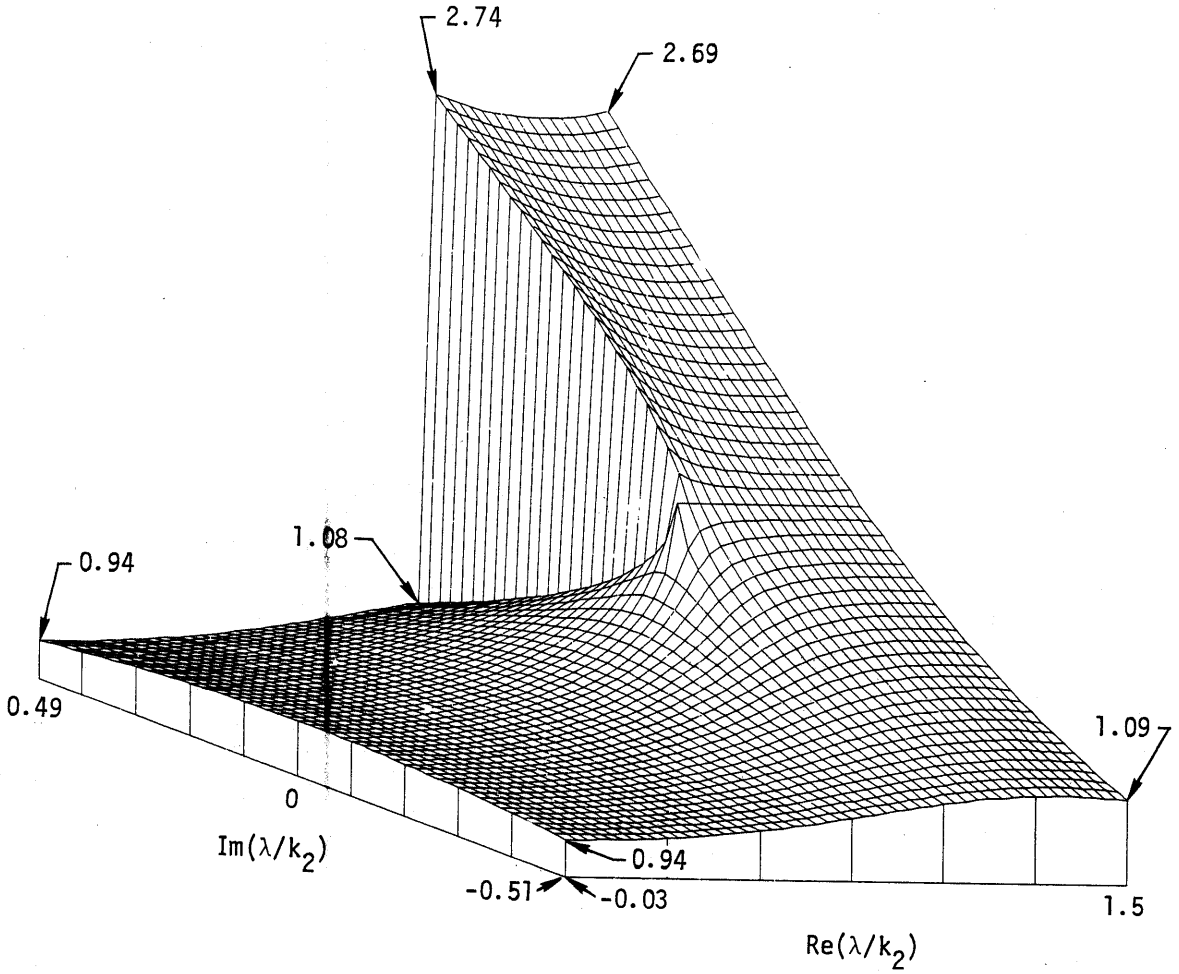

Fig. 25. The magnitude of $1/(\gamma_1 + \gamma_2)$ is well behaved except along the vertical branch cut emanating from $\lambda = k_2$. The case shown is for $\epsilon_r = 4$ and $p = 0$.

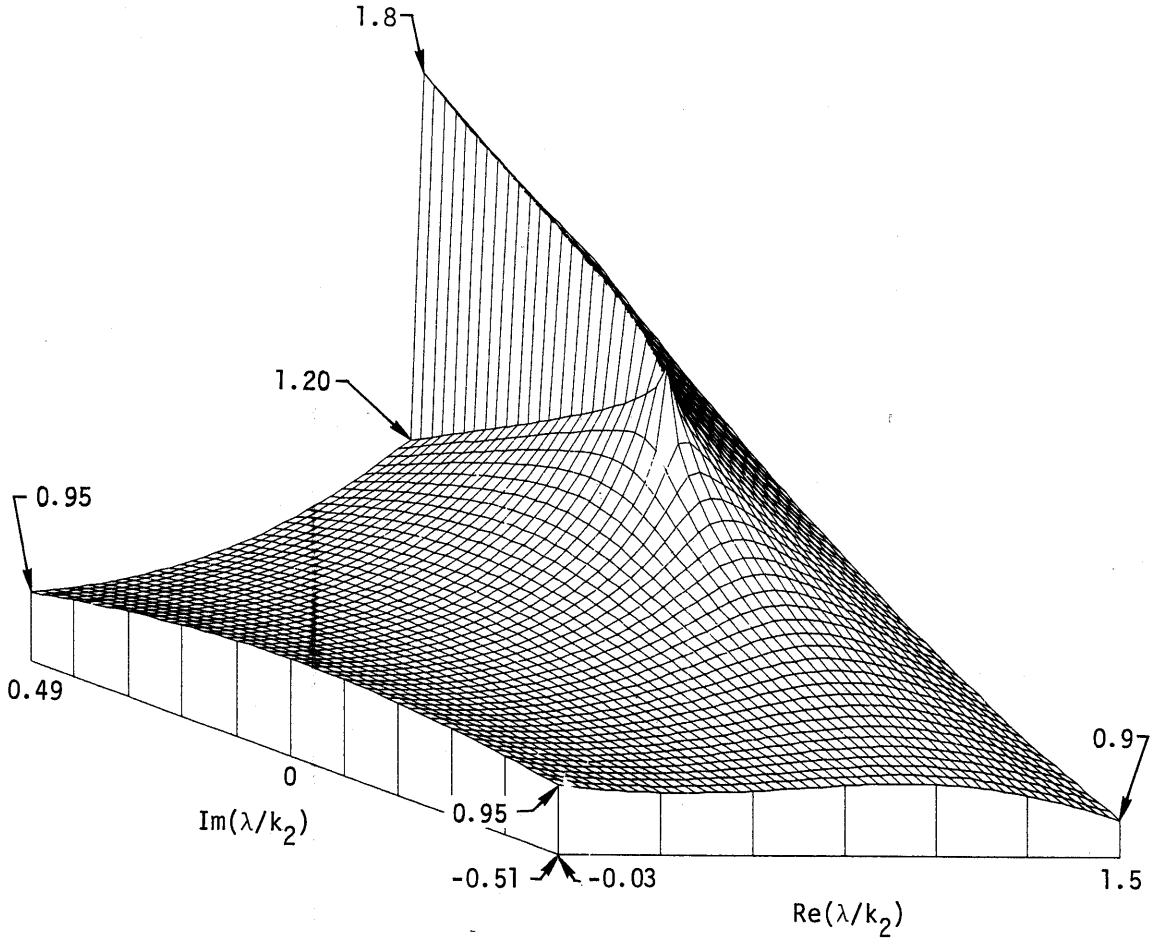

Fig. 26. The magnitude of $1/(\gamma_1 + \gamma_2)$ is well behaved except along the vertical branch cut emanating from $\lambda = k_2$. The case shown is for $\epsilon_r = 4$ and $p = 1$.

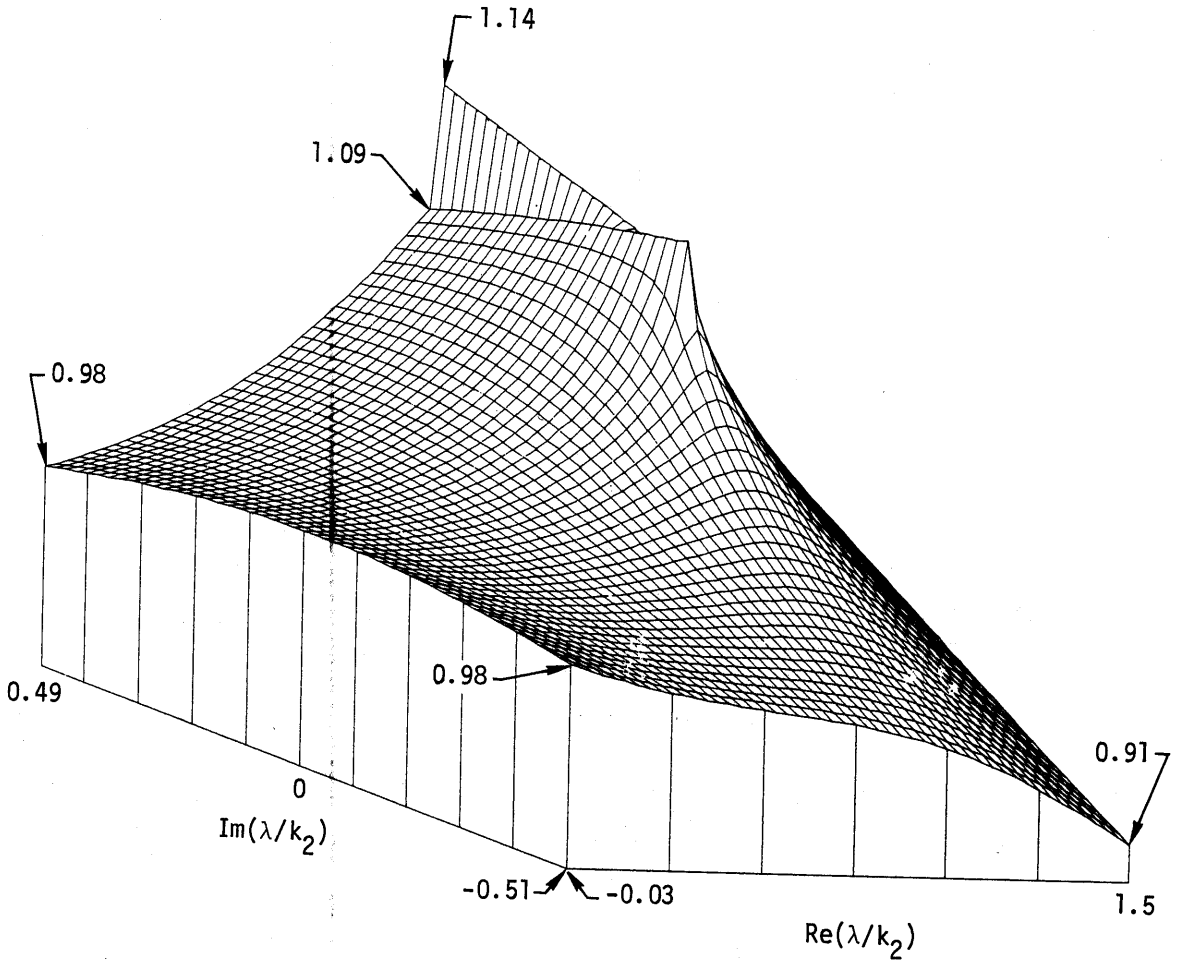

Fig. 27. The magnitude of $1/(\gamma_1 + \gamma_2)$ is well behaved except along the vertical branch cut emanating from $\lambda = k_2$. The case shown is for $\epsilon_r = 4$ and $p = 10$.

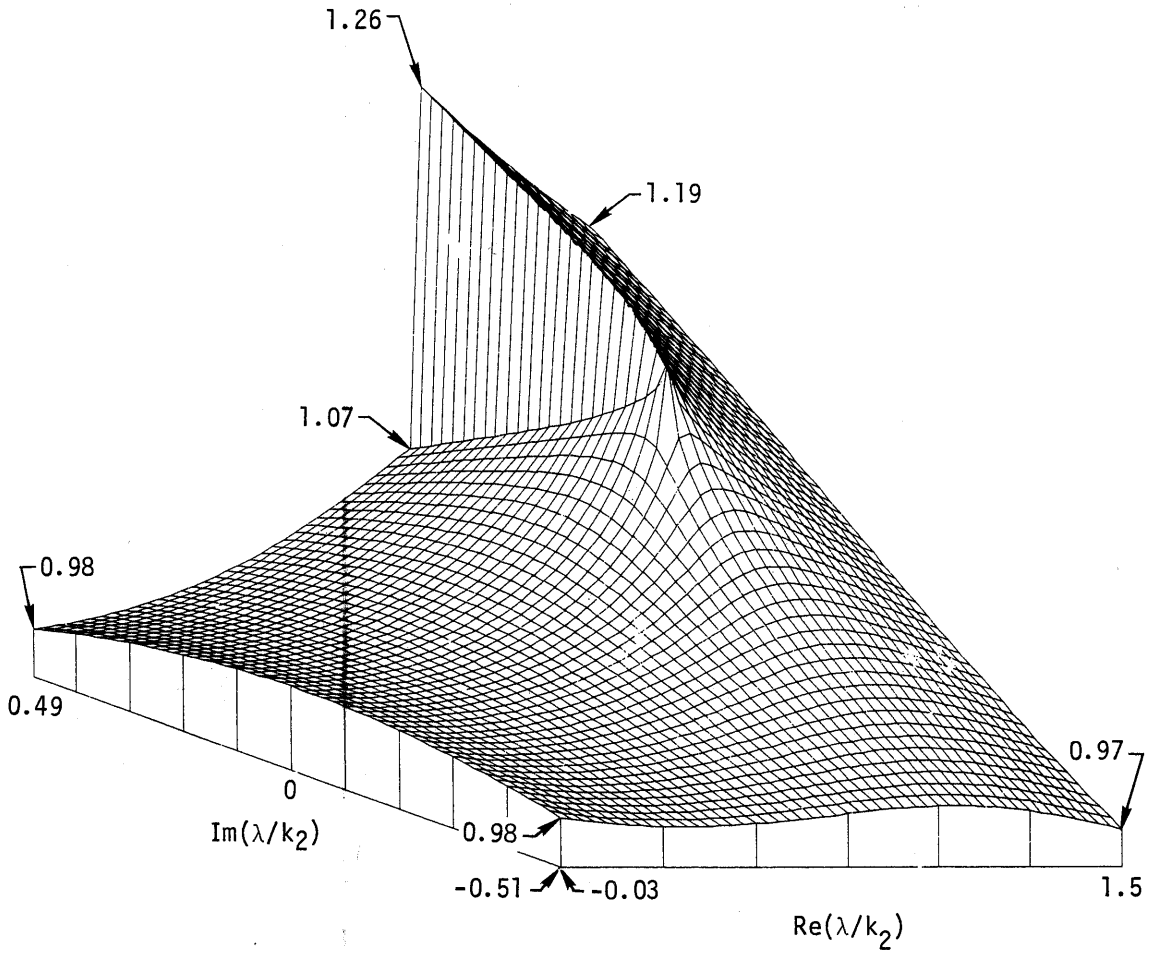

Fig. 28. The magnitude of $1/(\gamma_1 + \gamma_2)$ is well behaved except along the vertical branch cut emanating from $\lambda = k_2$. The case shown is for $\epsilon_r = 25$ and $p = 1$.

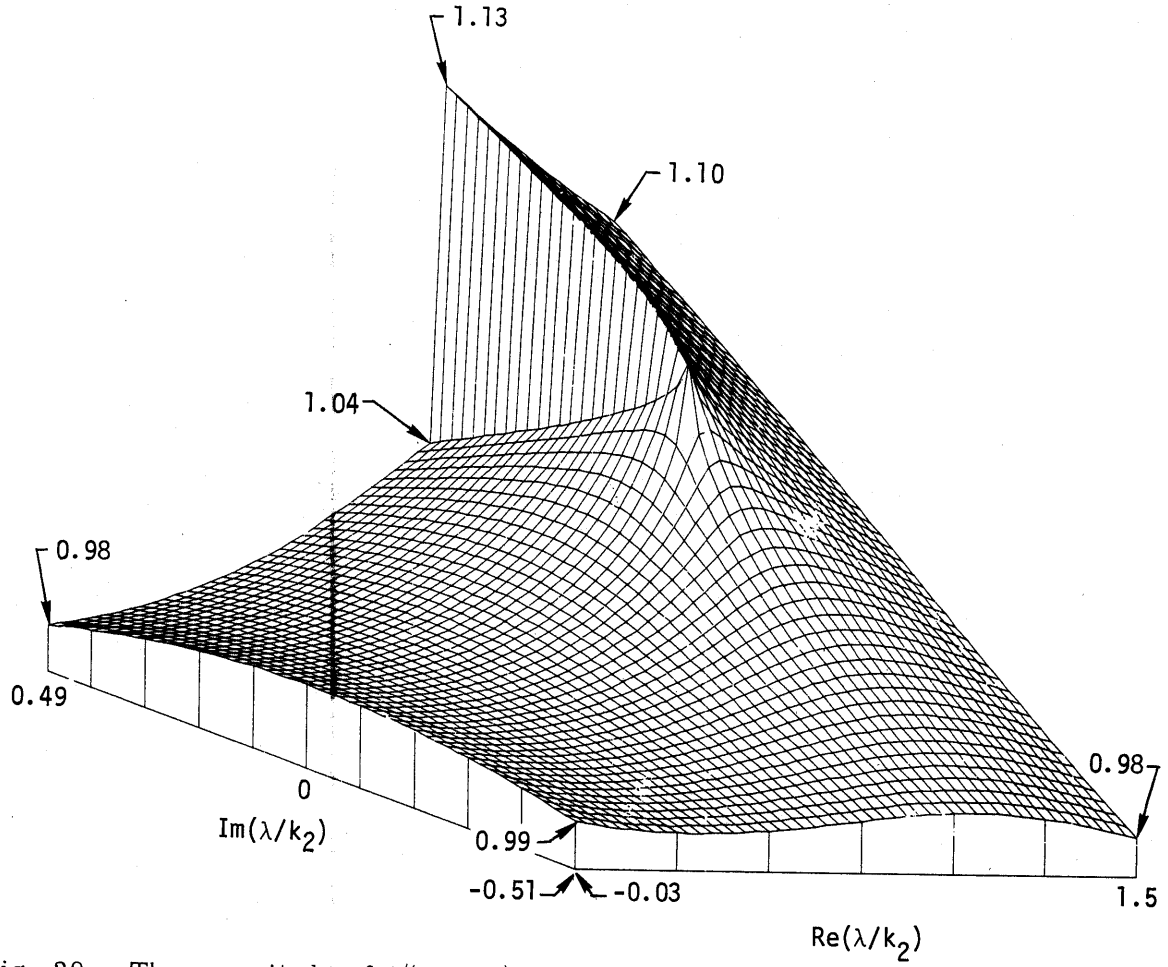

Fig. 29. The magnitude of $1/(\gamma_1 + \gamma_2)$ is well behaved except along the vertical branch cut emanating from $\lambda = k_2$. The case shown is for $\epsilon_r = 81$ and $p = 1$.

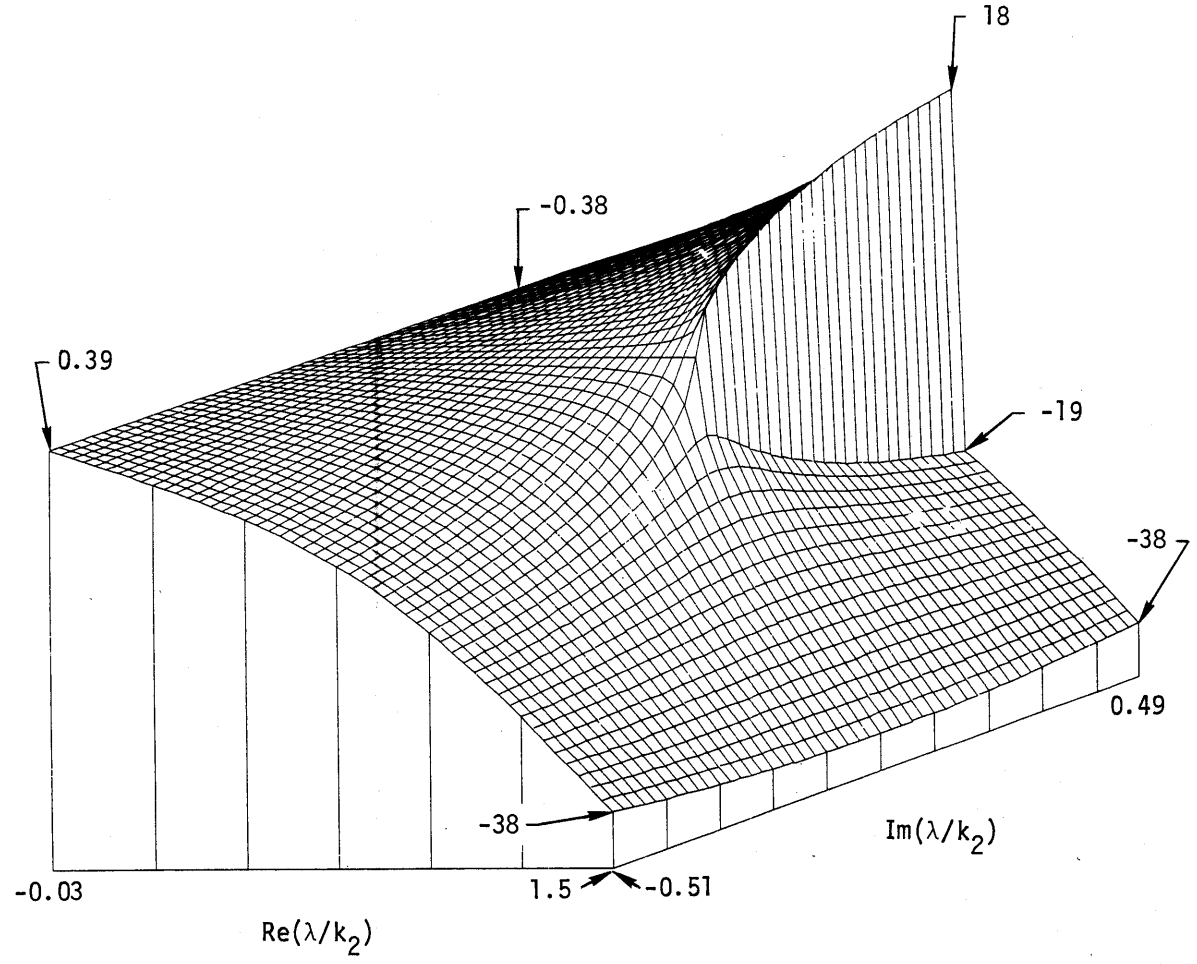

Fig. 30. The phase of $1/(\gamma_1 + \gamma_2)$ is well behaved except along the vertical branch cut emanating from $\lambda = k_2$. The case shown is for $\epsilon_r = 4$ and $p = 0$.

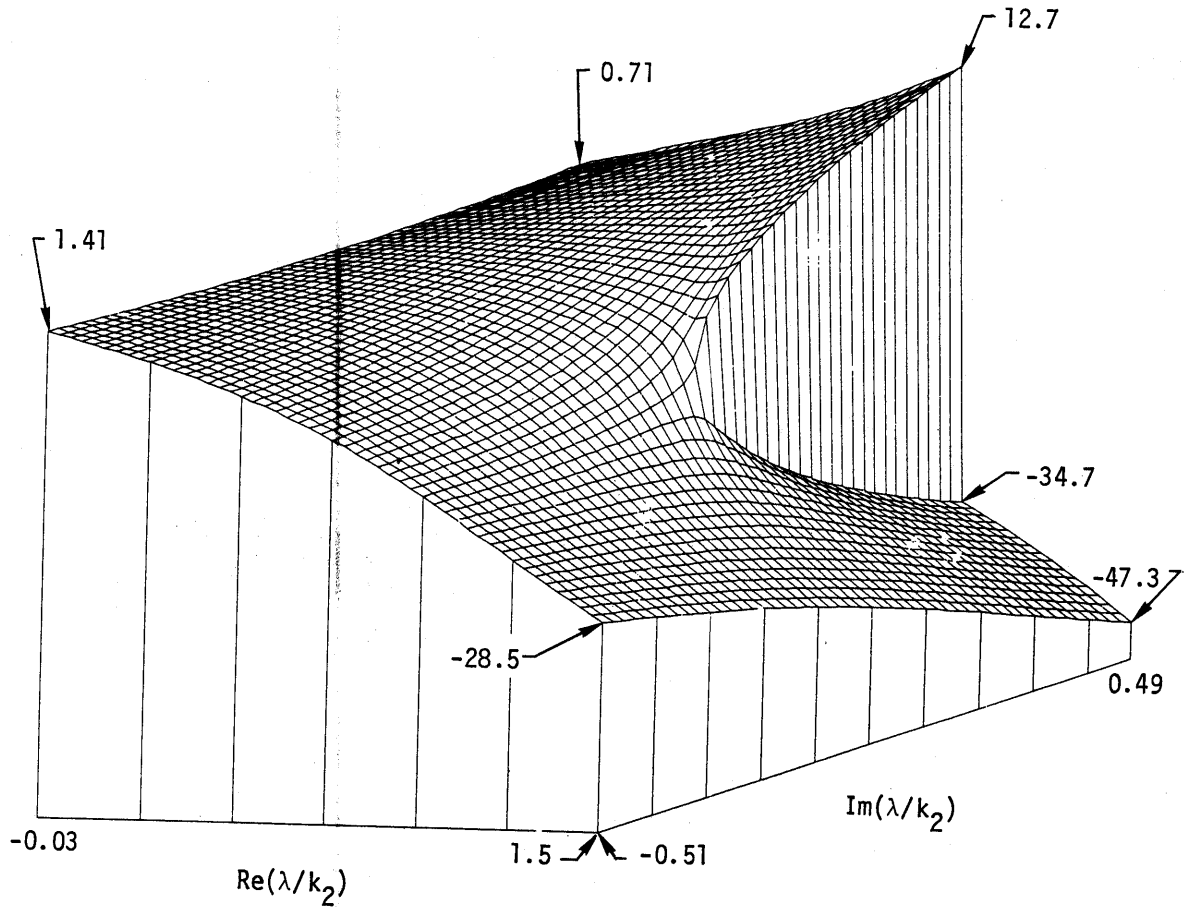

Fig. 31. The phase of $1/(\gamma_1 + \gamma_2)$ is well behaved except along the vertical branch cut emanating from $\lambda = k_2$. The case shown is for $\epsilon_r = 4$ and $p = 1$.

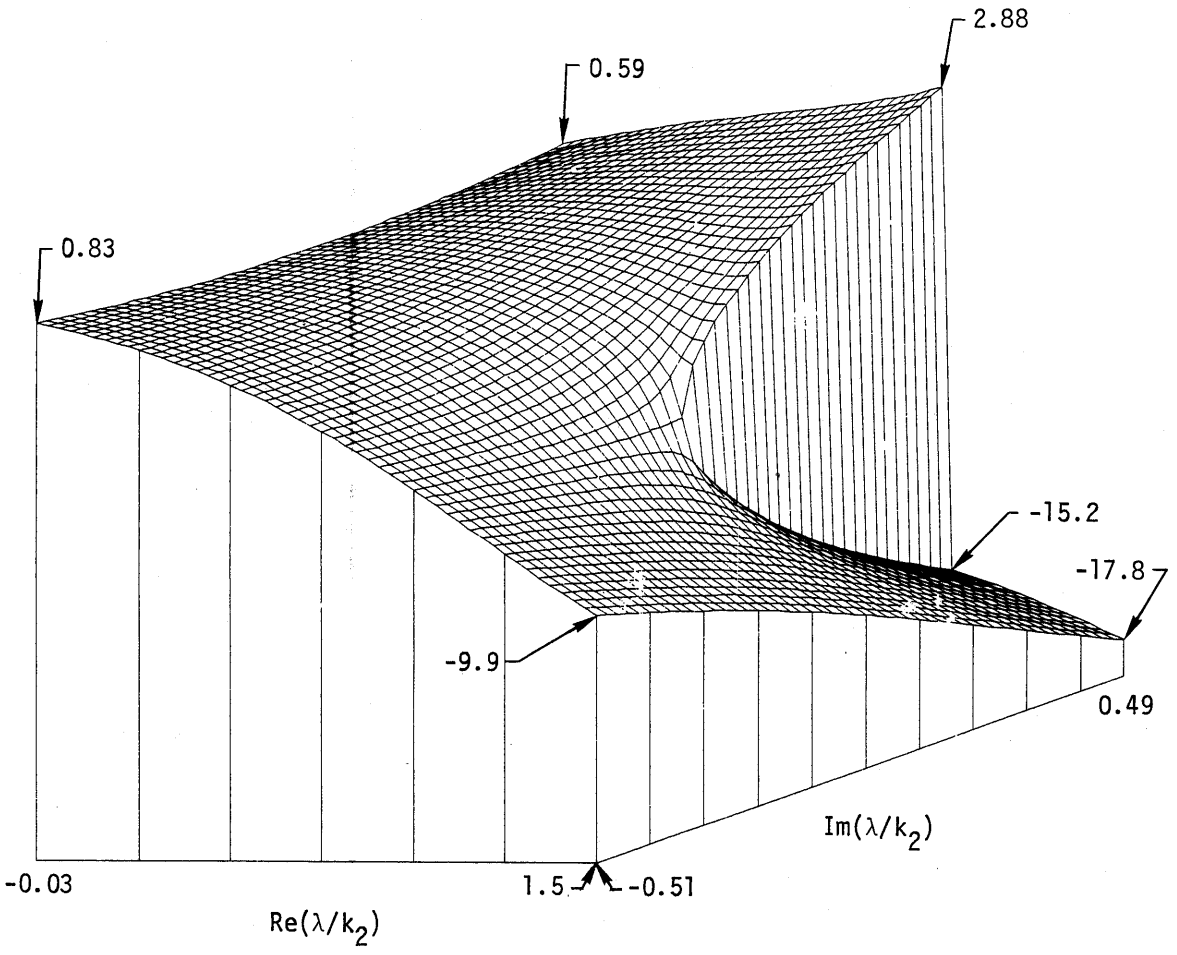

Fig. 32. The phase of $1/(\gamma_1 + \gamma_2)$ is well behaved except along the vertical branch cut emanating from $\lambda = k_2$. The case shown is for $\epsilon_r = 4$ and $p = 10$.

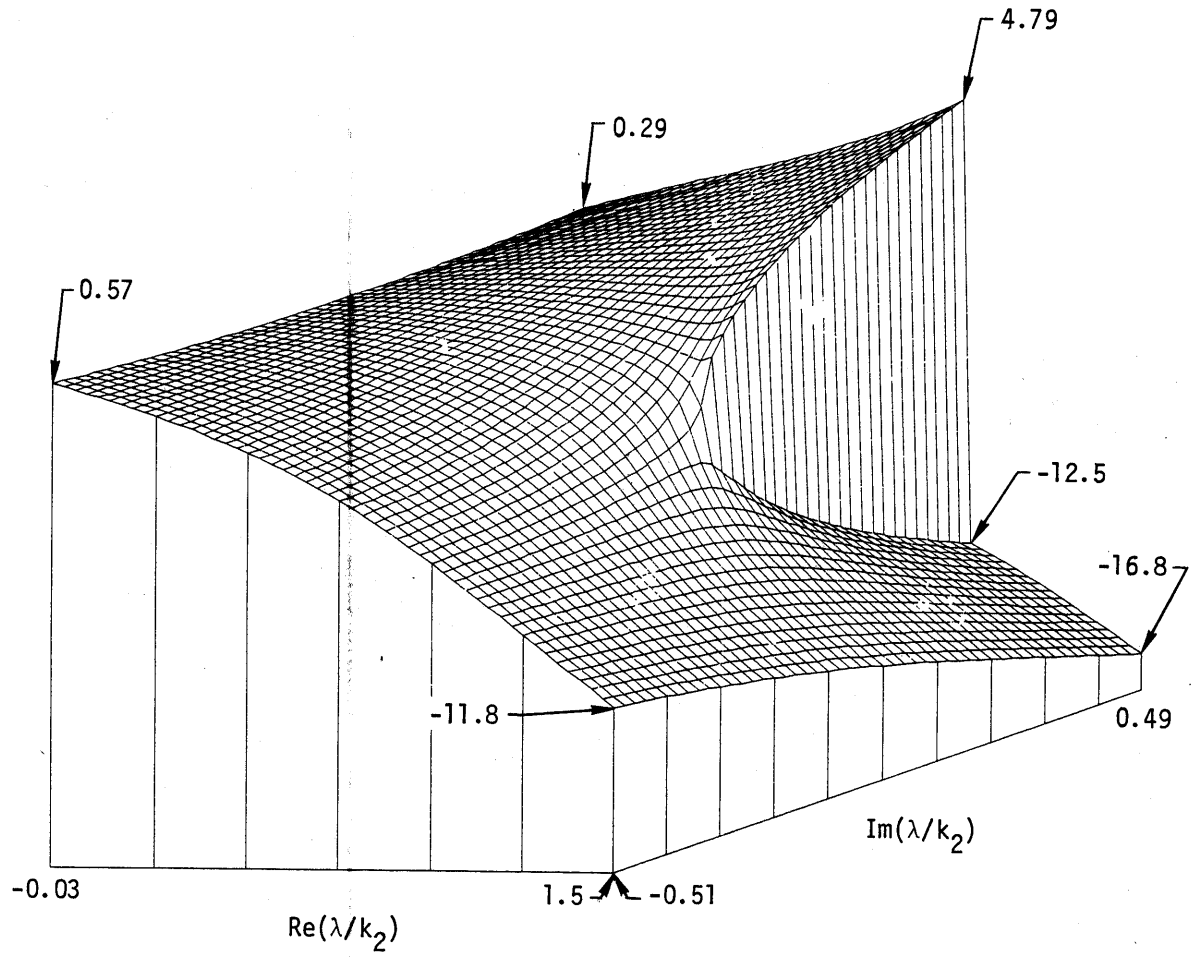

Fig. 33. The phase of $1/(\gamma_1 + \gamma_2)$ is well behaved except along the vertical branch cut emanating from $\lambda = k_2$. The case shown is for $\epsilon_r = 25$ and $p = 1$.

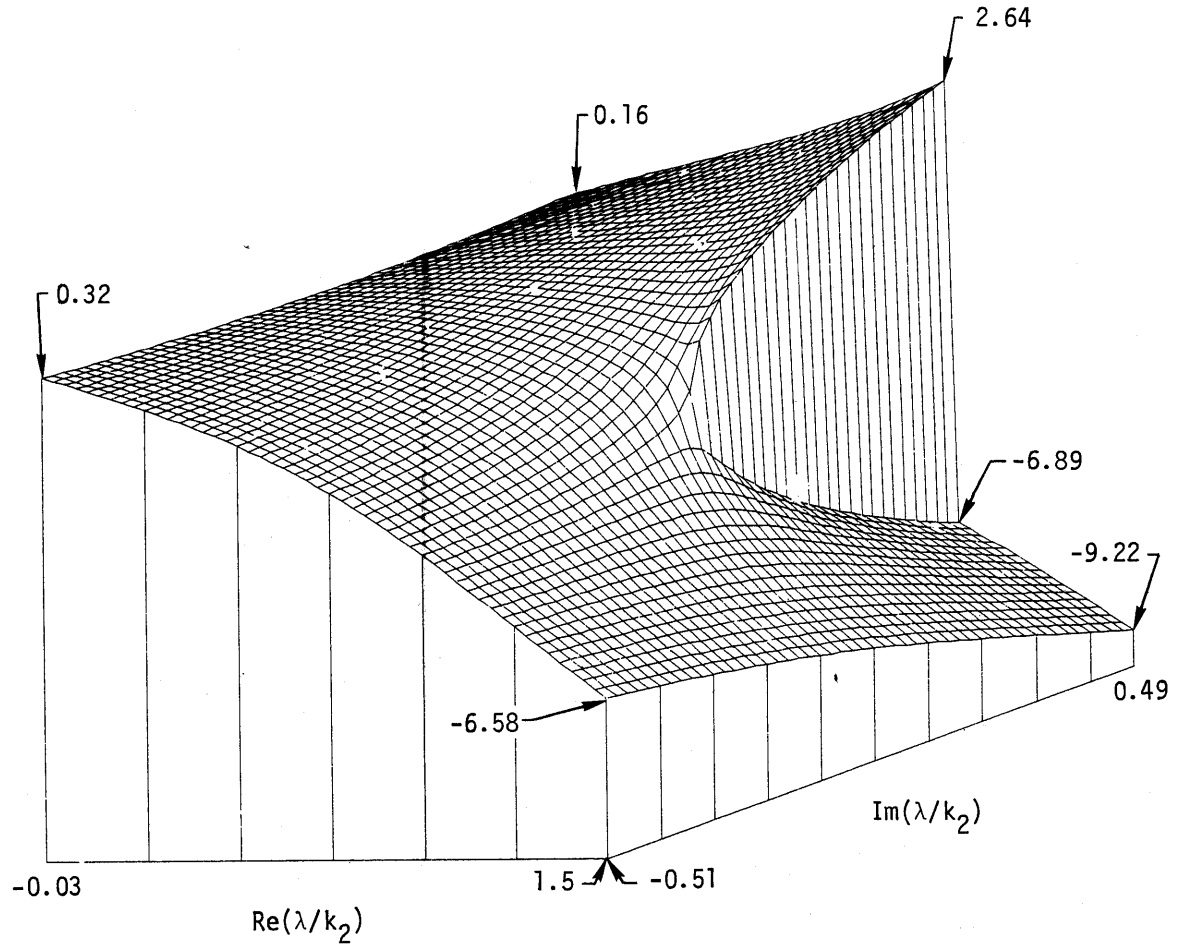

Fig. 34. The phase of $1/(\gamma_1 + \gamma_2)$ is well behaved except along the vertical branch cut emanating from $\lambda = k_2$. The case shown is for $\epsilon_r = 81$ and $p = 1$.

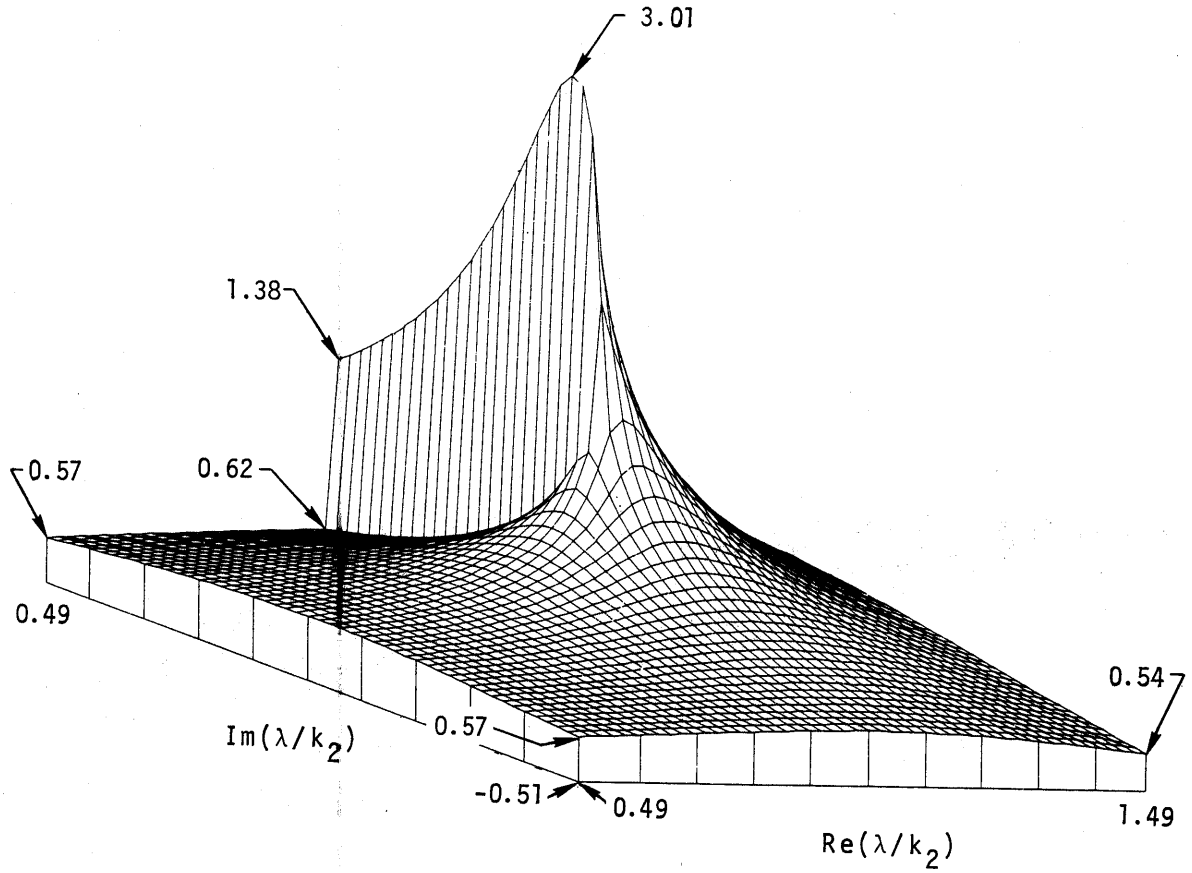

Fig. 35. The magnitude of $1/N(\lambda)$ is peaked along the vertical branch cut. The case shown is for $\epsilon_r = 4$ and $p = 0$.

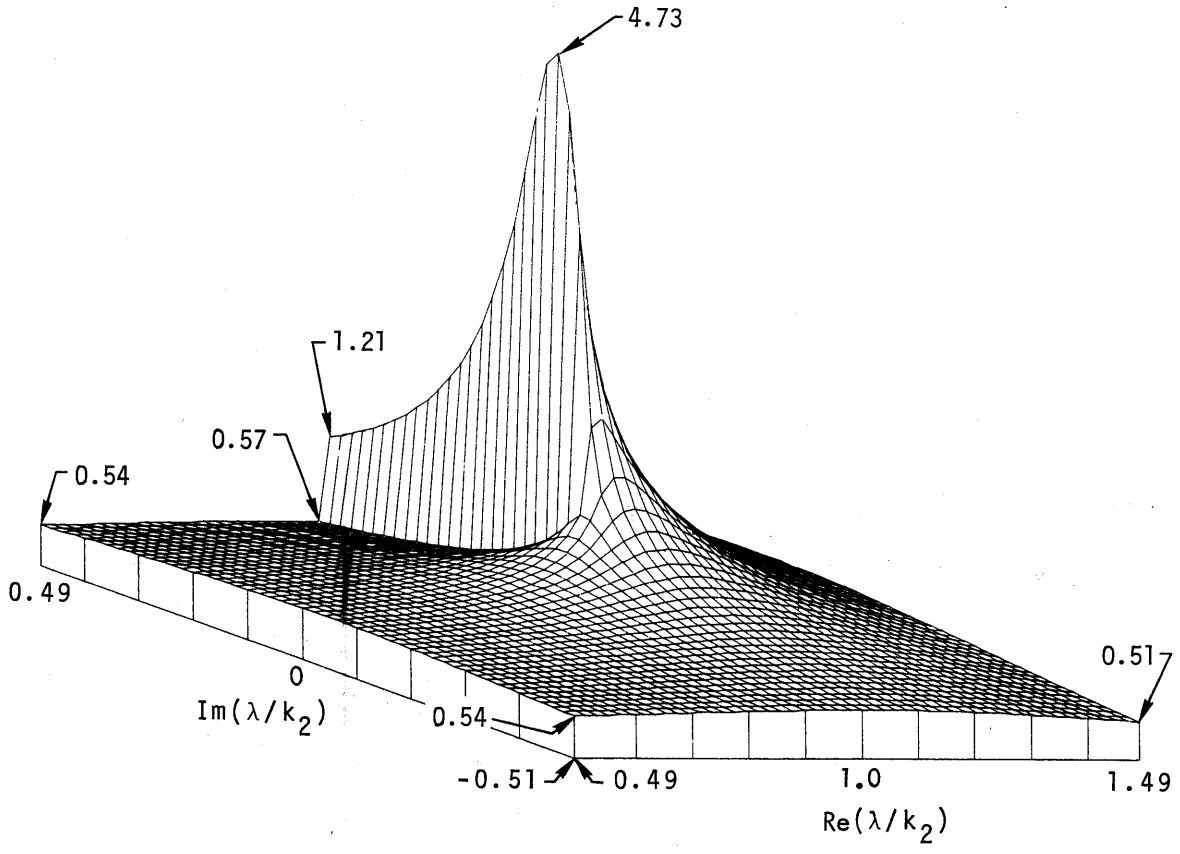

Fig. 36. The magnitude of $1/N(\lambda)$ is peaked along the vertical branch cut. The case shown is for $\epsilon_r = 4$ and $p = 1$.

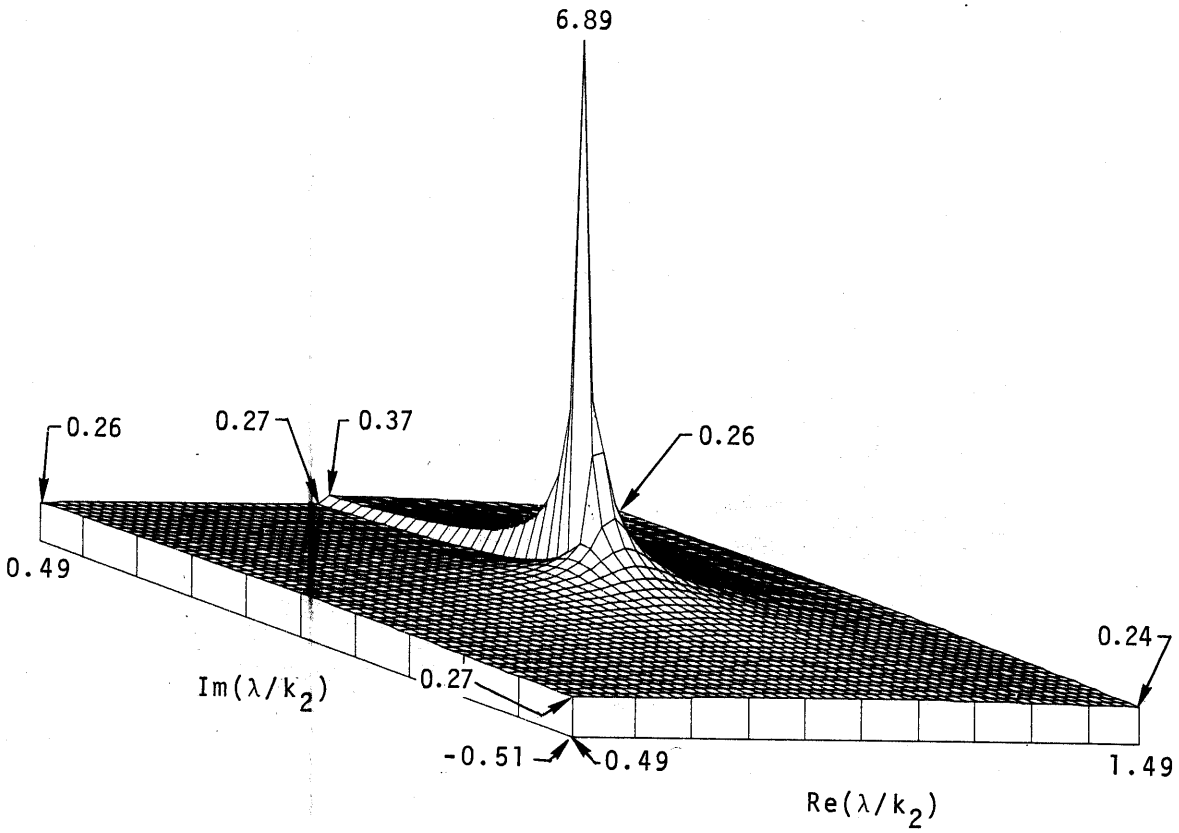

Fig. 37. The magnitude of $1/N(\lambda)$ is peaked along the vertical branch cut. The case shown is for $\epsilon_r = 4$ and $p = 10$.

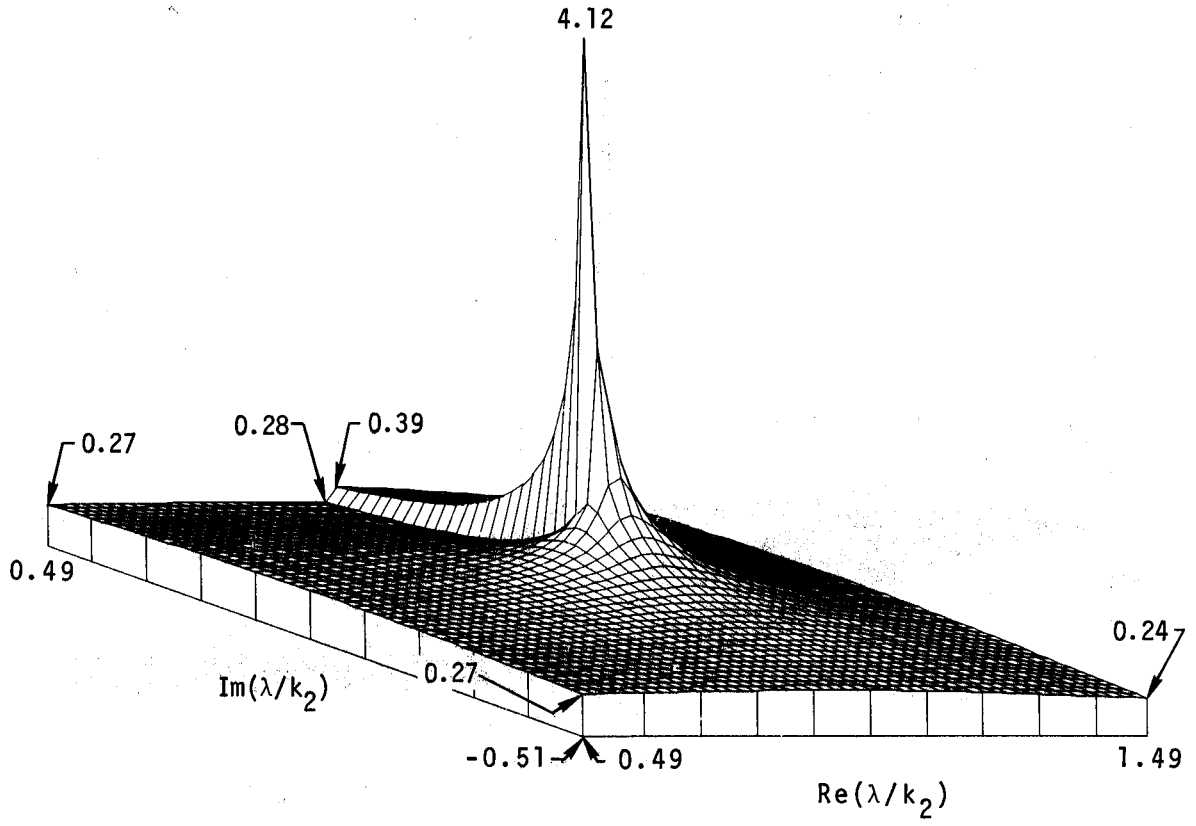

Fig. 38. The magnitude of $1/N(\lambda)$ is peaked along the vertical branch cut. The case shown is for $\epsilon_r = 25$ and $p = 1$.

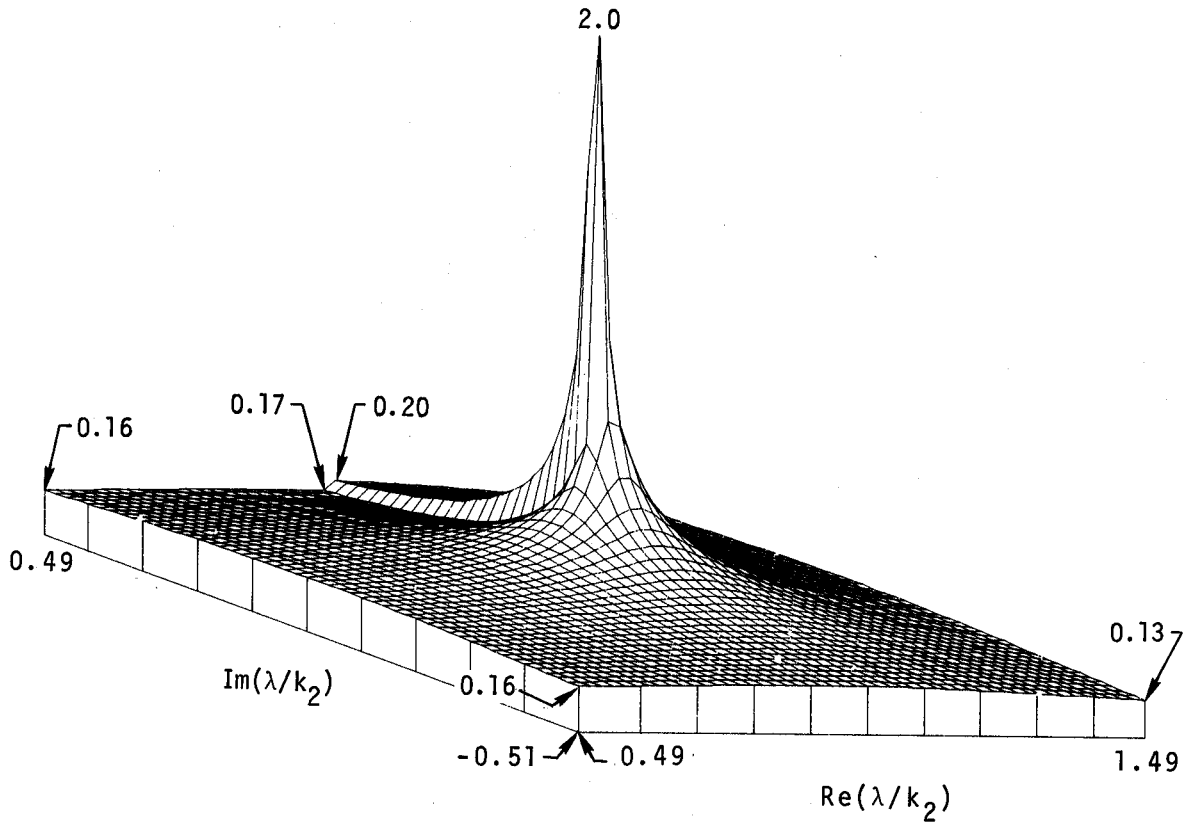

Fig. 39. The magnitude of $1/N(\lambda)$ is peaked along the vertical branch cut. The case shown is for $\epsilon_r = 81$ and $p = 1$.

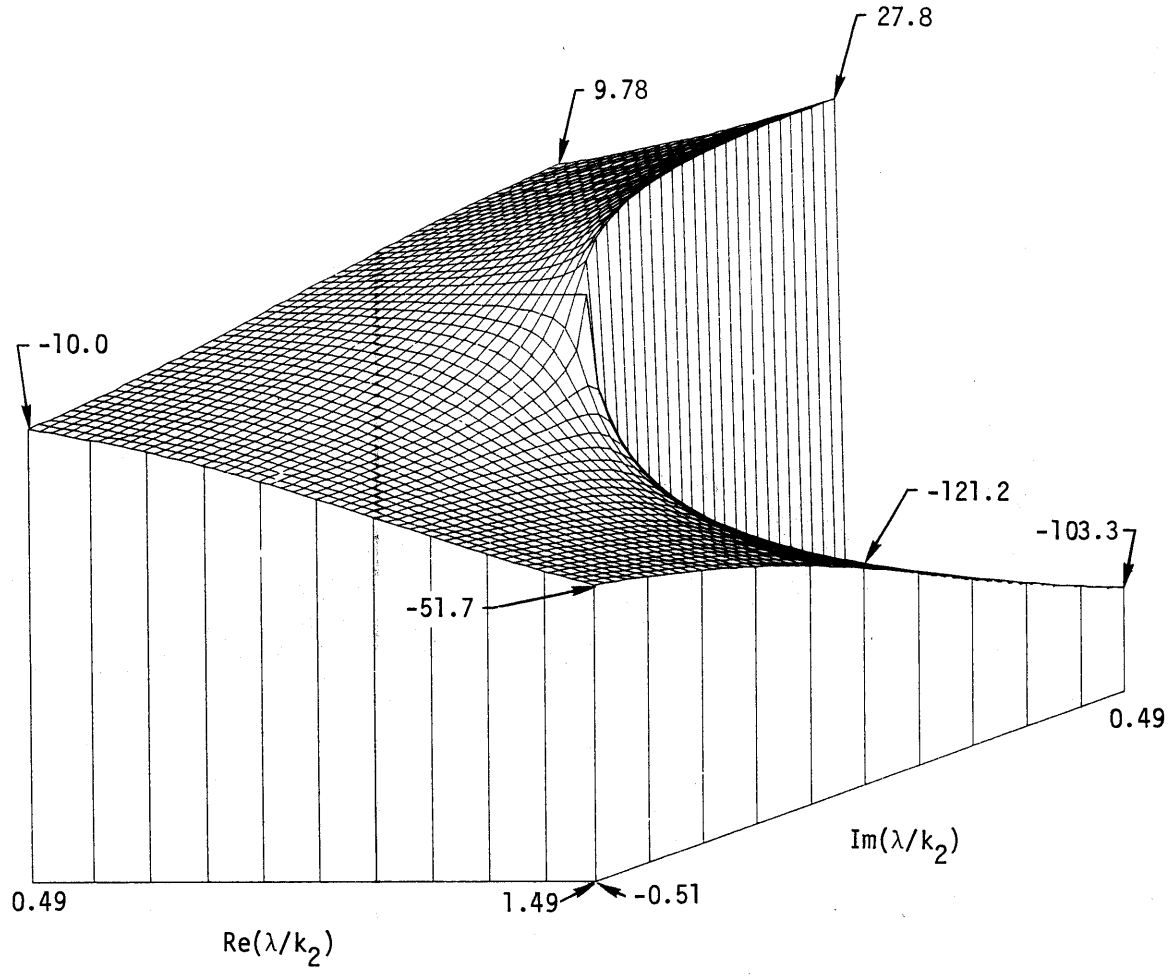

Fig. 40. The phase of $1/N(\lambda)$ is well behaved except along the vertical branch cut emanating from $\lambda = k_2$. The case shown is for $\epsilon_r = 4$ and $p = 0$.

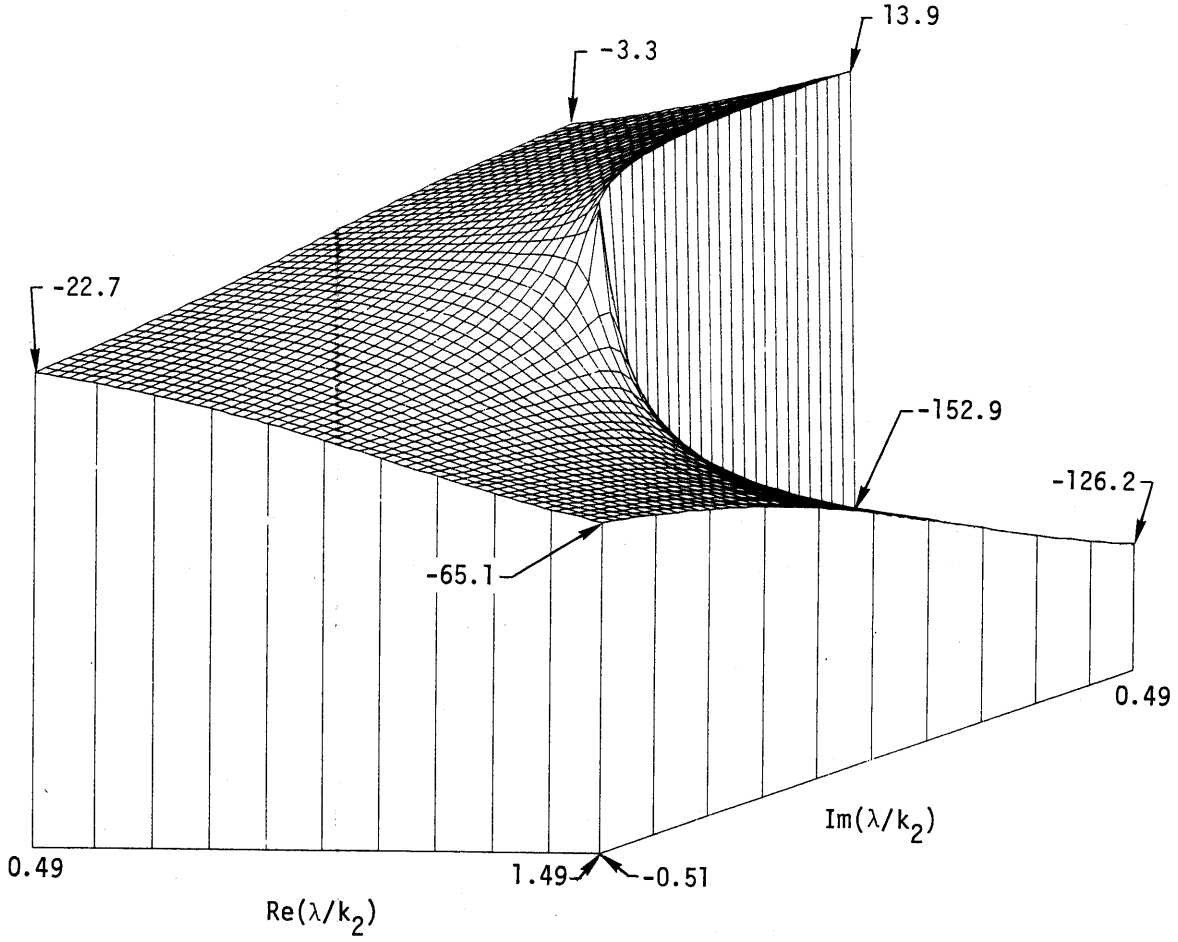

Fig. 41. The phase of $1/N(\lambda)$ is well behaved except along the vertical branch cut emanating from $\lambda = k_2$. The case shown is for $\epsilon_r = 4$ and $p = 1$.

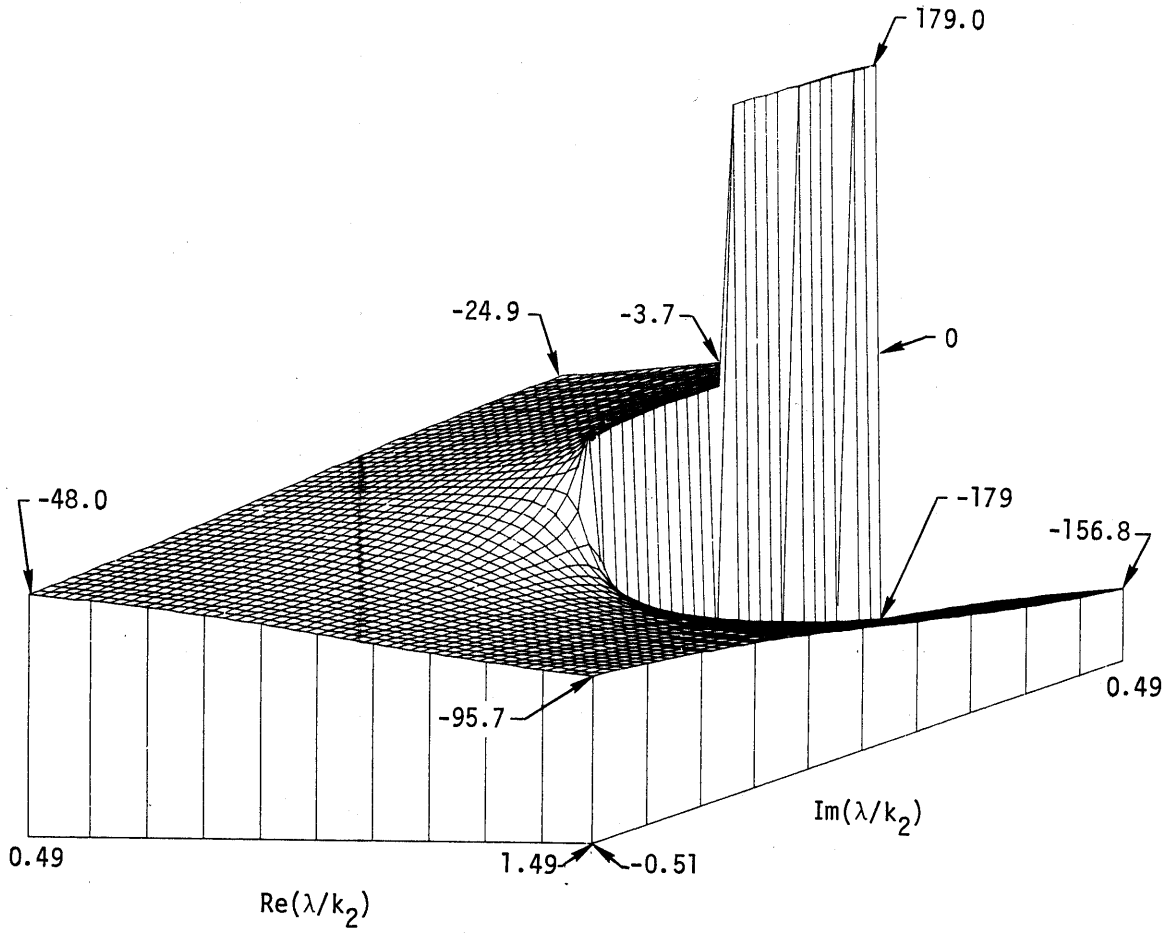

Fig. 42. The phase of $1/N(\lambda)$ is well behaved except along the vertical branch cut emanating from $\lambda = k_2$. The case shown is for $\epsilon_r = 4$ and $p = 10$.

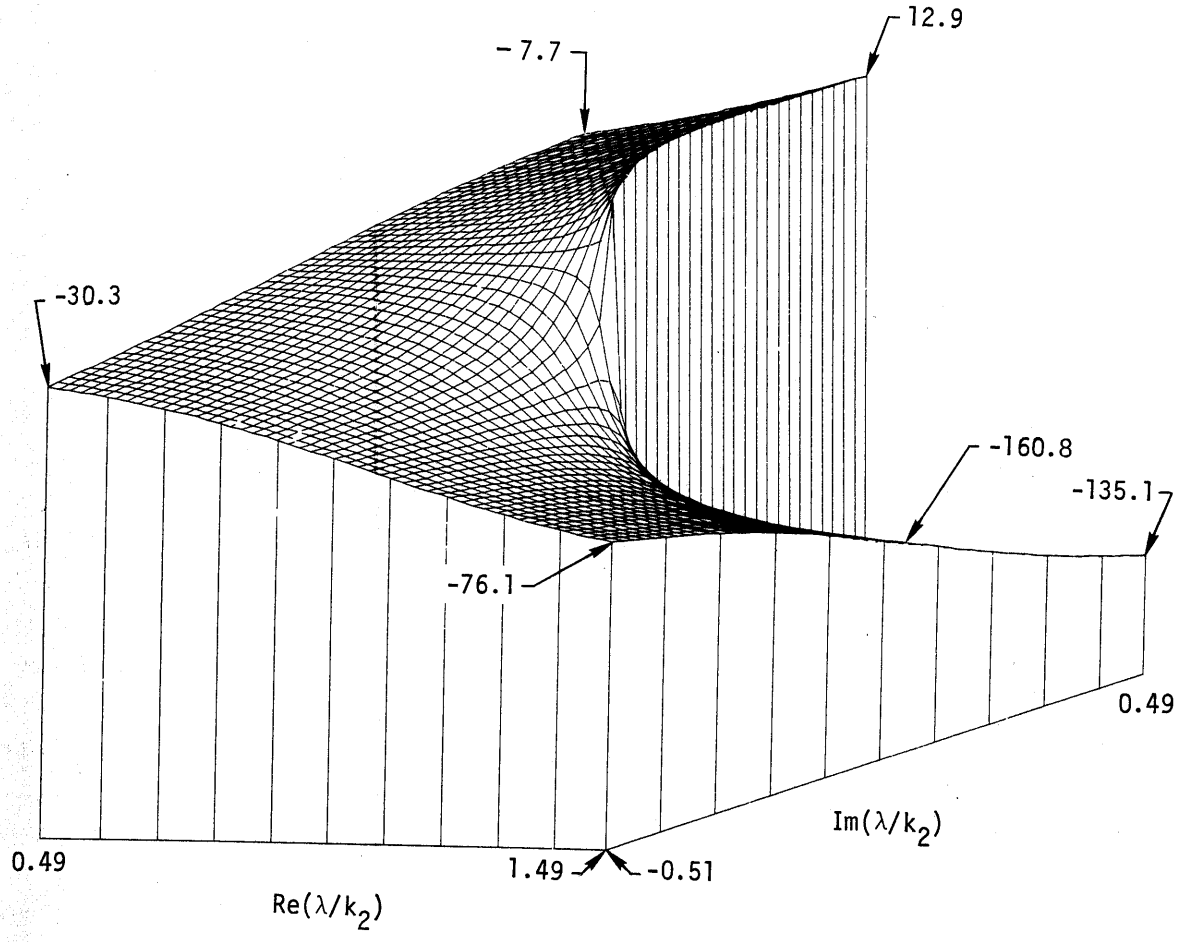

Fig. 43. The phase of $1/N(\lambda)$ is well behaved except along the vertical branch cut emanating from $\lambda = k_2$. The case shown is for $\epsilon_r = 25$ and $p = 1$.

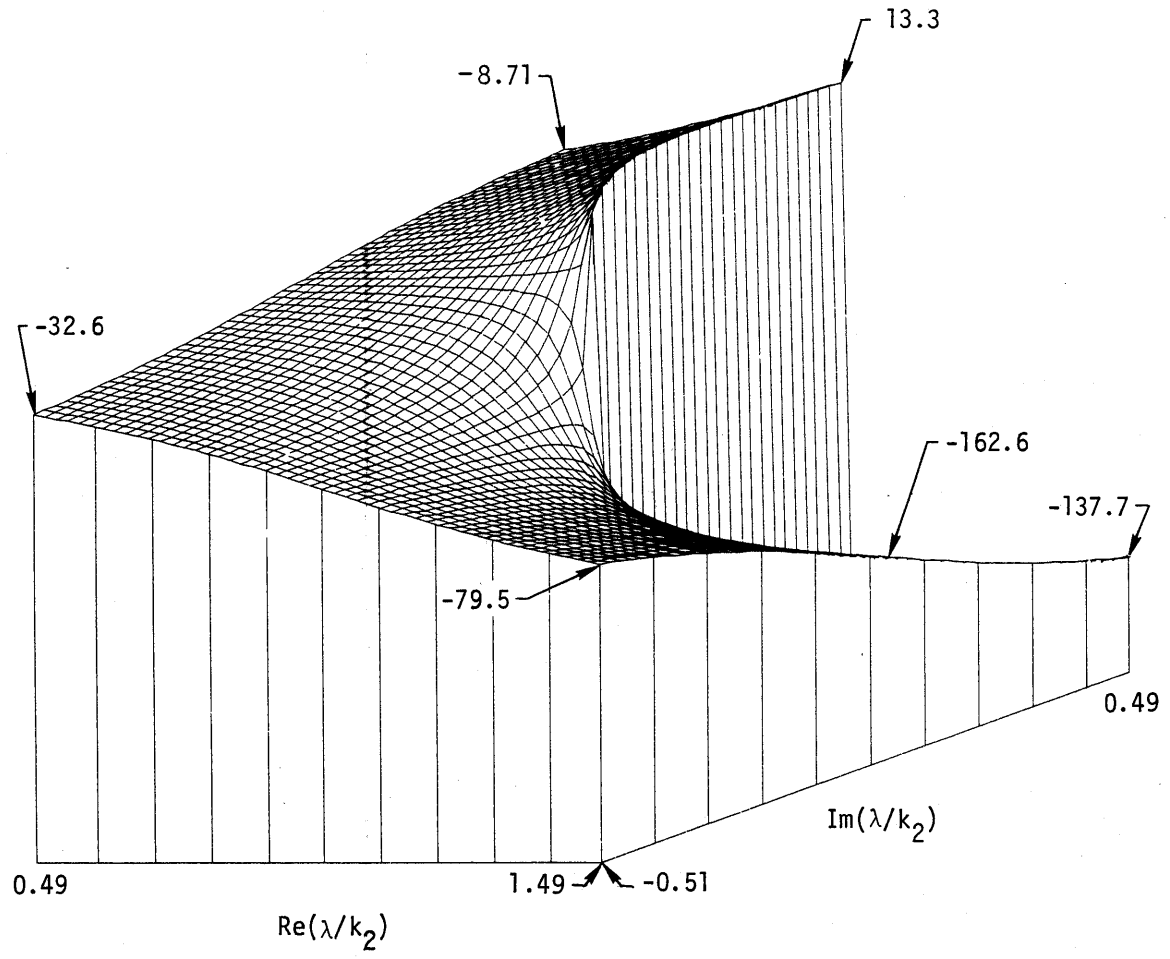

Fig. 44. The phase of $1/N(\lambda)$ is well behaved except along the vertical branch cut emanating from $\lambda = k_2$. The case shown is for $\epsilon_r = 81$ and $p = 1$.

Deformations of the Integration Path

We found it useful to consider not only paths of integration along the real axis for the Bessel and Hankel formations, but also to consider deformations of the paths of integration. These alternative paths have been studied to determine if a more rapid convergence is feasible for a deformed path than for a real axis path.

We considered many paths which we thought might enhance the convergence rate. Although a number of paths were considered, we present only those we found to be particularly helpful.

We first discuss deformation of the paths for the U and V integrals when the formulation is expressed in terms of Bessel functions. The deformations for the Hankel function formulation are elaborated later. The utility of the approach combining approximate analytic results with numerical integration results is discussed later in this report for both the Bessel and Hankel formulations.

BESSEL FUNCTION FORMULATION

The Bessel function representation dictates that the integration path be confined to within a distance about the real axis of the order of $|\lambda_I| \lesssim 2/\rho$. This is because $J_0(\lambda\rho)$ grows exponentially as $|\lambda_I|$ increases. The exponential increase is not dramatic for $|\lambda_I| \lesssim 2/\rho$; however, for λ_I outside this bound, we would likely encounter numerical difficulties.

Because $J_0(\lambda\rho)$ oscillates and does not decay especially rapidly as $\lambda_R\rho \to \infty$, the Bessel function formulation would thus not be numerically effective if a large number of cycles of the Bessel function are needed before convergence is achieved From experience, it is known that a major contribution to the U and V integrals occurs within the region $0 \leq \lambda_R \lesssim k_2$. From the above facts, it can be argued that the Bessel function formulation should not be used if $k_2\rho \gtrsim 10$ because many cycles of the Bessel would need to be calculated before convergence occurs.

We want to modify the integration contour so that the integral converges rapidly. The various components of the U and V integrands influence the convergence rate, and we want to determine the contour in the λ plane which leads to rapid convergence. From the section Integrand Component Behavior, we see that the exponential term (see Figs. 13 to 24) is not dramatically affected by its location within the region $0 \geq \lambda_I - k_2/2$, $0 < \lambda_R \leq 1.5\, k_2$. The exponential term decay would be slightly enhanced for a path closer to $\lambda_I = -k_2/2$ than to $\lambda_I = 0$, but the difference would generally not be dramatic. The exponential term oscillation would be slightly less for a path closer to $\lambda_I = 0$ than for $\lambda_I = -k_2/2$, but again the difference would generally be small. These statements about the exponential dependence upon the path of integration are true for both the $\exp(-\gamma_2 b)$ term and the $\exp(-\gamma_1 a)$ term. There is a dependence of the actual numbers upon the medium parameters (ϵ_r and p). However, in a qualitative sense, the above observations are valid.

The nonexponential/non-Bessel function dependence upon the location of the integration path is also illustrated in the section Integrand Component Behavior. Dropping the explicit λ multiplier, the nonexponential/non-Bessel function dependence of the U and V integrands upon the integration path is respectively contained in the $1/(\gamma_1 + \gamma_2)$ and the $1/N(\lambda)$ terms. These have both previously been illustrated. Regardless of the medium parameters, as λ_I is increasingly negative, the functional behavior of the terms $1/(\gamma_1 + \gamma_2)$ and $1/N(\lambda)$ becomes smoother. Thus, a deformation of the integration path to a larger negative λ_I is preferred to enhance convergence.

A few remarks regarding the calculation time of the various integrand components is also pertinent to this discussion. The calculation time for computing the exponential terms and nonexponential/non-Bessel terms is relatively independent of location of λ_R and λ_I. However, the calculation time for the Bessel functions is less for real arguments than it is for complex arguments. Thus, with no other considerations involved, an integration contour along the real axis is preferred (see Fig. 45). However, the behavior of the $1/(\gamma_1 + \gamma_2)$ and $1/N(\lambda)$ terms on the real axis is severe enough so that a

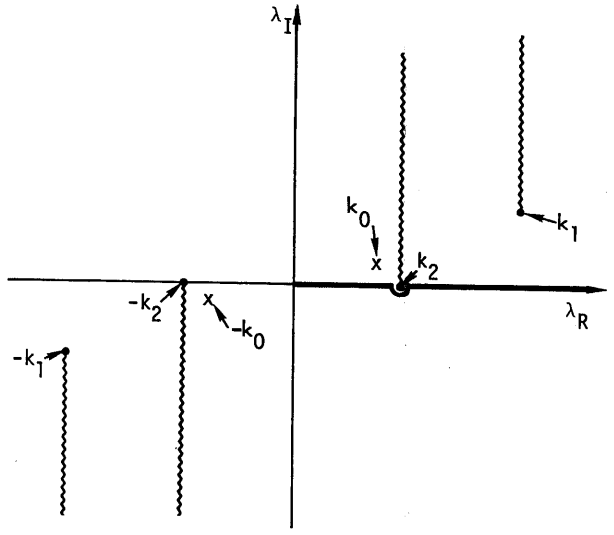

Fig. 45. The original path of integration is along the positive real λ axis.

numerical integration in the near vicinity of $\lambda = k_2$ will encounter convergence difficulties. The numerical difficulties can be overcome either from an approximate analytic integration (see the Approximate Real Axis Integration section) or by deforming the contour to avoid the spiky behavior near $\lambda = k_2$. The approximate real axis integration result generally requires evaluation of special functions. There is no fundamental difficulty in using this approach. Nevertheless, an alternate approach which is useful is to deform the contour near $\lambda = k_2$. The contour which has been found effective for this formulation is shown in Fig. 46. For the Bessel function routines available to us, the contour shown in Fig. 46 has been found to be generally more efficient than the real axis numerical integration only, or the real axis numerical integration done in conjunction with the approximate analytic contribution result near $\lambda = k_2$.

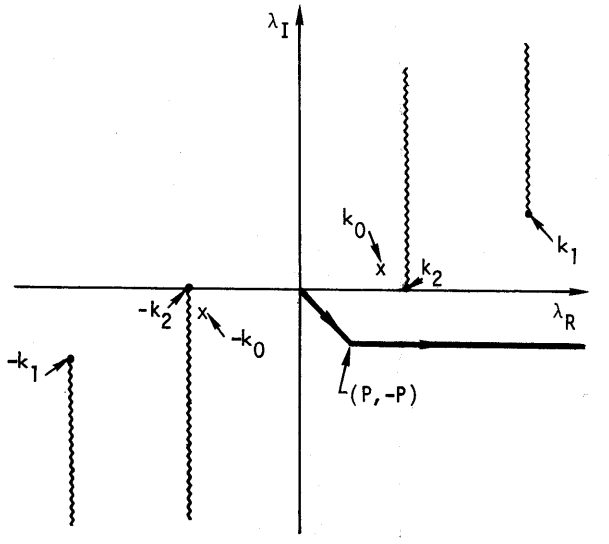

Fig. 46. One of the possible deformations is a "down-and-out" path. Note: P = minimum of $\left(\frac{1}{\rho} \text{ or } \frac{1}{|z| + h}\right)$.

HANKEL FUNCTION FORMULATION

The asymptotic behavior of the Hankel function is $H_0^{(1)}(\lambda\rho) \xrightarrow[\lambda\rho \to \infty]{} [2/(i\pi\lambda\rho)]^{1/2} \exp(i\lambda\rho)$. The asymptotic behavior of the exponential factor is $\exp(-\gamma_1 a - \gamma_2 b) \xrightarrow[\lambda \to \infty]{} \exp[-|\lambda|(a + b)]$. This asymptotic behavior of the exponential holds except in the region Re $\gamma < 0$, a region which will be avoided. The combination of the Hankel and exponential factors thus has an asymptotic behavior of

$$H_0^{(1)}(\lambda\rho) \exp(-\gamma_1 a - \gamma_2 b) \xrightarrow[\lambda\rho \to \infty]{} \left(\frac{2}{i\pi\lambda\rho}\right)^{1/2} \exp[i\lambda\rho - |\lambda|(a + b)].$$

It is judicious to align the path of integration so that it minimizes the numerical computations. For large λ, two choices are worthy of study. One path is chosen so that it maximizes the exponential decay as λ is increased, and another path that may be chosen is one that minimizes the oscillatory behavior.

For large λ, the path maximizing the decay rate is described by

$$\lambda_I = \frac{\rho}{a+b} |\lambda_R| + \text{constant},$$

and the path minimizing the oscillatory behavior is described by

$$\lambda_I = \frac{a+b}{\rho} |\lambda_R| + \text{constant}.$$

For a large disparity between ρ and $a+b$, the least oscillation and most rapid decay contours are almost perpendicular to each other, with the most rapid decay path being almost vertical, and the least oscillation path being almost horizontal.

We have found from a number of numerical model results that it is better to maximize the decay rate than to minimize the oscillatory behavior. Thus, for large λ, the path described by the former equation is used in the Hankel function integration.

"Good" choices for the constant in the maximum decay rate equation have been found to be

$$\text{constant} = \text{Im}(k_1) - \frac{\rho}{a+b} \text{Re}(k_1)$$

for the right-hand asymptotic path, and for the left-hand asymptotic path

$$\text{constant} = \frac{k_2}{2}.$$

The preceding discussion pertains to the large argument Hankel formulation contour. The Hankel formulation contour also has to be specified for smaller λ. This choice was based on the behavior of the Hankel function and of the $1/(\gamma_1 + \gamma_2)$ and $1/N(\lambda)$ terms. As discussed in the Bessel function formulation section, the influence of the exponential terms is not significant in the range of λ such that $0 \leq \text{Re}\,\lambda \leq 1.5\lambda$ and $|\lambda_I| \leq k_2/2$.

The Hankel function is well-behaved except in the near vicinity of the origin. Thus, it is desirable either to avoid the origin or to analytically integrate about the origin so that stringent numerical integration requirements are not encountered. Both approaches have been tried and the most effective procedure has been to choose a contour which avoids the origin.

The behavior of the $1/(\gamma_1 + \gamma_2)$ and $1/N(\lambda)$ terms is depicted in the section on Integrand Component Behavior and is reasonably well behaved for $\lambda_R \lesssim k_2/2$. For $\lambda_R \gtrsim 1.3\, k_2$, these functions are also reasonably well-behaved. However, for $-0.2\, k_2 \lesssim \lambda_I \leq k_2$ and $0.75\, k_2 \lesssim \lambda_R \lesssim 1.3\, k_2$, these functions can vary over a wide range. Hence, if feasible, a numerical integration over a contour in this region should be avoided.

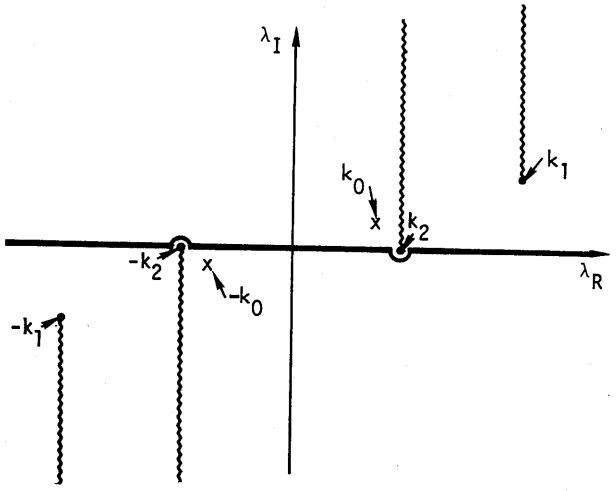

Fig. 47. The original path of integration for the Hankel function formulation is along the real λ axis.

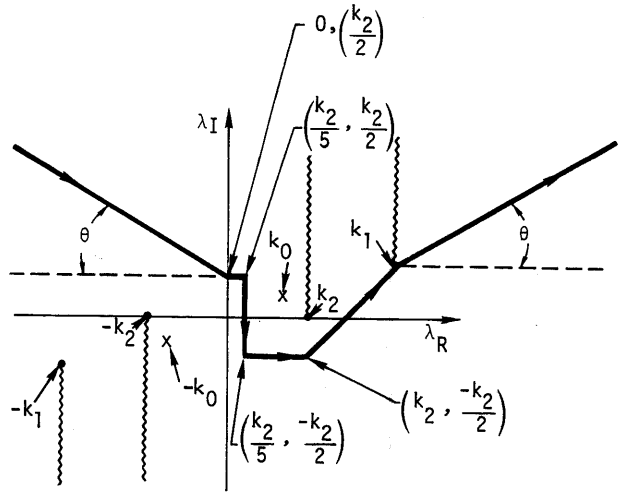

Fig. 48. A useful deformation of the contour used in the Hankel function formulation is the multisegmented path shown $\left[\theta = \tan^{-1}\left(\frac{\rho}{|z| + h}\right)\right]$.

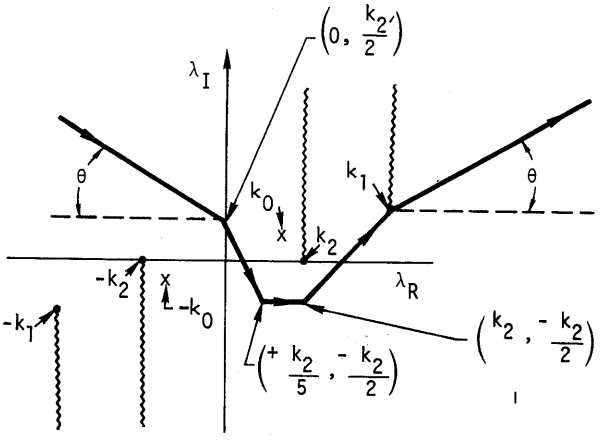

Fig. 49. Another useful deformation of the contour used in the Hankel function formulation is the multisegmented path shown $\left[\theta = \tan^{-1}\left(\frac{\rho}{|z| + h}\right)\right]$.

By letting the path of integration lie below the real axis for $0.75\ k_2 \leq \lambda_R \lesssim 1.3\ k_2$, the numerical difficulties associated with the $1/(\gamma_1 + \gamma_2)$ and $1/N(\lambda)$ terms can be circumvented. However, as the Hankel function $H_0^{(1)}(\lambda\rho)$ grows exponentially for $\lambda_I < 0$, an integration path into the region $\lambda_I < 0$ with $|\lambda_I| > 2/\rho$ can encounter numerical difficulties.

Taking all of the above factors into account, the original Hankel function formulation contour (see Fig. 47) of integration has been chosen to be deformed as depicted in Fig. 48. Alternatives to this path have been considered (see a representative example in Fig. 49); however, the contour shown in Fig. 48 has generally been found to be most effective.

Helpful Approximate Analytic Results

We felt a hybrid approach combining approximate analytic results with numerical results would yield answers of sufficient accuracy with a significant improvement in efficiency. More exactly, if an approximate analytic result could be obtained for the contribution of the U and V integrals in the regions where they are not numerically nice (e.g., in the near vicinity of $\lambda = k_2$, especially near the vertical branch cut), and numerical methods used over the remainder of the contour then the combination of these two results (the analytic and numerical results for the different portions of the contour) should then efficiently yield sufficiently accurate results for the U and V integrals. This approach was tried for both the Bessel and Hankel function formulations. Approximate analytic results were determined for the Bessel function real axis (near $\lambda = k_2$) U and V integral contributions.

Approximate analytic results were also determined for the Hankel function vertical axis (around the vertical branch cut) U and V integral contributions. These helpful analytic results follow.

APPROXIMATE REAL AXIS INTEGRATION

The U and V integrals are moderately well-behaved along the positive real axis, except in the near vicinity of $\lambda = k_2$. Thus, integration along the positive real axis can be effective if an analytic expression is developed for the contribution to the U and V integrals due to the integrand behavior in the near vicinity of $\lambda = k_2$. That is, a sufficiently accurate analytic expression is needed for the following contributions to the U and V integrals:

$$U_{\substack{\text{near}\\ k_2}} = \int_{k_2-\Delta}^{k_2+\Delta} \frac{J_0(\lambda\rho)\, \exp(-\gamma_1 a - \gamma_2 b)\lambda d\lambda}{\gamma_1 + \gamma_2},$$

$$V_{\substack{\text{near}\\ k_2}} = \int_{k_2-\Delta}^{k_2+\Delta} \frac{J_0(\lambda\rho)\, \exp(-\gamma_1 a - \gamma_2 b)\lambda d\lambda}{k_1^2\gamma_2 + k_2^2\gamma_1}$$

The quantity Δ is assumed to be small relative to k_2 (discussed later). If we let

$$\lambda = k_2 + s,$$

then

$$\gamma_1 \cong \left(k_2^2 - k_1^2\right)^{1/2}, \quad \gamma_2 \cong (2k_2 s)^{1/2},$$

which leads to

$$U_{\substack{\text{near}\\ k_2}} \cong \int_{-\Delta}^{\Delta} \frac{J_0(k_2\rho)\, \exp\left[-\left(k_2^2 - k_1^2\right)^{1/2} a - (2k_2 s)^{1/2} b\right] (k_2 + s)\, ds}{\left(k_2^2 - k_1^2\right)^{1/2} + (2k_2 s)^{1/2}}$$

and

$$V_{\substack{\text{near}\\ k_2}} \cong \int_{-\Delta}^{\Delta} \frac{J_0(k_2\rho)\, \exp\left[-\left(k_2^2 - k_1^2\right)^{1/2} a - (2k_2 s)^{1/2} b\right] (k_2 + s)\, ds}{k_1^2(2k_2 s)^{1/2} + k_2^2\left(k_2^2 - k_1^2\right)^{1/2}}$$

Using a change of variable and the integral definitions for G_i (see the Helpful Integral Relations section), one can show that

$$U_{\substack{\text{near}\\ k_2}} \cong 2J_0(k_2\rho)\, \exp\left[-\left(k_2^2 - k_1^2\right)^{1/2} a\right]$$

$$\times \left[\left(-\frac{k_2}{\alpha\beta} - \frac{2}{\alpha^3\epsilon} - \frac{2t}{\alpha^2\epsilon} + \frac{\beta}{\alpha^2\epsilon^2} - \frac{t^2}{\alpha\epsilon} + \frac{\beta t}{\alpha\epsilon^2} - \frac{\beta^2}{\alpha^3\epsilon}\right) \exp(-\alpha t) + \left(\frac{k_2\beta}{\epsilon^2} + \frac{\beta^3}{\epsilon^4}\right) \exp\left(\frac{\alpha\beta}{\epsilon}\right) E_1\left(\frac{\alpha\beta}{\epsilon} + \alpha t\right)\right] \Bigg|_{t=(-\Delta)^{1/2}}^{t=(\Delta)^{1/2}}$$

$$V_{\substack{\text{near}\\ k_2}} \cong 2J_0(k_2\rho)\, \exp\left[-\left(k_2^2 - k_1^2\right)^{1/2} a\right]$$

$$\times \left[\left(-\frac{k_2}{\alpha\beta_1} - \frac{2}{\alpha^3\epsilon_1} - \frac{2t}{\alpha^2\epsilon_1} + \frac{\beta_1}{\alpha^2\epsilon_1^2} - \frac{t^2}{\alpha\epsilon_1} + \frac{\beta_1 t}{\alpha\epsilon_1^2} - \frac{\beta_1^2}{\alpha\epsilon_1^3}\right) \exp(-\alpha t) + \left(\frac{k_2\beta_1}{\epsilon_1^2} + \frac{\beta_1^3}{\epsilon_1^4}\right) \exp\left(\frac{\alpha\beta_1}{\epsilon_1}\right) E_1\left(\frac{\alpha\beta_1}{\epsilon_1} + \alpha t\right)\right] \Bigg|_{t=(-\Delta)^{1/2}}^{t=(\Delta)^{1/2}}$$

where E_1 is the exponential integral function, and

$$\alpha = (2k_2)^{1/2} b$$

$$\beta = \left(k_2^2 - k_1^2\right)^{1/2}$$

$$\epsilon = (2k_2)^{1/2}$$

$$\beta_1 = k_2^2\left(k_2^2 - k_1^2\right)^{1/2}$$

$$\epsilon_1 = k_1^2(2k_2)^{1/2}$$

In the special case when b = 0, it can be shown that

$$U_{\substack{\text{near} \\ k_2}} \cong 2J_0(k_2\rho)\exp\left[-\left(k_2^2 - k_1^2\right)^{1/2} a\right]$$

$$\times \left[\left(-\frac{k_2\beta}{\epsilon^2} - \frac{\beta^3}{\epsilon^4}\right)\ln(\beta + \epsilon t) + \frac{t^3}{3\epsilon} - \frac{\beta t^2}{2\epsilon^2} + \frac{\beta^2 t}{\epsilon^3} + \frac{k_2 t}{\epsilon}\right]\Bigg|_{t = (-\Delta)^{1/2}}^{t = (\Delta)^{1/2}}$$

$$V_{\substack{\text{near} \\ k_2}} \cong 2J_0(k_2\rho)\exp\left[-\left(k_2^2 - k_1^2\right)^{1/2} a\right]$$

$$\times \left[\left(-\frac{k_2\beta_1}{\epsilon_1^2} - \frac{\beta_1^3}{\epsilon_1^4}\right)\ln(\beta_1 + \epsilon_1 t) + \frac{t^3}{3\epsilon_1} - \frac{\beta_1 t^2}{2\epsilon_1^2} + \frac{\beta_1^2 t}{\epsilon_1^3} + \frac{k_2 t}{\epsilon_1}\right]\Bigg|_{t = (-\Delta)^{1/2}}^{t = (\Delta)^{1/2}}$$

The choice of the size of Δ is dictated not only by the requirement that $\Delta \ll k_2$ but also that it be large enough that the spiky behavior of the integrand on the real axis is contained within the interval $k_2 - \Delta \le \lambda \le k_2 + \Delta$. It can be shown that the spiky behavior of the integrand occurs within a distance equal to the difference between k_2 and k_0. Since

$$k_0 = \left(\frac{k_1^2 k_2^2}{k_1^2 + k_2^2}\right)^{1/2} \cong k_2\left(1 - \frac{1}{2}\frac{k_2^2}{k_1^2} + \ldots\right),$$

then for $|k_1^2| \gg k_2^2$,

$$|k_2 - k_0| \cong \frac{1}{2}\frac{k_2^3}{|k_1^2|} = \frac{1}{2}k_2\left|\frac{k_2^2}{k_1^2}\right|.$$

We designate this as Δ, or

$$\Delta = \frac{1}{2}k_2\left|\frac{k_2^2}{k_1^2}\right|$$

Note that if indeed $|k_1^2| \gg k_2^2$, then $\Delta \ll k_2$, which is consistent with the original assumption.

APPROXIMATE VERTICAL BRANCH CUT INTEGRATION

For certain situations, we have found it helpful to deform the Hankel function formulation contour of integration (see Fig. 47) so that it lies along both sides of the vertical branch cuts (see Fig. 50). This path of integration is useful in numerical evaluations of the U and V integrals when $k_2\rho \gtrsim 5$.

From the figures depicting the behavior of the components of the integrands of the U and V integrals, one might suspect that a numerical evaluation of the U and V

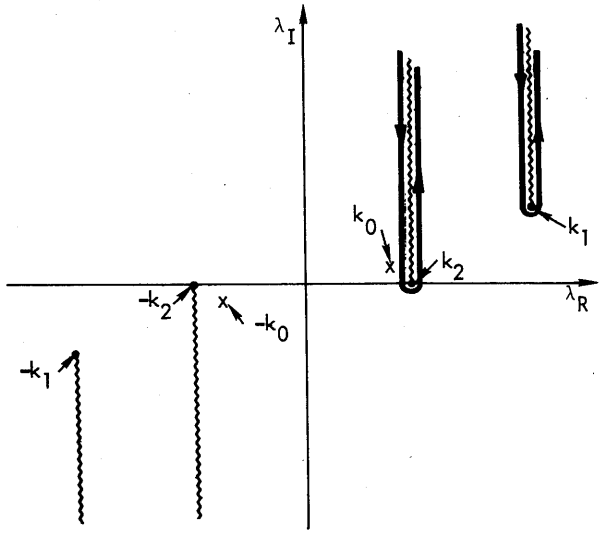

Fig. 50. A useful deformation of the contour used in the Hankel function formulation is the vertically aligned contour shown.

integrals would be difficult to evaluate along a path close to the vertical k_2 branch cut, and this is indeed true. However, the difficult numerical integration can be avoided by an approximate, but sufficiently accurate, analytic integration.

The U and V integrals are evaluated in the following manner. Let $F(\lambda)$ represent the integrand behavior of either the U or V integrands along the vertical k_2 branch cut. Let $F_A(\lambda)$ be an approximation to the behavior of $F(\lambda)$, where $F_A(\lambda) \cong F(\lambda)$ in the near vicinity of k_2 [i.e., in the region where $F(\lambda)$ is not well behaved]. By definition,

$$\int_0^\infty F(\lambda)d\lambda = \int_0^\infty [F(\lambda) - F_A(\lambda)]d\lambda + \int_0^\infty F_A(\lambda)d\lambda .$$

The second integral on the right hand side will be analytically integrated. The first integral on the right hand side is handled via

$$\int_0^\infty [F(\lambda) - F_A(\lambda)]d\lambda \cong \int_{\lambda_A}^\infty [F(\lambda) - F_A(\lambda)]d\lambda.$$

This approximate relation holds as $F(\lambda) \cong F_A(\lambda)$ along the vertical k_2 branch cut for $\lambda \lesssim \lambda_A$. In this way, the numerically troublesome integral behavior of $F(\lambda)$ near k_2 is circumvented.

The U and V integrand behavior is smoothly varying along the vertical k_2 branch cut except for the region defined by $\mathrm{Re}(\lambda) = k_2$, $0 \le \mathrm{Im}(\lambda) \lesssim 0.5\, k_2$. An analytic expression which sufficiently approximates the behavior of the U and V integrands will be used for this region. This approximate expression can be integrated analytically if its domain of definition is extended to the complete region $\mathrm{Re}(\lambda) = k_2$, $0 \le \mathrm{Im}(\lambda) < \infty$.

The extended approximate expression, as well as the actual U and V integrands, are well-behaved functions in the region $\mathrm{Re}(\lambda) = k_2$, $0.5k_2 \le \lambda < \infty$. Hence, the contribution to the U and V integrals from this segment of the total path along the vertical k_2 branch cut can be effectively evaluated numerically. The details of this procedure follow.

The following integral definitions will be helpful in expressing the U and V integral results.

$$\int_{-\infty}^{\infty} \frac{\exp(-\alpha t^2 - 2\beta t)}{t + t_0}\, dt = -\pi i \times \exp(-\alpha t_0^2 + 2\beta t_0)\, \mathrm{erfc}\left(i\frac{\beta}{\sqrt{\alpha}} - i\sqrt{\alpha}\, t_0\right)$$

$$\int_{-\infty}^{\infty} \exp(-\alpha t^2 - 2\beta t)dt = \frac{1}{2}\sqrt{\frac{\pi}{\alpha}} \times \exp\left(\frac{\beta}{2\alpha}\right) \mathrm{erfc}(\sqrt{\alpha}\,\beta)$$

By using the definition of the U and V integrands and approximate expressions for several of the integrand components, one can construct, in the region of $[\mathrm{Re}(\lambda) = k_2,\ 0 \le \mathrm{Im}(\lambda) \le 0.5\, k_2]$, sufficiently valid analytic approximations to the U and V integrands. Using the representation $\lambda = k_2 + is$, the approximations used are

$$\gamma_1 \cong \left(k_2^2 - k_1^2\right)^{1/2} + i\,\frac{k_2 s}{\left(k_2^2 - k_1^2\right)^{1/2}}$$

$$\gamma_2 \cong (i2k_2 s)^{1/2} - \frac{s^2}{(i8k_2 s)^{1/2}}$$

$$H_0^{(1)}(\lambda\rho) \cong \left(\frac{2}{i\pi\lambda\rho}\right)^{1/2} \exp(+i\lambda\rho)\left[1 - \frac{i}{8\lambda\rho}\right]$$

$$\frac{1}{(k_2 + is)^{1/2}} \cong \frac{1}{(k_2)^{1/2}}\left[1 - \frac{is}{2k_2}\right]$$

$$\exp(\mp\gamma_2 b) \cong \exp\left[\mp(i2k_2 s)^{1/2}\, b\right] \times \left[1 \pm \frac{s^2 b}{(i8k_2 s)^{1/2}}\right]$$

$$\exp(\mp\gamma_1 a) \cong \exp\left[\mp\left(k_2^2 - k_1^2\right)^{1/2} a \mp \frac{ik_2 sa}{\left(k_2^2 - k_1^2\right)^{1/2}}\right]$$

We now let $s = q^2$. Substituting the approximate expressions for the appropriate integrand components, one can show that the locally $\left[\mathrm{Re}(\lambda) = k_2,\ 0 \le \mathrm{Im}(\lambda) \lesssim 0.5k_2\right]$ approximate contribution to the U integral along the vertical k_2 branch cut (this approximate contribution is designated by $\int_{U,C_2}$) is

$$\int_{U,C_2} \cong \frac{i2k_2}{k_2^2 - k_1^2} \times \exp\left[-\left(k_2^2 - k_1^2\right)^{1/2} a\right]\left(\frac{2}{i\pi k_2\rho}\right)^{1/2} \times \exp(+ik_2\rho)\int_0^{q_L} qdq\, \exp(-\rho q^2) \times \exp\left[-\frac{ik_2 a}{\left(k_2^2 - k_1^2\right)^{1/2}} q^2\right]\left[1 - \frac{i}{8\rho k_2} + \frac{q^2}{k_2}\left(\frac{i}{2} - \frac{1}{16k_2\rho}\right) + \frac{q^4}{k_2^2}\left(\frac{1}{2} - \frac{i3}{16k_2\rho}\right)\right] \times \left(\left\{\exp\left[-(i2k_2)^{1/2} qb\right] + \exp\left[+(i2k_2)^{1/2} qb\right]\right\} \times \left\{-\frac{q}{(k_2)^{1/2}}(i2)^{1/2} k_2 + \frac{q^3}{k_2^{3/2}} \times \left[\frac{k_2}{(i8)^{1/2}} + \frac{k_2\left(k_2^2 - k_1^2\right)^{1/2} b}{(i8)^{1/2}}\right]\right\} + \left\{\exp\left[-(i2k_2)^{1/2} qb\right] - \exp\left[+(i2k_2)^{1/2} qb\right]\right\} \times \left[\left(k_2^2 - k_1^2\right)^{1/2} + \frac{q^2}{k_2}\frac{ik_2^2}{\left(k_2^2 - k_1^2\right)^{1/2}}\right]\right)$$

By letting the upper limit of integration q_L go to infinity, one obtains

$$\int_{U,C_2} \cong \frac{i2k_2}{k_2^2 - k_1^2}$$

$$\times \exp\left[-\left(k_2^2 - k_1^2\right)^{1/2} a\right] \left(\frac{2}{i\pi k_2 \rho}\right)^{1/2}$$

$$\times \exp(+ik_2\rho) \left(\frac{\pi}{\alpha}\right)^{1/2} \frac{1}{\alpha} \exp\left(\frac{\beta^2}{\alpha}\right)$$

$$\times \left\{\operatorname{erfc}\left[\frac{\beta}{(\alpha)^{1/2}}\right] + \operatorname{erfc}\left[-\frac{\beta}{(\alpha)^{1/2}}\right]\right\}$$

$$\times \left[-\frac{1}{2}\beta\, AF + \frac{1}{4}\left(1 + \frac{2\beta^2}{\alpha}\right) AD\right.$$

$$- \frac{1}{8}\left(\frac{6\beta}{\alpha} + \frac{4\beta^3}{\alpha^2}\right)(AG + BF)$$

$$+ \frac{1}{16}\left(\frac{6}{\alpha} + \frac{24\beta^2}{\alpha^2} + \frac{8\beta^4}{\alpha^3}\right)(AE + BD)$$

$$- \frac{1}{32}\left(\frac{60\beta}{\alpha^2} + \frac{80\beta^3}{\alpha^3} + \frac{16\beta^5}{\alpha^4}\right)(BG + CF)$$

$$+ \frac{1}{64}\left(\frac{60}{\alpha^2} + \frac{360\beta^2}{\alpha^3}\right.$$

$$\left.\left. + \frac{240\beta^4}{\alpha^4} + \frac{32\beta^6}{\alpha^5}\right)(BE + CD)\right]$$

where

$$A = 1 - \frac{i}{8k_2\rho}$$

$$B = \frac{i}{2} - \frac{i}{16k_2\rho}$$

$$C = \frac{1}{2} - \frac{i3}{16k_2\rho}$$

$$D = -(i2)^{1/2} k_2$$

$$E = \frac{k_2}{(i8)^{1/2}}\left[1 + \left(k_2^2 - k_1^2\right)^{1/2} b\right]$$

$$F = \left(k_2^2 - k_1^2\right)^{1/2}$$

$$G = \frac{ik_2^2}{\left(k_2^2 - k_1^2\right)^{1/2}}$$

$$\alpha = \rho + \frac{ik_2 a}{\left(k_2^2 - k_1^2\right)^{1/2}}$$

$$\beta = (i2k_2)^{1/2} b$$

In deriving the above equation, use has been made of the previously given integral relations and the derivatives with respect to b of these relations. These integral relations are also given in the section on Helpful Integral Relations. The use of the approximate relations beyond their range of applicability has to be corrected by later subtracting from the accumulative answer the numerical result for the integral (evaluated between an upper limit of ∞ and a lower limit of q_L). The factor q_L is specified as the bound beyond which the integrand is not sufficiently equal to the integrand of the U integral in the range $0 \le q \le q_L$ $\left[\text{or } \mathrm{Re}(\lambda) = k_2,\ 0 \le \mathrm{Im}(\lambda) \le q_L^2\right]$.

An approach similar to that used for the U integrand can be used to circumvent the numerically stringent region of the V integrand. By a change of variable, using the approximate relations, and utilizing the additional approximation (valid along the vertical branch cut near k_2) that

$$\frac{1}{q^2 - ik_0 - ik_2} \cong +\frac{i}{k_0 + k_2}$$

$$\times \left(1 - \frac{iq^2}{k_0 + k_2}\right),$$ one can show that

$$\int_{V,C_2} \cong \frac{2\exp\left[-\left(k_2^2 - k_1^2\right)^{1/2} a\right]}{k_2^4\left(\frac{k_1^4}{k_2^4} - 1\right)} \left(\frac{2}{i\pi k_2 \rho}\right)^{1/2} \exp(+ik_2\rho)$$

$$\times \int_0^\infty q\,dq\, \frac{1}{q^2 - q_p^2} \exp\left[-\rho q^2 - i\frac{k_2 a}{\left(k_2^2 - k_1^2\right)^{1/2}} q^2\right]$$

$$\times \frac{k_2}{k_0 + k_2}\left(A' + B'q^2/k_2\right)\left(\left\{\exp\left[-(i2k_2)^{1/2} qb\right] - \exp\left[+(i2k_2)^{1/2} qb\right]\right\}\right.$$

$$\times \left[C' + D'q^2/k_2 + E'q^4/k_2^2\right] + \left\{\exp\left[-(i2k_2)^{1/2} qb\right] + \exp\left[+(i2k_2)^{1/2} qb\right]\right\}$$

$$\left.\times \left[F'q/(k_2)^{1/2} + G'q^3/k_2^{3/2}\right]\right)$$

with

$$A' = 1 - \frac{i}{8k_2\rho}$$

$$B' = -\frac{ik_2}{k_0 + k_2} - \frac{3}{16k_2\rho}$$

$$C' = k_2^2\left(k_2^2 - k_1^2\right)^{1/2}$$

$$D' = \frac{ik_2^4}{\left(k_2^2 - k_1^2\right)^{1/2}}$$

$$E' = -\frac{k_2^2 k_1^2 b}{2}$$

$$F' = -(i2)^{1/2} k_2 k_1^2$$

$$G' = \frac{1}{(i8)^{1/2}}\left[k_2 k_1^2 + k_2^3\left(k_2^2 - k_1^2\right)^{1/2} b\right]$$

$$q_p^2 = i(k_2 - k_0)$$

Using results given in the section on Helpful Integral Relations, one can show that

$$\int_{V,C_2} \cong -\frac{2\exp\left[-\left(k_2^2 - k_1^2\right)^{1/2} a\right]}{k_2^4\left(\frac{k_1^4}{k_2^4} - 1\right)}$$

$$\times \left(\frac{2}{i\pi k_2\rho}\right)^{1/2} \exp(+ik_2\rho)\, \frac{k_2}{k_0 + k_2}\, \frac{1}{2q_p}$$

$$\times \{A'C'(H_1^- - H_1^+) + (A'D' + B'C')(H_3^- - H_3^+)$$

$$+ (A'E' + B'D')(H_5^- - H_5^+)$$

$$+ A'F'(H_2^- + H_2^+) + (A'G' + B'F')$$

$$\times (H_4^- + H_4^+)\}$$

where

$$H_i^\pm = \int_{-\infty}^{\infty} \frac{\exp(-\alpha t^2 \pm 2\beta t) t^i dt}{t + t_0}$$

$$\alpha = k_2\rho + \frac{ik_2^2 a}{\left(k_2^2 - k_1^2\right)^{1/2}}$$

$$\beta = \left(\frac{i}{2}\right)^{1/2} k_2 b$$

$$t_0 = q_p = i(k_2 - k_0)^{1/2}.$$

The results for the $H_i^\pm$ in terms of the complex error function are given in the Helpful Integral Relations section.

Numerical Procedure Details

The numerical integration of the U and V integrals requires rapidly convergent means of computing integrals over finite and semi-infinite intervals, even when the integrand may have numerous oscillations in the interval. There are several

techniques for handling problems of this type (e.g., Euler transformation, G-transform, Gaussian integration between zeros of Bessel function, Laguerre integration, Monte Carlo methods, etc.). The methods we have used are adaptive Romberg integration for the finite intervals of the complex contours in Figs. 45 to 50, and a combination of adaptive Romberg integration and Shank's nonlinear transformation (used to accelerate the convergence) for the semi-infinite intervals. An alternative technique used for the semi-infinite intervals was progressive Romberg integration with a check on the relative contribution of the last subinterval. When the last five subintervals each contributed less than 10^{-3} of the accumulated sum, then the progressive semi-infinite integration was terminated and said to be converged. The choice of these procedures, rather than alternative procedures, was based upon our past experience that these methods work quite well. It is not expected that alternate methods would dramatically improve the accuracy or computation time required for the integrands of interest.

The width of the subintervals used in the numerical scheme is based upon the known oscillation rate of Bessel and Hankel functions, and also the asymptotic oscillation and decay rate of the exponential term. An arbitrary subinterval width of

$$\Delta\lambda = \frac{\pi}{5\rho}$$

was chosen. This choice has proven satisfactory in the numerical studies conducted thus far.

Special functions were required to evaluate the Sommerfeld integrals. For example, the Hankel formulation requires Hankel function evaluations; the Bessel formulation requires Bessel function evaluations; the approximate Bessel function integration along the real axis is expressed in terms of complex exponential functions; and the approximate Hankel function integration around the vertical branch cuts is expressed in terms of complementary error functions. Computer routines for evaluating Bessel, Hankel, complex exponential integral function, and complementary error functions were thus generated. Details of the computational algorithms are not discussed herein; a separate manual will present these details.

The use of the vertical branch cuts in specifying which root to use in evaluating γ_1 and γ_2 necessitated that the usual choice of the complex square root routine used in our mathematical routines library be modified. The complex square root algorithm employed in most mathematical routine libraries assume the branch cut lies along the negative real axis. This causes no problems except in the determination of γ_1 and γ_2. By definition, $\gamma_1 = [(\lambda - k_1)(\lambda + k_1)]^{1/2}$ and $\gamma_2 = [(\lambda - k_2)(\lambda + k_2)]^{1/2}$. For integration paths on the upper Riemann sheet, with λ lying somewhere in the first, second, or fourth quadrant (the location of the paths of integration used), the quantities $\lambda + k_1$ and $\lambda + k_2$ can be computed using the standard square root algorithm. However, the quantities $\lambda - k_1$ and $\lambda - k_2$ require special consideration for λ lying in the first or second quadrant, to the left of and above (see Fig. 8) k_1 (for $\lambda - k_1$), or

to the left of and above (see Fig. 7) k_2 (for $\lambda - k_2$). If λ lies in the first or second quadrant to the left of the above k_1, the correct square root choice for $\lambda - k_1$ should be the negative of the usual complex square root result for $\lambda - k_1$. If λ lies in the first or second quadrant, to the left of and above k_2, the correct square root choice for $\lambda - k_2$ should be the negative of the usual complex square root result for $\lambda - k_2$. These observations can be seen to be valid by referring to Fig. 51 which depicts the location in the z plane (upper and lower Riemann sheets) of three choices of $(z)^{1/2}$ branch cut location. The branch cut along the negative

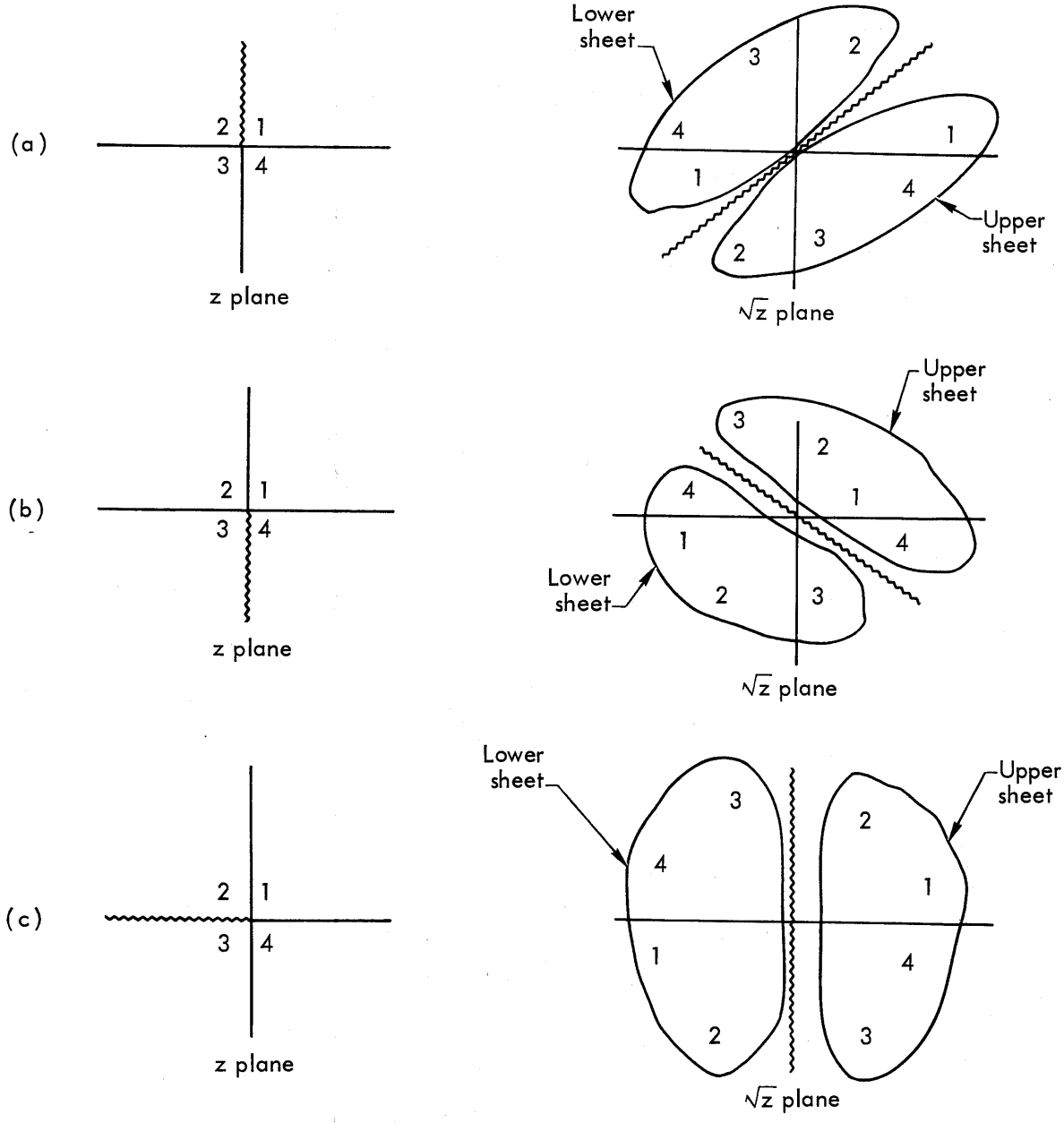

Fig. 51. Some possible locations of the branch cuts (z plane) and their locations in the $(z)^{1/2}$ plane. The numbers 1, 2, 3, and 4, respectively, refer to the location of the first, second, third, and fourth quadrants in the z plane and the location of these quadrants when mapped into the $\sqrt{z}$ plane.

real axis is the usual complex square root algorithm choice, the upward vertical branch cut is analogous to the upward vertical branch cut at $\lambda = k$ (where $z = \lambda - k$), and the downward vertical branch cut is analogous to the downward vertical branch cut at $\lambda = -k$ (where $z = \lambda + k$). Note that on the upper sheet, the second quadrant of the upward vertical branch cut (Fig. 51a) and the third quadrant of the downward vertical branch cut (Fig. 51b) are displaced from their locations on the upper sheet for the negative real axis branch cut (Fig. 51c). Hence, the sign of the standard square root has to be changed when in these quadrants.

For further details regarding the varied numerical algorithms, the reader is referred to the computer program manuals.

Numerical Integration Validation

Various checks on the validity of the integration procedure were performed to ensure that our methods yielded valid answers. One validation method involved performing integration of the U and V integrands along a path connecting two points on the upper Riemann sheet of the λ domain. Integrations along other paths that also connected these two points were also performed. When there were no poles interior to two paths, the integral results should be the same, regardless of the path. It was, for the cases considered.

Another check involved evaluating the Bessel formulation and Hankel formulation of the free-space Green's function, which is a Sommerfeld-type integral with a known analytic result. All cases of ρ/λ and z/λ considered yielded accurate results. This included a variety of orientations of source and receiver, and separation distances that were in the very near, near, intermediate, and far-field (in free space) regions.

A third check on the validity of the integration procedures was to compare numerical results with results based on known approximate formulas for Sommerfeld integrals (in the regions where the approximate formulas were known to be sufficiently valid). In all cases considered, the comparisons were quite good.

The fourth check used was to check boundary conditions at the air-ground interface. That is, the continuity of tangential electric fields and normal electric displacement was checked for a number of cases with the source buried, elevated, or on the surface. This was a severe test of the numerical procedure in that one formulation (the receiver in the same medium as the source) includes Green's function terms, whereas the second formulation (the receiver not in the same medium as the source) does not include Green's function terms. All cases considered met the boundary condition constraint within an acceptable accuracy.

Sample test case results for the boundary condition checks are presented in Tables 3, 4, and 5 to provide a demonstration of the validity of the above remarks, and to provide numerical results which others can check on their own computer to ensure that their copy of the Sommerfeld integral program is yielding satisfactory answers. Note that the

boundary conditions are reasonably well-satisfied for the cases given in Tables 3, 4, and 5. The tangential fields (E_ϕ, E_ρ) are approximately equal at the positions just above ($z = +10^{-6}$ m) and below ($z = -10^{-6}$ m), the ground-air interface ($z = 0$). This is true for an elevated source, a source at the interface, and a buried source. It is also shown to be valid for both horizontal (H) and vertical (V) sources. The normal electric field (E_z) is discontinuous across the interface by a factor which is approximately N^2, as dictated by boundary conditions.

Table 3. A check on the computer results via a comparison of boundary conditions for an elevated source.

	$z = +10^{-6}$ m	$z = -10^{-6}$ m	Note 1
ρ = 1 m	$E_\phi^H = 2.826 \times 10^{-2}$ /-17.76°	$E_\phi^H = 2.828 \times 10^{-2}$ /-17.75°	
	$E_\rho^H = 2.824 \times 10^{-2}$ /162.2°	$E_\rho^H = 2.825 \times 10^{-2}$ /162.2°	
	$E_\rho^V = 1.555 \times 10^{-3}$ /167.2°	$E_\rho^V = 1.567 \times 10^{-3}$ /166.7°	
	$E_z^V = 3.812 \times 10^{-1}$ /114.9°	$E_z^V = 6.269 \times 10^{-3}$ /33.48°	(a)
	$E_z^H = 2.435 \times 10^{-2}$ /-83.79°	$E_z^H = 4.018 \times 10^{-4}$ /-165.2°	(b)
ρ = 20 m	$E_\phi^H = 1.026 \times 10^{-3}$ /-106.4°	$E_\phi^H = 1.026 \times 10^{-3}$ /-106.4°	
	$E_\rho^H = 4.851 \times 10^{-4}$ /90.75°	$E_\rho^H = 4.851 \times 10^{-4}$ /90.75°	
	$E_\rho^V = 4.348 \times 10^{-3}$ /82.43°	$E_\rho^V = 4.344 \times 10^{-4}$ /82.43°	
	$E_z^V = 3.338 \times 10^{-2}$ /122.7°	$E_z^V = 5.521 \times 10^{-4}$ /41.42°	(c)
	$E_z^H = 5.048 \times 10^{-3}$ /159.1°	$E_z^H = 8.332 \times 10^{-5}$ /77.68°	(d)
ρ = 200 m	$E_\phi^H = 2.624 \times 10^{-4}$ /-113.6°	$E_\phi^H = 2.624 \times 10^{-4}$ /-113.6°	
	$E_\rho^H = 7.010 \times 10^{-5}$ /160.6°	$E_\rho^H = 7.010 \times 10^{-5}$ /160.6°	
	$E_\rho^V = 2.099 \times 10^{-3}$ /83.67°	$E_\rho^V = 2.100 \times 10^{-3}$ /83.62°	
	$E_z^V = 1.654 \times 10^{-2}$ /124.2°	$E_z^V = 2.729 \times 10^{-4}$ /42.77°	(e)
	$E_z^H = 8.553 \times 10^{-4}$ /-159.4°	$E_z^H = 1.411 \times 10^{-5}$ /119.0°	(f)

NOTES: (1) Ratios of E_z at $z = +10^{-6}$ m to E_z at $z = -10^{-6}$ m:

(a) Ratio = 60.80 /81.42°

(b) Ratio = 60.60 /81.41°

(c) Ratio = 60.46 /81.28°

(d) Ratio = 60.58 /81.42°

(e) Ratio = 60.60 /81.43°

(f) Ratio = 60.61 /81.6°

(2) f = 3 MHz, $\epsilon_r = 9$, $\sigma = 10^{-2}$ S/m, h = 20 m, $N^2 = 60.67$ /81.47°

Table 4. A check on the computer results via a comparison of boundary conditions for a source at the interface.

	$z = +10^{-6}$ m	$z = -10^{-6}$ m	Note 1
ρ = 1 m	$E_\phi^H = 1.595 \times 10^1 \angle 4.020°$	$E_\phi^H = 1.595 \times 10^1 \angle 4.020°$	
	$E_\rho^H = 3.132 \times 10^1 \angle 12.25°$	$E_\rho^H = 3.132 \times 10^1 \angle 12.25°$	
	$E_\rho^V = 1.854 \times 10^0 \angle 95.79°$	$E_\rho^V = 1.852 \times 10^0 \angle 96.20°$	
	$E_z^V = 9.478 \times 10^2 \angle -89.10°$	$E_z^V = 1.564 \times 10^1 \angle -170.5°$	(a)
	$E_z^H = 1.851 \times 10^0 \angle -84.19°$	$E_z^H = 3.060 \times 10^{-2} \angle -165.6°$	(b)
ρ = 20 m	$E_\phi^H = 6.417 \times 10^{-3} \angle 32.86°$	$E_\phi^H = 6.417 \times 10^{-3} \angle 32.86°$	
	$E_\rho^H = 2.888 \times 10^{-3} \angle -20.62°$	$E_\rho^H = 2.888 \times 10^{-3} \angle -20.62°$	
	$E_\rho^V = 3.217 \times 10^{-2} \angle 167.9°$	$E_\rho^V = 3.221 \times 10^{-2} \angle 167.9°$	
	$E_z^V = 1.959 \times 10^{-1} \angle -127.2°$	$E_z^V = 3.214 \times 10^{-3} \angle 150.9°$	(c)
	$E_z^H = 3.217 \times 10^{-2} \angle -12.05°$	$E_z^H = 5.310 \times 10^{-4} \angle -93.51°$	(d)
ρ = 200 m	$E_\phi^H = 4.650 \times 10^{-5} \angle -61.12°$	$E_\phi^H = 4.650 \times 10^{-5} \angle -61.12°$	
	$E_\rho^H = 2.847 \times 10^{-4} \angle -133.5°$	$E_\rho^H = 2.847 \times 10^{-4} \angle -133.5°$	
	$E_\rho^V = 2.280 \times 10^{-3} \angle 86.91°$	$E_\rho^V = 2.279 \times 10^{-3} \angle 86.83°$	
	$E_z^V = 1.805 \times 10^{-2} \angle 127.4°$	$E_z^V = 2.978 \times 10^{-4} \angle 45.95°$	(e)
	$E_z^H = 2.280 \times 10^{-3} \angle -93.08°$	$E_z^H = 3.764 \times 10^{-5} \angle -174.5°$	(f)

NOTES: (1) Ratios of E_z at $z = +10^{-6}$ m to E_z at $z = -10^{-6}$ m:

(a) Ratio = $60.60 \angle 81.40°$

(b) Ratio = $60.49 \angle 81.41°$

(c) Ratio = $60.95 \angle 81.9°$

(d) Ratio = $60.58 \angle 81.46°$

(e) Ratio = $60.61 \angle 81.45°$

(f) Ratio = $60.57 \angle 81.42°$

(2) f = 3 MHz, $\epsilon_r = 9$, $\sigma = 10^{-2}$ S/m, h = 0 m, $N^2 = 60.67 \angle 81.47°$

Table 5. A check on the computer results via a comparison of boundary conditions for a buried source.

	$z = +10^{-6}$ m	$z = -10^{-6}$ m	Note 1
ρ = 1 m	$E_\phi^H = 2.959 \times 10^{-4}$ /-18.82°	$E_\phi^H = 2.959 \times 10^{-4}$ /-18.82°	
	$E_\rho^H = 2.943 \times 10^{-4}$ /161.2°	$E_\rho^H = 2.943 \times 10^{-4}$ /161.2°	
	$E_\rho^V = 1.915 \times 10^{-5}$ /-9.973°	$E_\rho^V = 1.930 \times 10^{-5}$ /-10.12°	
	$E_z^V = 1.465 \times 10^{-4}$ /13.66°	$E_z^V = 2.418 \times 10^{-6}$ /-67.68°	(a)
	$E_z^H = 4.010 \times 10^{-5}$ /150.5°	$E_z^H = 6.619 \times 10^{-7}$ /69.10°	(b)
ρ = 20 m	$E_\phi^H = 2.594 \times 10^{-5}$ /107.7°	$E_\phi^H = 2.594 \times 10^{-5}$ /107.7°	
	$E_\rho^H = 1.042 \times 10^{-5}$ /3.426°	$E_\rho^H = 1.042 \times 10^{-5}$ /3.426°	
	$E_\rho^V = 1.026 \times 10^{-5}$ /159.3°	$E_\rho^V = 1.026 \times 10^{-5}$ /159.3°	
	$E_z^V = 1.328 \times 10^{-5}$ /-118.5°	$E_z^V = 2.194 \times 10^{-7}$ /159.7°	(c)
	$E_z^H = 6.591 \times 10^{-5}$ /-124.3°	$E_z^H = 1.087 \times 10^{-6}$ /154.15°	(d)
ρ = 200 m	$E_\phi^H = 7.498 \times 10^{-8}$ /-17.83°	$E_\phi^H = 7.505 \times 10^{-8}$ /-25.38°	
	$E_\rho^H = 4.565 \times 10^{-7}$ /-72.46°	$E_\rho^H = 4.563 \times 10^{-7}$ /-72.47°	
	$E_\rho^V = 6.035 \times 10^{-8}$ /66.57°	$E_\rho^V = 6.032 \times 10^{-8}$ /66.47°	
	$E_z^V = 4.780 \times 10^{-7}$ /107.1°	$E_z^V = 7.930 \times 10^{-9}$ /25.25°	(e)
	$E_z^H = 3.654 \times 10^{-6}$ /147.9°	$E_z^H = 6.032 \times 10^{-8}$ /66.50°	(f)

NOTES: (1) Ratio of E_z at $z = +10^{-6}$ m to E_z at $z = -10^{-6}$ m:

(a) Ratio = 60.58 /81.34°
(b) Ratio = 60.58 /81.4°
(c) Ratio = 60.58 /81.8°
(d) Ratio = 60.63 /81.55°
(e) Ratio = 60.77 /81.85°
(f) Ratio = 60.57 /81.4°

(2) f = 3 MHz, $\epsilon_r = 9$, $\sigma = 10^{-2}$ S/m, h = 20, $N^2 = 60.67$ /81.47°

Which Integration Path to Use When

A rough "rule-of-thumb" has been developed for when to use which path of integration. These rules are not to be considered "cast-in-concrete," but only as a guide. For example, as the equations for the approximate vertical branch cut integration have not been written or debugged yet, the authors have used the

Hankel function path shown in Fig. 48 for $\rho > \lambda/2$. This has been true regardless of the values of a and b. This procedure is contrary to the guidelines given below. The reason for this contrariness is explained below.

When $\rho \leq \lambda$, regardless of the values of a and b, the path chosen is that shown in Fig. 46. This requires a numerical integration.

When $\rho > \lambda$, with $\rho < (a + b)/2$, the path chosen is that shown in Fig. 48. This requires a numerical integration.

When $\rho > \lambda$, with $\rho \geq (a + b)/2$, the path chosen is that shown in Fig. 50. This requires a numerical integration and an analytic evaluation.

The guidelines given above have been established from the various reasons given previously, from the authors' computational experience for various parameters when using the paths depicted in Figs. 46 and 48, and from the shared experiences of Dr. James F. Fuller of NOAA when using the integration path of Fig. 50 (for the particular situation of a vertically oriented source and receiver in the ground).

Various modifications of the paths in Figs. 46 and 48 have been tried to see if the convergence could be improved. A path which generally was more effective has not been encountered. However, it is possible that there are one or more paths which are more effective but have not been tried. It is also possible that there are paths that are more effective for a specific problem.

Acknowledgments

The list of investigators who have contributed to a better understanding of the behavior of Sommerfeld integrals is quite extensive. No attempt has been made herein to prepare an exhaustive reference list of these contributors. However, the authors would like to acknowledge the assistance and insight provided by the papers listed in the bibliography.

The authors have also benefited from extended discussions with a number of individuals. We especially welcome the opportunity to thank them for their constructive critical comments, assistance on varied points, and their pursuing interest in this work. These people include: Mr. James Goodwyn of the Defense Advanced Research Projects Agency; Dr. Donald E. Barrick, Dr. James R. Wait, and Dr. James A. Fuller, of the National Oceanographic and Atmospheric Administration (now with Texas Instruments, Inc.); Prof. Raj Mittra of the University of Illinois; and Dr. Edmund K. Miller, Mr. Frederick J. Deadrick, Dr. Robert M. Bevensee, and Dr. Andrew J. Poggio of the Lawrence Livermore Laboratory.

The authors are particularly indebted to Dr. James A. Fuller for his shared experiences. There are many similarities between some of the aspects of the work described herein and those described by Dr. Fuller in his Ph.D thesis, performed under Dr. James R. Wait at the University of Colorado. Most of the work described herein was performed independently but concurrently with that of Dr. Fuller.

Some of the conclusions however have been based on the collective observations of Dr. Fuller and the authors (e.g., when to use and the effectiveness of using the approximate vertical branch cut integration. This idea of performing a vertical branch cut integration was suggested to the authors by Prof. Raj Mittra during his employment at LLL during the summer of 1973.

References

1. A Sommerfeld, Ann. Phys. 28, 665 (1909).
2. W. C. Kuo and K. K. Mei, Approximation of the Sommerfeld's Integral for Fast Convergence. Presented at the 1973 IEEE Group on Antennas and Propagation International Symposium, Boulder, Colorado.
3. J. E. Lindsay, Jr., A Direct Approach to the Numerical Evaluation of E. M. Fields Due to Sources Buried Beneath the Earth's Surface. Presented at the 1973 IEEE Group on Antennas and Propagation International Symposium, Boulder, Colorado.
4. M. Siegel and R. W. P. King, J. Appl. Phys. 41 (6), 2415 (May 1970).
5. A. Fuller, Electromagnetic Radiation and Propagation in the Presence of Dispersive Geological Media, Ph.D. thesis at the Department of Electrical Engineering, University of Colorado (1974).
6. E. K. Miller, Computer Models for Antennas, Lawrence Livermore Laboratory, Rept. UCRL-51515 (1974).
7. A. Baños, Dipole Radiation in the Presence of a Conducting Half-Space (Pergamon Press, New York, 1966).

Bibliography

M. Abramowitz and I. A. Stegun, Handbook of Mathematical Functions with Formulas, Graphs, and Mathematical Tables, National Bureau of Standards Applied Mathematics Series 55 (1965).

A. Alaylioglu, G. A. Evans, and J. Hyslop, "The Evaluation of Oscillatory Integrals with Infinite Limits," J. Comp. Phys. 13, 433 (1973).

T. A. Atchinson and H. L. Gray, "Nonlinear Transformations Related to the Evaluation of Improper Integrals. II," SIAM Journal of Numerical Analysis, 5 (2), 451 (1968).

A. Baños, Dipole Radiation in the Presence of a Conducting Half-Space (Pergamon Press, New York, 1966).

D. E. Barrick, "Theory of Ground-Wave Propagation Across a Rough Sea at Dekameter Wavelengths," Battelle Memorial Institute, ARPA Order No. 1178, January 1970.

A. W. Biggs, "Radiation Fields from a Horizontal Electric Dipole in a Semi-Infinite Conducting Medium," IRE Transactions on Antennas and Propagation (July 1962).

W. E. Blair, "Experimental Verification of Dipole Radiation in a Conducting Half-Space," IEEE Transactions on Antennas and Propagation (May 1963).

L. M. Brekhovskikh, Waves in Layered Media, translated by D. Lieberman and edited by R. T. Beyer (Academic Press, New York, 1960).

C. R. Burrows, "The Surface Wave in Radio Propagation over Plane Earth," Proc. IRE 25, 219 (1937).

G. A. Campbell and R. M. Foster, Fourier Integrals for Practical Applications (D. Van Nostrand Co., Inc., Princeton, 1948).

J. S. R. Chisholm, A. Genz, and G. E. Rowlands, "Accelerated Convergence of Sequences of Quadrature Approximations," J. Comp. Phys. 10 (2), 284 (1972).

P. David and J. Voge, Propagation of Waves (Pergamon Press, New York, 1969).

D. Dence and T. Tamir, "Radio Loss of Lateral Waves in Forest Environments," Radio Science 4 (4), 307 (April 1969).

A. Dey and H. F. Morrison, "Electromagnetic Coupling in Frequency and Time-Domain Induced-Polarization Surveys over a Multilayered Earth," Geophysics 38 (2), 380 (1973).

L. Felsen, "Lateral Waves," in Electromagnetic Theory, Part I, edited by John Brown (Pergamon Press, London, 1967) pp. 11-44.

R. C. Fenwick and W. L. Weeks, "Submerged Antenna Characteristics," IEEE Trans. Antennas Propagation AP-11, 296 (May 1963).

Y. L. Feynberg, The Propagation of Radio Waves Along the Surface of the Earth, Foreign Technology Division Wright-Patterson AFB, Ohio (March 1967) AD 660 951.

J. A. Fuller, "Electromagnetic Radiation and Propagation in the Presence of Dispersive Geological Media," Ph.D. thesis at the Department of Electrical Engineering, University of Colorado (1974).

R. W. Hamming, Numerical Methods for Scientists and Engineers (McGraw-Hill Book Co., Inc., New York, 1962).

R. C. Hansen, "Radiation and Reception with Buried and Submerged Antennas," IEEE Trans. Antennas Propagation AP-11, 207 (May 1963).

R. J. King, "Electromagnetic Wave Propagation Over a Constant Impedance Plane," Radio Science 4 (3), 255 (March 1969).

R. J. King, S. H. Cho, D. L. Jaggard, and V. Sokolov, "Height-gain Experimental Data for Groundwave Propagation, 1, Homogeneous Paths," Radio Science 8 (1), 7 (January 1973).

R. J. King, S. H. Cho, and D. L. Jaggard, "Height-gain Experimental Data for Groundwave Propagation, 2, Heterogeneous Paths," Radio Science 8 (1), 17 (January 1973).

R. W. P. King, The Theory of Linear Antennas (Harvard University Press, Cambridge, Mass., 1956) pp. 695-817.

W.C. Kuo and K. K. Mei, "Approximation of the Sommerfeld's Integral for Fast Convergence," paper presented at the 1973 IEEE Group on Antennas and Propagation International Symposium, Boulder, Colorado.

D. L. Lager and R. J. Lytle, Manual for Subroutines Pertaining to Numerical Evaluation of Sommerfeld Integrals, Lawrence Livermore Laboratory Rept. (in preparation).

D. L. Lager, F. J. Deadrick, E. K. Miller, R. W. Adams, and R. J. Lytle, A Program for Analyzing Thin Wire Structures Above, Below, and Penetrating the Ground: WF-LLL2A, Lawrence Livermore Laboratory Rept. (in preparation).

G. A. Lavrov and A. S. Knyazev, Near Earth and Buried Antennas, U.S. Dept. Commerce Clearinghouse for Federal Scientific and Technical Information, Joint Publications Research Service No. 41131 (1967).

J. E. Lindsay, Jr., "A Direct Approach to the Numerical Evaluation of E. M. Fields Due to Sources Buried Beneath the Earth's Surface," paper presented at the 1973 IEEE Group on Antennas and Propagation International Symposium, Boulder, Colorado.

Y. L. Luke, "On the Computation of Oscillating Integrals," Cambridge Philosophical Society, Proceedings 50, 269 (1954).

R. J. Lytle, A Computer Program for Calculating the Fields of an Arbitrarily Oriented Sub-surface Electric Current Source, Lawrence Livermore Laboratory, internal rept. Technical Note No. 125 (March 1, 1971).

R. J. Lytle, "Ground Reflection Effects Upon Radiated and Received Signals as Viewed Via Image Theory," IEEE Transactions on Antennas and Propagation, AP-20 (6), 736 (1972).

R. J. Lytle and D. L. Lager, Extending the Range of Validity of Formulas Approximating Sommerfeld Integrals, Lawrence Livermore Laboratory Rept. (in preparation).

R. J. Lytle and E. K. Miller, A Physical Explanation of Electromagnetic Surface Wave Formulas, Lawrence Livermore Laboratory Rept. UCRL-51654 (1974).

E. K. Miller, "A Variable Interval Width Quadrature Technique Based on Romberg's Method," J. Comp. Phys. 5 (1970).

E. K. Miller, A. J. Poggio, G. J. Burke, and E. S. Selden, "Analysis of Wire Antennas in the Presence of a Conducting Half-Space. Part I. The Vertical Antenna in Free Space," Canadian J. Physics 50, 879 (1972).

E. K. Miller, A. J. Poggio, G. J. Burke, and E. S. Selden, "Analysis of Wire Antennas in the Presence of a Conducting Half-Space. Part II. The Horizontal Antenna in Free Space," Canadian J. Physics 50, 2614 (1972).

G. D. Monteath, Applications of the Electromagnetic Reciprocity Principle (Pergamon Press, New York, 1973).

R. K. Moore and W. E. Blair, "Dipole Radiation in a Conducting Half-Space," J. Res. Natl. Bur. Std. (U.S.) 65D (radio prop.), 547 (November-December 1961).

K. A. Norton, "The Propagation of Radio Waves Over the Surface of the Earth and in the Upper Atmosphere," Proc. IRE 24 (10), 1367 (1936).

K. A. Norton, "The Physical Reality of Space and Surface Waves in the Radiation Field of Radio Antennas," Proc. IRE 25 (9), 1192 (September 1937).

K. A. Norton, "The Propagation of Radio Waves Over the Surface of the Earth and in the Upper Atmosphere," Proc. IRE 25 (9), 1203 (1937).

A. Ralston, A First Course in Numerical Analysis (McGraw-Hill Book Co., Inc., New York, 1965).

S. O. Rice, "Series for the Wave Function of a Radiating Dipole at the Earth's Surface," Bell System Tech. J. 16, 101 (January 1937).

D. Shanks, "Non-linear Transformations of Divergent and Slowly Convergent Sequences," Journal of Math. Physics 34, 1 (1955).

M. Siegel and R. W. P. King, "Electromagnetic Fields in a Dissipative Half-Space: A Numerical Approach," J. Appl. Phys. 41 (6), 2415 (May 1970).

A. Sommerfeld, "Über die Ausbreitung der Wellen in der drahtlosen Telegraphie," Ann. Phys. 28, 665 (1909).

A. Sommerfeld, "Über die Ausbreitung der Wellen in der drahtlosen Telegraphie," Ann. Physik, Ser. 4 81 (17), 1135 (December 1926).

D. Staiman and T. Tamir, "Nature and Optimization of the Ground (Lateral) Wave Excited by Submerged Antennas," Proc. IEE 113 (8), 1299 (1966).

J. A. Stratton, Electromagnetic Theory (McGraw-Hill Book Company, New York, 1941).

M. J. O. Strutt, "Strachlung von Antennen unter den Einfluss der Erdbodeneigenschaften," Ann. Physik 1 (1), 721 (1929).

C. T. Tai, Radiation of a Hertzian Dipole Immersed in a Dissipative Medium, Cruft Lab. Tech. Rept. 21, Office of Naval Research, Harvard University, Cambridge, Mass (Oct. 10, 1947).

T. Tamir, "Experimental Verification of a Lateral Wave Above a Lossy Interface," Electronics Letters 6 (12), 357 (June 1970).

B. van der Pol, "On Discontinuous Electromagnetic Waves and the Occurrence of a Surface Wave," IRE Trans. on Antennas and Propagation AP-4 (3), 288 (1956).

H. Weyl, "Ausbreitung elektromagnetischer Wellen über einem ebenen Leiter," Ann. Physik, Ser. 4 60, 481 (1919).

W. H. Wise, "The Physical Reality of Zenneck's Surface Wave," Bell System Tech. J. 16, 35 (January, 1937).

J. R. Wait, "Impedance Characteristics of Electric Dipoles Over a Conducting Half-space," Radio Science 4 (10), 971 (October 1969).

J. R. Wait, "Characteristics of Antennas Over Lossy Earth," in Antenna Theory Part 2, edited by R. E. Collin and F. J. Zucker (McGraw-Hill Book Co., Inc., New York, 1969), p. 386.

J. R. Wait, "Electromagnetic Fields of Sources in Lossy Media," in Antenna Theory Part 2, edited by R. E. Collin and F. J. Zucker (McGraw-Hill Book Co., Inc., New York), p. 438.

J. R. Wait, Electromagnetic Waves in Stratified Media (Pergamon Press, New York, 1970).

J. R. Wait and J. R. Fuller, "On Radio Propagation Through Earth," IEEE Trans. on Antennas and Propagation AP-19 (6), 796 (Nov. 1971), pp. 796-798.

A. Yokoyama, "Radiation of a Dipole in a Lossy Half-Space," Journal of the Physical Society of Japan 32 (1), 270 (Jan. 1972).

A. Yokoyama, "Comments on the Solutions of Dipoles in Semi-Infinite Media," IEEE Trans. on Antennas and Propagation AP-22 (2), 339 (March 1974).

Appendix A
Mathematical Formulas

The mathematical formulas describing the fields due to either a vertical electric or a horizontal electric dipole located either above or below the ground-air interface are given below. These formulae were obtained from Baños, and are expressed in his notation (with the exception that the cylindrical radius is herein expressed as ρ, rather than r). The air is assumed to be medium 2, the ground medium 1. The current moment of the source is denoted as $I\ell$ amp meter. The operating frequency is $\omega = 2\pi f$ radians/second. The propagation constants in the ground and in the air are respectively

$$k_1^2 = \omega^2 \mu_0 \epsilon_0 \epsilon_r + i\omega\mu_0\sigma ,$$

$$k_2^2 = \omega^2 \mu_0 \epsilon_0 ,$$

where μ_0 is the free space permeability, ϵ_0 is the free space permittivity, ϵ_r is the relative dielectric constant of the ground, and σ is the conductivity of the ground. The ratio of conduction currents to displacement currents in the ground is designated as $p = \frac{\sigma}{\omega\epsilon_0\epsilon_r}$.

The usual cylindrical coordinate system notation (ρ, ϕ, z) is used. $E_{1\rho}^H$ designates the radial electric field intensity in region 1 (ground) due to a horizontal electric current source. H_{2z}^V designates the vertical component of magnetic field intensity in region 2 (air) due to a vertical electric current source. Note that the location of the source is not explicitly designated using this notation. The source height is designated as h, and h is assumed positive, regardless of whether the source is buried or elevated. The receiver height is designated as z, where z is negative if the receiver is buried, and z is positive if the receiver is elevated. The radial separation between source and receiver is ρ. The source is assumed to lie in the x-z plane, and the receiver lies in a plane oriented at an angle of ϕ relative to the x-z plane. With this notation, the electromagnetic fields due to elevated and buried electric current sources can be expressed in terms of what are designated as U, V, and W integrals (defined below).

Vertical Electric Dipole in Medium 1 (Ground)

$$E_{1\rho}^V = \frac{i\omega I\ell\mu_0}{4\pi k_1^2} \frac{\partial^2}{\partial\rho\partial z} \left\{\left[G_{11} - G_{12} + k_2^2 V_{11}\right]\right\}$$

$$E_{1z}^V = \frac{i\omega I\ell\mu_0}{4\pi k_1^2} \left\{\left(\frac{\partial^2}{\partial z^2} + k_1^2\right)\left[G_{11} - G_{12} + k_2^2 V_{11}\right]\right\}$$

$$H^V_{1\phi} = -\frac{I\ell}{4\pi}\left\{\frac{\partial}{\partial\rho}\left[G_{11} - G_{12} + k_2^2 V_{11}\right]\right\}$$

$$E_{2\rho} = \frac{i\omega I\ell\mu_0}{4\pi}\left\{\frac{\partial^2 V_{12}}{\partial\rho\partial z}\right\}$$

$$E_{2z} = \frac{i\omega I\ell\mu_0}{4\pi}\left\{\left(\frac{\partial^2}{\partial z^2} + k_2^2\right) V_{12}\right\}$$

$$H_{2\phi} = -\frac{I\ell k_2^2}{4\pi}\left\{\frac{\partial V_{12}}{\partial\rho}\right\}$$

Vertical Electric Dipole in Medium 2 (Air)

$$E^V_{2\rho} = \frac{i\omega I\ell\mu_0}{4\pi k_2^2}\left\{\frac{\partial^2}{\partial\rho\partial z}\left[G_{22} - G_{21} + k_1^2 V_{22}\right]\right\}$$

$$E^V_{2z} = \frac{i\omega I\ell\mu_0}{4\pi k_2^2}\left\{\left(\frac{\partial^2}{\partial z^2} + k_2^2\right)\left[G_{22} - G_{21} + k_1^2 V_{22}\right]\right\}$$

$$H^V_{2\phi} = \frac{-I\ell}{4\pi}\left\{\frac{\partial}{\partial\rho}\left[G_{22} - G_{21} + k_1^2 V_{22}\right]\right\}$$

$$E_{1\rho} = \frac{i\omega I\ell\mu_0}{4\pi}\left\{\frac{\partial^2 V_{21}}{\partial\rho\partial z}\right\}$$

$$E_{1z} = \frac{i\omega I\ell\mu_0}{4\pi}\left\{\left(\frac{\partial^2}{\partial z^2} + k_1^2\right) V_{21}\right\}$$

$$H_{1\phi} = \frac{-I\ell k_1^2}{4\pi}\left\{\frac{\partial V_{21}}{\partial\rho}\right\}$$

Horizontal Electric Dipole in Medium 1 (Ground)

$$E^H_{1\rho} = \frac{i\omega I\ell\mu_0}{4\pi k_1^2}\cos\phi\left\{\frac{\partial^2}{\partial\rho^2}\left[G_{11} - G_{12} + k_1^2 V_{11}\right] + k_1^2\left[G_{11} - G_{12} + U_{11}\right]\right\}$$

$$E^H_{1\phi} = \frac{-i\omega I \ell \mu_0}{4\pi k_1^2} \sin\phi \left\{ \frac{1}{\rho} \frac{\partial}{\partial \rho} \left[G_{11} - G_{12} + k_1^2 V_{11} \right] + k_1^2 \left[G_{11} - G_{12} + U_{11} \right] \right\}$$

$$E^H_{1z} = \frac{i\omega I \ell \mu_0}{4\pi k_1^2} \cos\phi \left\{ \frac{\partial^2}{\partial z \partial \rho} \left[G_{11} + G_{12} - k_2^2 V_{11} \right] \right\}$$

$$E^H_{2\rho} = \frac{i\omega I \ell \mu_0}{4\pi} \cos\phi \left\{ \frac{\partial^2 V_{12}}{\partial \rho^2} + U_{12} \right\}$$

$$E^H_{2\phi} = - \frac{i\omega I \ell \mu_0}{4\pi} \sin\phi \left\{ \frac{1}{\rho} \frac{\partial V_{12}}{\partial \rho} + U_{12} \right\}$$

$$E^H_{2z} = \frac{i\omega I \ell \mu_0}{4\pi} \cos\phi \left\{ \frac{\partial^2 V_{12}}{\partial h \partial \rho} \right\}$$

$$H^H_{1\rho} = \frac{I \ell \sin\phi}{4\pi} \left\{ \frac{\partial}{\partial z} \left[G_{11} - G_{12} + U_{11} \right] - \frac{1}{\rho} \frac{\partial W_{11}}{\partial \rho} \right\}$$

$$H^H_{1\phi} = \frac{I \ell \cos\phi}{4\pi} \left\{ \frac{\partial}{\partial z} \left[G_{11} - G_{12} + U_{11} \right] - \frac{\partial^2 W_{11}}{\partial \rho^2} \right\}$$

$$H^H_{1z} = - \frac{I \ell \sin\phi}{4\pi} \left\{ \frac{\partial}{\partial \rho} \left[G_{11} - G_{12} + U_{11} \right] \right\}$$

$$H^H_{2\rho} = \frac{I \ell \sin\phi}{4\pi} \left\{ \frac{\partial U_{12}}{\partial z} - \frac{1}{\rho} \frac{\partial W_{12}}{\partial \rho} \right\}$$

$$H^H_{2\phi} = \frac{I \ell \cos\phi}{4\pi} \left\{ \frac{\partial U_{12}}{\partial z} - \frac{\partial^2 W_{12}}{\partial \rho^2} \right\}$$

$$H^H_{2z} = - \frac{I \ell \sin\phi}{4\pi} \left\{ \frac{\partial U_{12}}{\partial \rho} \right\}$$

Horizontal Electric Dipole in Medium 2 (Air)

$$E^H_{2\rho} = \frac{i\omega I\ell\mu_0}{4\pi k_2^2} \cos\phi \left\{ \frac{\partial^2}{\partial\rho^2} \left[G_{22} - G_{21} + k_2^2 V_{22} \right] + k_2^2 \left[G_{22} - G_{21} + U_{22} \right] \right\}$$

$$E^H_{2\phi} = - \frac{i\omega I\ell\mu_0}{4\pi k_2^2} \sin\phi \left\{ \frac{1}{\rho} \frac{\partial}{\partial\rho} \left[G_{22} - G_{21} + k_2^2 V_{22} \right] + k_2^2 \left[G_{22} - G_{21} + U_{22} \right] \right\}$$

$$E^H_{2z} = \frac{i\omega I\ell\mu_0}{4\pi k_2^2} \cos\phi \left\{ \frac{\partial^2}{\partial z \partial\rho} \left[G_{22} + G_{21} - k_1^2 V_{22} \right] \right\}$$

$$E^H_{1\rho} = \frac{i\omega I\ell\mu_0}{4\pi} \cos\phi \left\{ \frac{\partial^2 V_{21}}{\partial\rho^2} + U_{21} \right\}$$

$$E^H_{1\phi} = - \frac{i\omega I\ell\mu_0}{4\pi} \sin\phi \left\{ \frac{1}{\rho} \frac{\partial V_{21}}{\partial\rho} + U_{21} \right\}$$

$$E^H_{1z} = - \frac{i\omega I\ell\mu_0}{4\pi} \cos\phi \left\{ \frac{\partial^2 V_{21}}{\partial h \partial\rho} \right\}$$

$$H^H_{2\rho} = \frac{I\ell\sin\phi}{4\pi} \left\{ \frac{\partial}{\partial z} \left[G_{22} - G_{21} + U_{22} \right] - \frac{1}{\rho} \frac{\partial W_{22}}{\partial\rho} \right\}$$

$$H^H_{2\phi} = \frac{I\ell\cos\phi}{4\pi} \left\{ \frac{\partial}{\partial z} \left[G_{22} - G_{21} + U_{22} \right] - \frac{\partial^2 W_{22}}{\partial\rho^2} \right\}$$

$$H^H_{2z} = - \frac{I\ell\sin\phi}{4\pi} \left\{ \frac{\partial}{\partial\rho} \left[G_{22} - G_{21} + U_{22} \right] \right\}$$

$$H^H_{1\rho} = \frac{I\ell\sin\phi}{4\pi} \left\{ \frac{\partial U_{21}}{\partial z} - \frac{1}{\rho} \frac{\partial W_{21}}{\partial\rho} \right\}$$

$$H^H_{1\phi} = \frac{I\ell\cos\phi}{4\pi} \left\{ \frac{\partial U_{21}}{\partial z} - \frac{\partial^2 W_{21}}{\partial\rho^2} \right\}$$

$$H^H_{1z} = - \frac{I\ell\sin\phi}{4\pi} \left\{ \frac{\partial U_{21}}{\partial\rho} \right\}$$

Green's Function Definitions

$$G_{11} = \frac{e^{ik_1 R_1}}{R_1}$$

$$G_{12} = \frac{e^{ik_1 R_2}}{R_2} .$$

$$G_{21} = \frac{e^{ik_2 R_1}}{R_1}$$

$$G_{22} = \frac{e^{ik_2 R_2}}{R_2}$$

$$R_1 = \sqrt{\rho^2 + (h + z)^2}$$

$$R_2 = \sqrt{\rho^2 + (h - z)^2}$$

The Fundamental Integrals (U, V, W)

$$U_{ij} = U(a, b, \rho)$$

$$V_{ij} = V(a, b, \rho)$$

$$W_{ij} = W(a, b, \rho)$$

$$U_{11} = U(h - z, 0, \rho)$$

$$U_{12} = U(h, z, \rho)$$

$$U_{22} = U(0, h + z, \rho)$$

$$U_{21} = U(-z, h, \rho)$$

$$V_{11} = V(h - z, 0, \rho)$$

$$V_{12} = V(h, z, \rho)$$

$$V_{22} = V(0, h + z, \rho)$$

$$V_{21} = V(-z, h, \rho)$$

$$W_{11} = W(h - z, 0, \rho)$$

$$W_{12} = W(h, z, \rho)$$

$$W_{22} = W(0, h + z, \rho)$$

$$W_{21} = W(-z, h, \rho)$$

$$U(a, b, \rho) = \int_{-\infty}^{\infty} \frac{e^{-\gamma_1 a - \gamma_2 b}}{\gamma_1 + \gamma_2} H_0^{(1)}(\lambda\rho)\lambda d\lambda$$

$$= \int_{-\infty}^{\infty} \frac{\gamma_2 - \gamma_1}{k_1^2 - k_2^2} e^{-\gamma_1 a - \gamma_2 b} H_0^{(1)}(\lambda\rho)\lambda d\lambda,$$

$$= \int_{-\infty}^{\infty} \frac{2e^{-\gamma_1 a - \gamma_2 b} J_0(\lambda\rho)\lambda d\lambda}{\gamma_1 + \gamma_2}$$

$$V(a, b, \rho) = \int_{-\infty}^{\infty} \frac{e^{-\gamma_1 a - \gamma_2 b}}{k_1^2\gamma_2 + k_2^2\gamma_1} H_0^{(1)}(\lambda\rho)\lambda d\lambda$$

$$= \int_{-\infty}^{\infty} \frac{k_1^2\gamma_2 - k_2^2\gamma_1}{(k_1^4 - k_2^4)(\lambda^2 - k_0^2)} e^{-\gamma_1 a - \gamma_2 b} H_0^{(1)}(\lambda\rho)\lambda d\lambda$$

$$= \int_{0}^{\infty} \frac{2e^{-\gamma_1 a - \gamma_2 b} J_0(\lambda\rho)\lambda d\lambda}{k_1^2\gamma_2 + k_2^2\gamma_1}$$

$$W(a, b, \rho) = \int_{-\infty}^{\infty} \frac{\gamma_2 - \gamma_1}{k_1^2\gamma_2 + k_2^2\gamma_1} e^{-\gamma_1 a - \gamma_2 b} H_0^{(1)}(\lambda\rho)\lambda d\lambda$$

$$= \int_{-\infty}^{\infty} \frac{2(\gamma_2 - \gamma_1)e^{-\gamma_1 a - \gamma_2 b} J_0(\lambda\rho)\lambda d\lambda}{k_1^2\gamma_2 + k_2^2\gamma_1}$$

$$= \frac{\partial V(a, b, \rho)}{\partial a} - \frac{\partial V(a, b, \rho)}{\partial b}$$

Appendix B
Helpful Integral Relations

$$I_0 = \int_0^\infty \exp(-\alpha t^2 - 2\beta t)\, dt = \frac{1}{2}\sqrt{\frac{\pi}{a}}\, \exp(+\beta^2/\alpha)\, \operatorname{erfc}(\beta/\sqrt{\alpha})$$

$$I_1 = \int_0^\infty \exp(-\alpha t^2 - 2\beta t)\, t\, dt = -\frac{\beta}{\alpha} I_0 + \frac{1}{2\alpha}$$

$$I_2 = \int_0^\infty \exp(-\alpha t^2 - 2\beta t) t^2 dt = \frac{1}{2\alpha}\left(1 + 2\frac{\beta^2}{\alpha}\right) I_0 - \frac{1}{2}\frac{\beta}{\alpha^2}$$

$$I_3 = \int_0^\infty \exp(-\alpha t^2 - 2\beta t) t^3 dt = -\frac{1}{4\alpha}\left(\frac{6\beta}{\alpha} + \frac{4\beta^3}{\alpha^2}\right) I_0 + \frac{1}{4\alpha^2}\left(2 + \frac{2\beta^2}{\alpha}\right)$$

$$I_4 = \int_0^\infty \exp(-\alpha t^2 - 2\beta t) t^4 dt = \frac{1}{8\alpha}\left(\frac{6}{\alpha} + \frac{24\beta^2}{\alpha^2} + \frac{8\beta^4}{\alpha^3}\right) I_0 - \frac{1}{8\alpha^2}\left(\frac{10\beta}{\alpha} + \frac{4\beta^3}{\alpha^2}\right)$$

$$I_5 = \int_0^\infty \exp(-\alpha t^2 - 2\beta t) t^5 dt = -\frac{1}{16\alpha}\left(\frac{60\beta}{\alpha^2} + \frac{80\beta^3}{\alpha^3} + \frac{16\beta^5}{\alpha^4}\right) I_0 + \frac{1}{16\alpha^2}\left(\frac{8}{\alpha} + \frac{36\beta^2}{\alpha^2} + \frac{8\beta^4}{\alpha^3}\right)$$

$$I_6 = \int_0^\infty \exp(-\alpha t^2 - 2\beta t) t^6 dt = \frac{1}{32\alpha}\left(\frac{60}{\alpha^2} + \frac{360\beta^2}{\alpha^3} + \frac{240\beta^4}{\alpha^4} + \frac{32\beta^6}{\alpha^5}\right) I_0$$

$$- \frac{1}{32\alpha^2}\left(\frac{132\beta}{\alpha^2} + \frac{112\beta^3}{\alpha^3} + \frac{16\beta^5}{\alpha^4}\right)$$

$$H_0 = \int_{-\infty}^\infty \frac{\exp(-\alpha t^2 - 2\beta t)\, dt}{t + t_0} = -i\pi \exp\left(-\alpha t_0^2 + 2\beta t_0\right) \operatorname{erfc}\left(i\frac{\beta}{\sqrt{\alpha}} - i\sqrt{\alpha}\, t_0\right)$$

$$H_1 = \int_{-\infty}^\infty \frac{\exp(-\alpha t^2 - 2\beta t)\, t\, dt}{t + t_0} = -t_0 H_0 + \sqrt{\frac{\pi}{\alpha}}\, \exp(+\beta^2/\alpha)$$

$$H_2 = \int_{-\infty}^\infty \frac{\exp(-\alpha t^2 - 2\beta t)\, t^2 dt}{t + t_0} = +t_0^2 H_0 - \sqrt{\frac{\pi}{\alpha}}\left(t_0 + \frac{\beta}{\alpha}\right) \exp(+\beta^2/\alpha)$$

$$H_3 = \int_{-\infty}^{\infty} \frac{\exp(-\alpha t^2 - 2\beta t)\, t^3 dt}{t + t_0} = - t_0^3 H_0 + \sqrt{\frac{\pi}{\alpha}} \left(t_0^2 + t_0 \frac{\beta}{\alpha} + \frac{\beta^2}{\alpha^2} + \frac{1}{2\alpha} \right) \exp(+\beta^2/\alpha)$$

$$H_4 = \int_{-\infty}^{\infty} \frac{\exp(-\alpha t^2 - 2\beta t)\, t^4 dt}{t + t_0} = + t_0^4 H_0 - \sqrt{\frac{\pi}{\alpha}} \left(t_0^3 + t_0^2 \frac{\beta}{\alpha} + t_0 \frac{\beta^2}{\alpha^2} + t_0 \frac{1}{2\alpha} + \frac{\beta^3}{\alpha^3} + \frac{3\beta}{2\alpha^2} \right)$$

$$\times \exp(+\beta^2/\alpha)$$

$$H_5 = \int_{-\infty}^{\infty} \frac{\exp(-\alpha t^2 - 2\beta t)\, t^5 dt}{t + t_0} = - t_0^5 H_0 + \sqrt{\frac{\pi}{\alpha}} \left(t_0^4 + t_0^3 \frac{\beta}{\alpha} + t_0^2 \frac{\beta^2}{\alpha^2} + t_0^2 \frac{1}{2\alpha} + t_0 \frac{\beta^3}{\alpha^3} \right.$$

$$\left. + t_0 \frac{3\beta}{2\alpha^2} + \frac{\beta^4}{\alpha^4} + \frac{3\beta^2}{\alpha^3} + \frac{3}{4\alpha^2} \right) \exp(+\beta^2/\alpha)$$

$$H_6 = \int_{-\infty}^{\infty} \frac{\exp(-\alpha t^2 - 2\beta t)\, t^6 dt}{t + t_0} = t_0^6 H_0 - \sqrt{\frac{\pi}{\alpha}} \left(t_0^5 + t_0^4 \frac{\beta}{\alpha} + t_0^3 \frac{\beta^2}{\alpha^2} + t_0^3 \frac{1}{\alpha} + t_0^2 \frac{\beta^3}{\alpha^3} \right.$$

$$\left. + t_0^2 \frac{5\beta}{2\alpha^2} + t_0 \frac{\beta^4}{\alpha^4} + t_0 \frac{9\beta^2}{2\alpha^2} + t_0 \frac{3}{2\alpha^2} + \frac{\beta^5}{\alpha^5} + \frac{7\beta^3}{\alpha^4} + \frac{21\beta}{4\alpha^3} \right) \exp(+\beta^2/\alpha)$$

$$G_1 = \int_{t_1}^{t_2} \frac{\exp(-\alpha t)\, t dt}{\beta + \epsilon t} = \left[- \frac{1}{\alpha\epsilon} \exp(-\alpha t) + \frac{\beta}{\epsilon^2} \exp\left(\frac{\alpha\beta}{\epsilon}\right) E_1 \left(\frac{\alpha\beta}{\epsilon} + \alpha t\right) \right] \Bigg|_{t_1}^{t_2}$$

$$G_2 = \int_{t_1}^{t_2} \frac{\exp(-\alpha t)\, t^2 dt}{\beta + \epsilon t} = \left[\left(- \frac{1}{\alpha^2 \epsilon} - \frac{t}{\alpha\epsilon} + \frac{\beta}{\alpha\epsilon^2} \right) \exp(-\alpha t) - \frac{\beta^2}{\epsilon^3} \exp\left(\frac{\alpha\beta}{\epsilon}\right) E_1 \left(\frac{\alpha\beta}{\epsilon} + \alpha t\right) \right] \Bigg|_{t_1}^{t_2}$$

$$G_3 = \int_{t_1}^{t_2} \frac{\exp(-\alpha t)\, t^3 dt}{\beta + \epsilon t} = \left[\left(- \frac{2}{\alpha^3 \epsilon} - \frac{2t}{\alpha^2 \epsilon} + \frac{\beta}{\alpha^2 \epsilon^2} - \frac{t^2}{\alpha\epsilon} + \frac{\beta t}{\alpha\epsilon^2} - \frac{\beta^2}{\epsilon^3 \alpha} \right) \exp(-\alpha t) \right.$$

$$\left. + \frac{\beta^3}{\epsilon^4} \exp\left(\frac{\alpha\beta}{\epsilon}\right) E_1 \left(\frac{\alpha\beta}{\epsilon} + \alpha t\right) \right] \Bigg|_{t_1}^{t_2}$$

$$F_1 = \int \frac{t\,dt}{\beta + \epsilon t} = \frac{t}{\epsilon} - \frac{\beta}{\epsilon^2} \ln(\beta + \epsilon t)$$

$$F_2 = \int \frac{t^2\,dt}{\beta + \epsilon t} = \frac{\epsilon t^2}{2} + \beta t - \frac{\beta}{\epsilon}\, t + \frac{\beta^2}{2\epsilon} - \frac{\beta^2}{\epsilon^2} + \frac{\beta^2}{\epsilon^3} \ln(\beta + \epsilon t)$$

$$F_3 = \int \frac{t^3\,dt}{\beta + \epsilon t} = \frac{t^3}{3\epsilon} - \frac{\beta t^2}{2\epsilon^2} + \frac{\beta^2 t}{\epsilon^3} - \frac{\beta^3 \ln(\beta + \epsilon t)}{\epsilon^4}$$

/ PBT/lc/lmc